2017

# Immunocytochemical evaluation of cellular changes in a mouse model of direct cranial blast and advanced chronic traumatic encephalopathy in human postmortem brains

BOSTON UNIVERSITY

GRADUATE SCHOOL OF ARTS AND SCIENCES

Dissertation

# IMMUNOCYTOCHEMICAL EVALUATION OF CELLULAR CHANGES IN A MOUSE MODEL OF DIRECT CRANIAL BLAST AND ADVANCED CHRONIC TRAUMATIC ENCEPHALOPATHY IN HUMAN POSTMORTEM BRAINS

by

**GLORIA JESSICA DEWALT**

B.S., Dickinson College, 2007
M.A., Boston University, 2014

Submitted in partial fulfillment of the

requirements for the degree of

Doctor of Philosophy

2017

Approved by

First Reader

William D. Eldred, PhD
Professor of Biology

Second Reader

Vincent E. Dionne, PhD
Professor Emeritus of Biology

Third Reader

Douglas L. Rosene, PhD
Professor of Anatomy and Neurobiology
Boston University, School of Medicine

**Acknowledgements**

Sincerest thanks to my advisor, Bill Eldred. Your mentorship, patience and kindness over the years will remain highly valued. This work would not be possible without the help of my incredible committee: Bill Eldred, Doug Rosene, Jen-Wei Lin, Shelley Russek, and Vince Dionne. Your encouragement, support, and expertise are inspiring. Thank you for many helpful discussions, patience, and your insight into what it takes to conduct quality science.

To Todd Blute, a great mentor (and an honorary committee member) thank you for all of the precious advice, humor, and support over the years.

All former lab members, E. Shirley Sanchez, Jan Blom, Tom Giove thank you for the guidance and providing a good foundation as I joined the lab and now as I make the transition in to the big wide world. Thanks also to the many undergrads over the years that showed me the importance of hard work and self-care.

My dearest friends at BU: Lauren Tereshko, Liz McCarthy, Ellen Witkowski and Tenzin Kunkhyen thank you for your comfort during the many highs and lows of grad school.

For my mom Veronica Small and my sister Monica DeWalt thank you for loving me unconditionally. Your patience, positivity (even when I didn't deserve it), and wisdom have been most valued.

Lastly, grad school would have been impossible without my four legged button nosed pumpkin pie tarts, Maggie and Ella-Lena, two amazing Shih Tzus that are little bundles of endless joy and love that cheered me up so much during this journey.

**IMMUNOCYTOCHEMICAL EVALUATION OF CELLULAR CHANGES IN A MOUSE MODEL OF DIRECT CRANIAL BLAST AND ADVANCED CHRONIC TRAUMATIC ENCEPHALOPATHY IN HUMAN POSTMORTEM BRAINS**

**GLORIA JESSICA DEWALT**

Boston University Graduate School of Arts and Sciences, 2017

Major Professor: William D. Eldred, Professor of Biology

ABSTRACT

Traumatic brain injury (TBI) is a serious public health concern. Although moderate and severe forms of TBI receive considerable attention, mild TBI accounts for the majority of all injuries. The first two aims of this work used a rodent model of mild blast to simulate primary injury (damage from the blast wave only). The first aim evaluated potential changes in interneurons containing the calcium-binding proteins calretinin or parvalbumin. In addition, morphological changes in astrocytes and microglia were assessed. Brains were analyzed 48 hours and one month following exposure to single or repeated blasts, with a focus on the hippocampus due to its integral role in learning and memory. Results showed significant region-specific alterations in microglia morphology 48 hours following blast. The absence of structural alterations in microglia one month following blast indicated that the regional hippocampal vulnerability may be transient. The second aim compared glial morphologies in the retina and brain (the lateral geniculate nucleus, superior colliculus, and visual cortex) 48 hours or one month following multiple blasts. Fiber degeneration has received considerable attention, however,

less is known about the status of glia throughout the visual pathway following mild blasts. Although no structural alterations were detected, it is possible that alterations in glia occurred at a more acute time scale as changes in glia can be rapid and reversible.

The final aim of this work focused on the immunocytochemical characterization of tau pathology in the visual cortices of human postmortem brains with advanced chronic traumatic encephalopathy (CTE). CTE is a devastating tauopathy associated with mild, repetitive TBIs. Although visual deficits are reported in CTE, the primary visual cortex is often spared. The main hypothesis under investigation was whether visual association areas would have tau pathology, despite sparing of primary visual cortex. In addition, a sub-class of interneurons containing parvalbumin was used to evaluate a potential cell-specific vulnerability. Results showed increased tau pathology in visual association areas in advanced CTE that was largely absent from the primary visual cortex. There was no effect on parvalbumin positive interneurons. The results of this work provide valuable insight regarding potential cell-specific resistance to CTE pathology.

## TABLE OF CONTENTS

## List of Tables

## List of Figures

## List of Abbreviations

| | |
|---|---|
| Aβ | Amyloid-beta |
| AD | Alzheimer's disease |
| AMPA | α-amino-3-hydroxy-5-methyl-4-isoxzolepropionic acid |
| ANOVA | Analysis of variance |
| APP | Amyloid precursor protein |
| AU | Arbitrary units |
| BA | Brodmann area |
| BBB | Blood brain barrier |
| BDC | Blast dissipation chamber |
| BU-ADC | Boston University Alzheimer's Disease Center |
| C | C-terminal |
| CA | Cornu ammonis |
| CBP | Calcium-binding protein |
| CCI | Controlled Cortical Impact |
| CDK5 | Cyclin dependent kinase 5 |
| CE | Coefficient of error |
| CNS | Central nervous system |
| COBIA | Cranium only blast injury apparatus |
| COD | Cause of death |
| CR | Calretinin |
| CSTE | Center for the Study of Traumatic Encephalopathy |
| CT | Computed tomography |

| | |
|---|---|
| CTE | Chronic traumatic encephalopathy |
| DAB | 3’3’-diaminobenzidine |
| DAI | Diffuse axonal injury |
| DG | Dentate gyrus |
| DLG | Dorsal lateral geniculate nucleus |
| DTI | Diffusion tensor imaging |
| EC | Entorhinal cortex |
| ERG | Electroretinogram |
| FPI | Fluid Percussion Injury |
| GABA | Gamma amino butyric acid |
| GCL | Granule cell layer |
| GCS | Glasgow coma scale |
| GFAP | Glial fibrillary acidic protein |
| GSK3b | Glycogen synthase 3 beta |
| Iba1 | Ionized calcium binding adapter molecule-1 |
| IML | Inner molecular layer |
| kHz | kilohertz |
| kPa | kilopascal |
| MARK | Microtubule affinity-regulating kinase |
| MAPK | Mitogen-activated protein kinase |
| MAPT | Microtubule-associated protein tau |
| MRI | Magnetic resonance imaging |
| NFT | Neurofibrillary tangle |
| NMDA | N-methyl-D-aspartate |

| | |
|---|---|
| NMDAR | N-methyl-D-aspartate receptor |
| OCT | Optical coherence tomography |
| OML | Outer molecular layer |
| N | N-terminal |
| PB | Phosphate buffer |
| PBTx | Phosphate buffer with Triton X-100 |
| PET | Positron emission tomography |
| PKA | Protein kinase A |
| PKC | Protein kinase C |
| PLP | Periodate-lysine-paraformaldehyde |
| PMI | Postmortem interval |
| PTA | Post traumatic amnesia |
| RGB | Red green blue |
| RGC | Retinal ganglion cell |
| ROI | Region of interest |
| s | Septal |
| S | Serine |
| SC | Superior colliculus |
| SD | Standard deviation |
| SEM | Standard error of the mean |
| SLM | Stratum lacunosm moleculare |
| Su | Subiculum |
| t | Temporal |
| T | Threonine |

| | |
|---|---|
| TBI | Traumatic brain injury |
| TBS | Tris buffered saline |
| VC | Visual cortex |
| VEP | Visually evoked potentials |

# CHAPTER 1

# INTRODUCTION

## What is traumatic brain injury?

Traumatic brain injury (TBI) is a general term used to describe any alteration in the structure and/or function of the brain from an external force (McAllister, 2011; Xiong et al., 2013). Sources of external forces include auto accidents, falls, contact sports, and blast-related injuries in military settings (Andriessen et al., 2010; McAllister, 2011). Symptoms following a TBI may include headaches, dizziness, fatigue, vertigo, and sensory impairments to memory and vision (DeKosky et al., 2013).

TBI severity is commonly classified as mild, moderate, or severe (Andriessen et al., 2010). Recently, a fourth category, 'penetrating', has been added by the department of defense to differentiate damage resulting from penetration of dura (Leo and McCrea, 2016). Clinical diagnosis regarding the extent of injury is based on neurological examinations and neuroimaging (Andriessen et al., 2010; Zhang et al., 2016). Neuroimaging assessments include computed tomography (CT), magnetic resonance imaging (MRI), and diffusion tensor imaging (DTI) (Adrian et al., 2016). Each of the aforementioned imaging techniques infer specific advantages. MRIs allow clinicians to monitor changes in brain activity while DTIs provide a metric to evaluate nerve fiber integrity

(Andriessen et al., 2010). Though helpful in visualizing the areas where severe trauma occurred, CT scans are less useful in detecting subtle injuries.

Clinically based scoring systems represent an important part of any neurological examination. The Glasgow Coma Scale (GCS) is a neurological scoring system that has been considered the gold standard since its inception in 1974 (Majdan et al., 2015). It uses a 15 point scale to assess a patient's motor, eye, and verbal responses following injury. The higher the GCS score the lower the severity of injury. Mild TBI has a GCS range of 13–15 (Andriessen et al., 2010) and is defined as confusion and/or disorientation that lasts less than 24 hours, a loss of consciousness less than 30 minutes, and post traumatic amnesia (PTA) less than 24 hours (Leo and McCrea, 2016). It has been reported that mild TBI represents the majority of all TBI cases (70–90%) (Ruff et al., 2009). However, the subtle deficits associated with mild TBI are not always detected by conventional neuroimaging (Ruff et al., 2009; Leo and McCrea, 2016). Moderate TBI entails confusion/disorientation over 24 hours but less than seven days, a loss of consciousness greater than 30 minutes but less than 24 hours and has a GCS range of 9–12 (Andriessen et al., 2010; Leo and McCrea, 2016). Similar to mild TBI, conventional neuroimaging results do not always detect structural abnormalities associated with moderate injuries (Leo and McCrea, 2016). Severe TBI is a confused/disorientated state and/or loss of consciousness that lasts more than 24 hours and has a GCS range less than or equal to 8 (Andriessen et al., 2010; Leo and McCrea, 2016).

## Experimental models used to study TBI

Damage resulting from TBI is traditionally defined as primary or secondary (Patt and Brodhun, 1999). Immediate damage from the resultant force is defined as primary injury, while secondary injury is the delayed onset (minutes to months) of cascades initiated from the primary injury (Patt and Brodhun, 1999; Andriessen et al., 2010). The pattern of damage from a TBI is often described as focal or diffuse. Focal injuries such as hematomas (subdural and epidural), contusions, and hemorrhages arise from the force(s) exerted onto the skull that compresses underlying tissue at the location of impact (coup) or opposite the impact (contre-coup) (Farkas and Povlishock, 2007; Andriessen et al., 2010). In contrast, diffuse (multifocal) injuries are widespread and exist in regions remote from the external force (Farkas and Povlishock, 2007; McAllister, 2011).

Several animal models have been developed to simulate TBI. Each model is broadly defined as penetrating or non-penetrating based on the method used to produce injury.

### *Penetrating models of TBI*

Fluid percussion injury (FPI) and controlled cortical impact (CCI) are two prevalent penetrating models of TBI (Figure 1.1). FPI uses a pendulum to strike a fluid filled reservoir that exerts a pulse of pressure from the fluid onto intact dura through a craniotomy centrally over the midline or laterally over the parietal bone between

bregma and lambda (Xiong et al., 2013). The strength of the pressure pulse determines the severity of injury**.** FPI is often used to reproduce focal injuries such as intracranial hemorrhage and to a lesser extent axonal injury (Finnie and Blumbergs, 2002; Xiong et al., 2013). In contrast to FPI, CCI is a rigid percussion model that employs a metallic piston to deliver a mechanical impact onto the intact dura (Cernak, 2005). The severity of injury is determined by the speed of impact and the extent of cortical deformation.

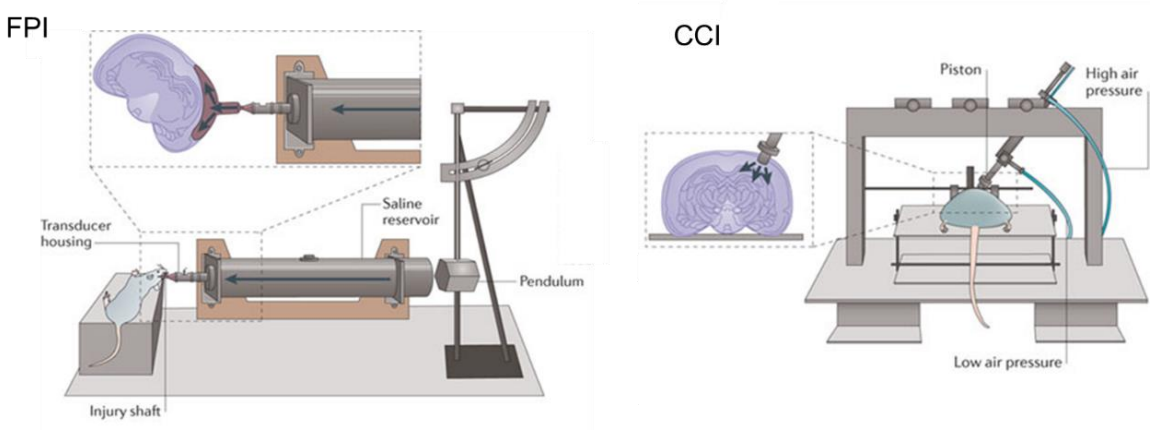


**Figure 1.1.** Penetrating models of TBI. Schematic modified from Xiong et al., 2013. CCI = controlled cortical impact. FPI = fluid percussion injury.

*Non-penetrating models of TBI*

Weight drop

To simulate concussive (mild) injury, several non-penetrating weight drop models have been constructed (Figure 1.2). Most use brass weights that are dropped from specified heights onto an exposed skull affixed with a steel protective disc located

centrally between bregma and lambda (Cernak, 2005; Hanrahan and Campbell, 2016). Progressive injury associated with weight drop models correlates with the mass and height of the weight used. Injuries modeled from weight drop include both focal and diffuse axonal injury (Xiong et al., 2013).

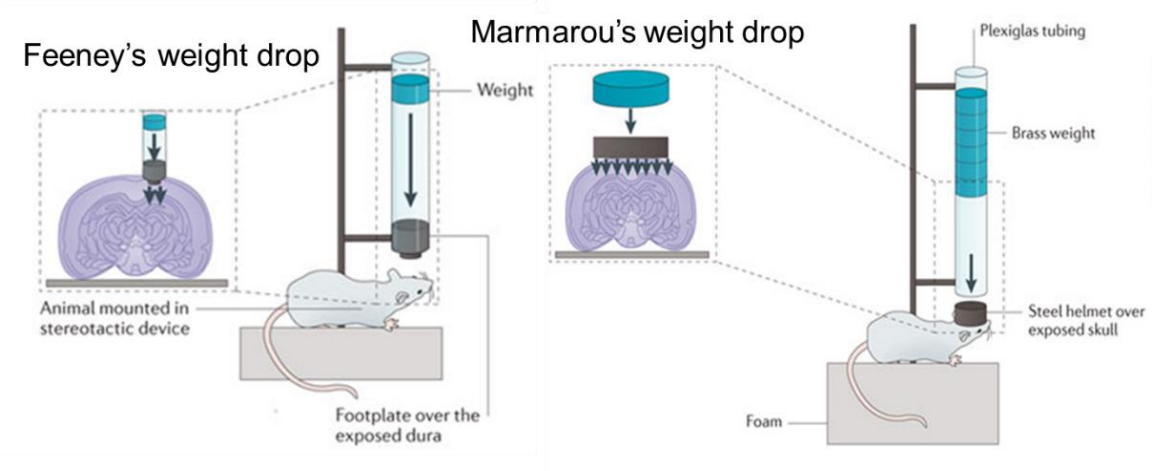


**Figure 1.2.** Common weight drop models of TBI. Schematic modified from Xiong et al., 2013.

Blast

TBI from blast exposures are categorized into four groups according to the nature of trauma. Primary injury is due to damage from the blast wave itself, secondary injury results from projectiles and penetrating fragments set in motion by the blast, while tertiary injury occurs from collisions with nearby objects, and quaternary injury is a consequence of burns and noxious fumes released from explosions (Chalioulias et al., 2007; Cernak and Noble-Haeusslein, 2010). Although primary

injury is known to cause neurological impairments, it remains the least understood type of injury (Elder and Cristian, 2009; Hicks et al., 2010; Svetlov et al., 2010; Courtney and Courtney, 2015; Nakagawa et al., 2016). In addition, primary injury is the most difficult to distinguish due to its co-occurrence with events that cause overt physical damage (Bhattacharjee, 2008). Because of this, many of the blast models to date focus on primary injury (Figure 1.3).

Acceleration-deceleration, direct cranial transmission of the blast wave, and thoracic transmission are the main pathological mechanisms attributed to blast exposure (Goldstein et al., 2012; Gullotti et al., 2014; Courtney and Courtney, 2015). Although neural damage due to acceleration-deceleration from blast waves traversing the skull is an accepted contributor of blast injury, thoracic transmission was initially the most widely cited mechanism. Thoracic transmission occurs when a blast wave propagates from the thorax to the head via major blood vessels (Simard et al., 2014). Although use of protective armor has significantly reduced injury via thoracic transmission, rotational and translational forces resulting in diffuse injuries remain prevalent contributors to injuries following blast (McAllister, 2011) and can exacerbate pathology (Svetlov et al., 2010; Goldstein et al., 2012; Gullotti et al., 2014). In addition, rotational forces can shear and stretch neurons beyond their elastic threshold. Direct transmission of the blast wave through the skull is a significant factor in neural damage (Risling et al., 2011; Courtney and Courtney, 2015). Although evidence to support each mechanism exists, it is likely that they are not mutually exclusive.

Most of the blast related models focus on damage following exposure to a single blast (Cernak, 2005; Goldstein et al., 2012; Xiong et al., 2013). However, within the last decade it has become increasingly evident that injuries from multiple blasts can offer better insight into TBI pathology as injuries are often due to repetitive insults (Wang et al., 2011). Many animal models of blast use cylindrical shock tubes containing two chambers separated by a membrane (Figure 1.3). When the first chamber is pressurized with compressed air, the membrane ruptures producing a blast onto the restrained animal in the second chamber (Hanrahan and Campbell, 2016). Recently, modified blast models have employed simpler methods to generate blasts, increasing their ease of use and providing more control in delivering blasts (Figure 1.3) (Kuehn et al., 2011; Heldt et al., 2014; Sajja et al., 2014).

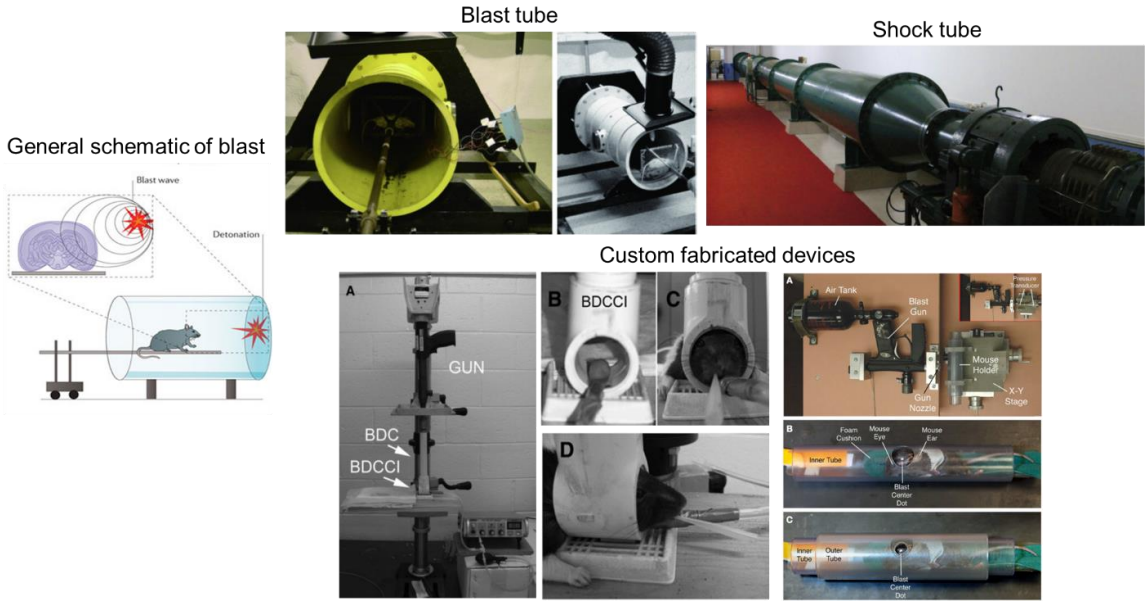


**Figure 1.3.** Blast models of TBI. General schematic of blast modified from Xiong et al., 2013. Blast tube and Shock tube images modified from Ning and Zhou, 2015. Images of custom fabricated devices modified from Kuehn et al., 2011 (left panel) and Heldt et al., 2014 (right panel).

*Caveats from animal models*

Although the experimental use of animals to reproduce specific TBI pathologies is invaluable, differences in experimental design, animal choice, and anesthetics are increasingly recognized as confounding factors.

Anesthetics and analgesics

Anesthetics and analgesics are typically required to immobilize animals and minimize pain and distress during and after injury. However, commonly used drugs can significantly affect TBI outcome by exerting a continuum of neuroprotection (Rowe et al., 2013). It has been shown that mild TBI and acute recovery following injury show the greatest susceptibility to neuroprotective effects, particularly in the presence of volatile anesthetics such as isoflurane (Kawaguchi et al., 2005). Much of this neuroprotection is due to the ability of drugs to mitigate excitotoxicity (Kawaguchi et al., 2005). For example, the gaseous anesthetic isoflurane has been shown to reduce the release of glutamate in addition to blocking N-methyl-D-aspartate (NMDA) and α-amino-d-hydroxy-5-methyl-4-isoxazole-propionate (AMPA) glutamate receptors in rats (Harada et al., 1999; Kimbro et al., 2000; Kawaguchi et al., 2005). In addition, the routinely used injectable anesthetic, ketamine, has been reported to significantly reduce memory dysfunction in TBI likely due to non-competitive inhibition of NMDARs that can mitigate deleterious consequences of their over-activation in a rat model of FPI (Smith et al., 1993).

Similarly, comparison of TBI outcome following the administration of seven commonly used anesthetics (diazepam, fentanyl, isoflurane, ketamine, morphine, pentobarbital, and propofol) in a rat model of CCI showed the least amount of neuronal death following exposure to isoflurane while ketamine treated animals had the greatest neuronal death (Statler et al., 2006). In contrast to evidence of neuroprotective effects, some studies report exacerbation of neurological pathology from anesthetics (Rowe et al., 2013). One study that evaluated the influence of isoflurane in a rat model of CCI found increased cell death that positively correlated with isoflurane dose and duration (Hertle et al., 2012). Although reports conflict regarding their benefit or detriment, awareness of the potential role that anesthetics and analgesics can have on TBI outcome is essential.

Animal choice

Animals used to study TBI have included: include pigs (Browne et al., 2011; Sherwood et al., 2014), rabbits (Jones et al., 2016), dogs (Shelah et al., 2007), mice and rats (Petras et al., 1997; Mohan et al., 2013; Zou et al., 2013; DeMar et al., 2016; Guley et al., 2016). Large animals such as pigs (Browne et al., 2011; Sherwood et al., 2014) and sheep (Xiong et al., 2013) can offer insight into the complex pathologies reported in humans due to similarities in brain size and the presence of sulci and gyri (gyrencephaly). However, mice are commonly used due

to their relatively low cost, ease of genetic manipulation, and well-mapped genomes (Steward et al., 1999; Cernak, 2005). In addition, studies using rats, though they offer less genetic manipulation in comparison to mice, are prevalent in animal models of TBI.

An emerging consideration in rodent studies is the confound resulting from species and strain-specific differences (Steward et al., 1999; Bricker-Anthony and Rex, 2015). One study using FPI evaluated two commonly used rat strains, Fisher 344 and Sprague-Dawley, found higher intracranial pressure, prolonged seizure activity, and significantly more degenerating neurons in Fisher 344 rats (Reid et al., 2010). Although C57BL/6 mice are most commonly used, and often serve as a background for many transgenic lines (Bricker-Anthony and Rex, 2015), work evaluating trauma in mice found a differential susceptibility to injury that can vary with strain and hybrid (Schauwecker and Steward, 1997; Majid et al., 2000). For example neurodegeneration and vision loss were more prevalent in DBA/2J mice compared with C57BL/6 (Bricker-Anthony and Rex, 2015). However, no standardization currently exists in model, anesthetic, or rodent strain. Therefore the aforementioned factors must always be considered when interpreting and comparing results.

## Primary and secondary cellular pathologies resulting from TBI

Although overt evidence of trauma such as contusions and lacerations have been detected postmortem, it has been well established that subtle cellular pathologies, evident only on a microscopic level, may be of greater importance to the progression of injury (Patt and Brodhun, 1999). Documentation of such pathologies includes but is not limited to cell death (Raghupathi, 2004; Andriessen et al., 2010; Wang et al., 2011), elevated free radicals (Huber et al., 2013), alterations in excitation and inhibition ratios (Buritica et al., 2009), and inflammation (de Lanerolle et al., 2011; Goodrich et al., 2016).

### *Alterations in excitation and inhibition following TBI*

Increased permeability of cell membranes is believed to initiate pathological events that contribute to TBI (Johnson et al., 2010). Direct consequences of altered membrane permeability include the excessive release of excitatory transmitters and ion imbalances (Werner and Engelhard, 2007). Additionally, disproportionate excitation (excitotoxicity) can also contribute to pathological alterations in calcium ion homeostasis (Andriessen et al., 2010). Calcium ions are the most abundant second messenger with vital roles in cellular processes such as growth, development, and synaptic transmission (Weber, 2012). Persistent elevation in intracellular calcium can activate degradative enzymes such as proteases and detrimental mediators such as reactive oxygen species that exacerbate signaling

cascades that ultimately result in cell death (Zhivotovsky and Orrenius, 2011). Although logical to assume that excessive excitation results from alterations in excitatory cells as glutamatergic pyramidal cells represent 75–80% of neuronal cells type (Freire et al., 2015), considerable evidence exists to the contrary. While interneurons only account for approximately 20% of the neuronal population (Freire et al., 2015), their regulation of proper brain functioning is essential (Xu et al., 2010). Diminished and/or total loss of inhibition are considered major contributors to the excitoxicity that can result from TBI (Cantu et al., 2015).

*Inflammation*

Previously the brain was considered spared due to the presence of the blood-brain barrier (BBB), an impermeable barrier comprised of endothelial cells encased by glia (Cederberg and Siesjo, 2010). Disruptive forces from TBI and/or damage to cells that maintain the BBB can allow access of peripheral immune cells, pathogens, and cytokines, all of which can further exacerbate BBB breakdown (Obermeier et al., 2013). Results of neuroimaging in humans and staining assays in animal models of injury support compromised BBB integrity and the inflammation that ensues as a common consequence of TBI.

Astrocytes and microglia are essential glial cell types involved in inflammatory responses following insults. Defining features common to both cell types are morphological changes (Figure 1.4) and secretion of soluble factors such

as cytokines, chemokines, and growth factors that modulate the extent of damage and repair following injury (Thored et al., 2009; Karve et al., 2016).

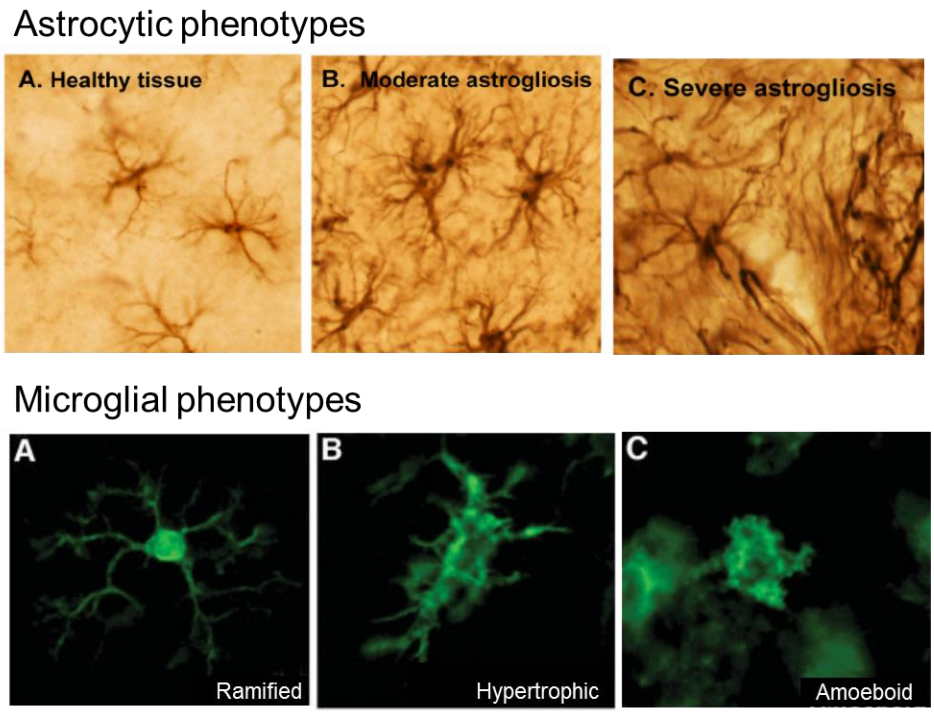


**Figure 1.4.** Range of glial morphologies in response to changes in the microenvironment. Astrocytic phenotypes modified from Sofroniew, 2009. Microglial phenotypes modified from Thored et al., 2009.

In healthy tissue, microglia are evenly distributed with dynamic properties that allow them to extend and retract thin (ramified) processes to survey their microenvironment (Jinno et al., 2007). In response to insult and interactions with neighboring cells, microglia can excrete soluble factors upon activation. Once activated, microglia can reversibly assume a variety of morphologies that range from hypertrophied somata and processes to complete contraction of processes

resulting in an amoeboid-like appearance (Figure 1.4, bottom panel) (Thored et al., 2009; Karperien et al., 2013). The spectrum of microglia polarization is broadly classified as cytotoxic M1 (classical activation) or neuroprotective M2 (alternative activation/acquired deactivation) (Tang and Le, 2016). The specific identity of microglia is based on a combination of secreted mediators, cell surface receptors, and alterations in gene expression. Similar to microglia, astrocytes normally tile the brain (Sofroniew and Vinters, 2010) and can undergo morphological changes (Figure 1.4, top panel) following insult and alterations in surrounding cells. In addition, astrocytes can secrete factors that affect the microenvironment and overall tissue integrity (Chen and Swanson, 2003). Studies evaluating astrocytes and microglia in the context of disease and trauma have demonstrated that responses are context and severity dependent (Schwartz et al., 2006; Zamanian et al., 2012). The autocrine and paracrine responses of astroglial reactivity can infer beneficial effects (neuroprotective) or exert deleterious (neurotoxic) exacerbation of cellular cascades (Karve et al., 2016).

**Long term complications associated with TBI**

The complex processes underlying TBI have been implicated in the initiation of long-term cognitive deficits (Faden and Loane, 2015). Specific neurodegenerative disorders following TBI include: amyotrophic lateral sclerosis, Alzheimer's disease (AD), Parkinson's disease, and chronic traumatic encephalopathy (CTE), the latter

of which is uniquely associated with repetitive head injuries (DeKosky et al., 2013; Elder et al., 2014; Faden and Loane, 2015).

Specific cellular events linking TBI with long-term neurodegenerative disorders center on the progressive accumulation of similar pathological components. Several studies have focused on the accumulation of amyloid precursor protein (APP) and amyloid-beta (Aβ) fragments that result from APP cleavage (Johnson et al., 2010; O'Brien and Wong, 2011). Accumulation of APP and Aβ plaques are common in degenerative disorders that are associated with TBI such as AD, and have been found soon after injury in animal models of TBI (Johnson et al., 2010). Results of one study found increases in Aβ immunoreactivity that persisted one month to one year following FPI in adult rats (Iwata et al., 2002). Interestingly, Aβ was found to accumulate in the absence of upregulated APP gene expression, suggesting a possible mechanism to account for neurodegeneration following TBI. In addition to APP and Aβ, a number of TBI studies have focused on accumulation of tau (Goldstein et al., 2012; McKee et al., 2013). Tau proteins are microtubule-associated proteins that function to stabilize microtubules (Avila et al., 2004). Figure 1.5 compares tau proteins in a healthy and disease neuron. Following trauma, or other pathological insults, deleterious aberrations such as hyperphosphorylation destabilize tau proteins causing them to disassociate from the microtubule and aggregate in the form of tangles and/or filaments in and around neurons and glia (Avila et al., 2004; Forman et al., 2005). Toxic accumulation of tau results in compromised axonal transport that contributes

to synaptic dysfunction, and ultimately degeneration (Ballatore et al., 2007). Particularly devastating is the ability of hyperphosphorylated tau to sequester normally functioning tau proteins leading to progressive retrograde neurodegeneration (Iqbal et al., 2005). Disrupted axonal integrity is posited to underlie the long-lasting cognitive deficits following TBI (DeKosky et al., 2013). Structural disorganization of axons can occur immediately following insults and/or over long intervals following injury (Iwata et al., 2002). However, environmental and genetic factors are emerging as active areas of research due to the variation and presentation of long-term impairments associated with single-incident versus repetitive TBIs.

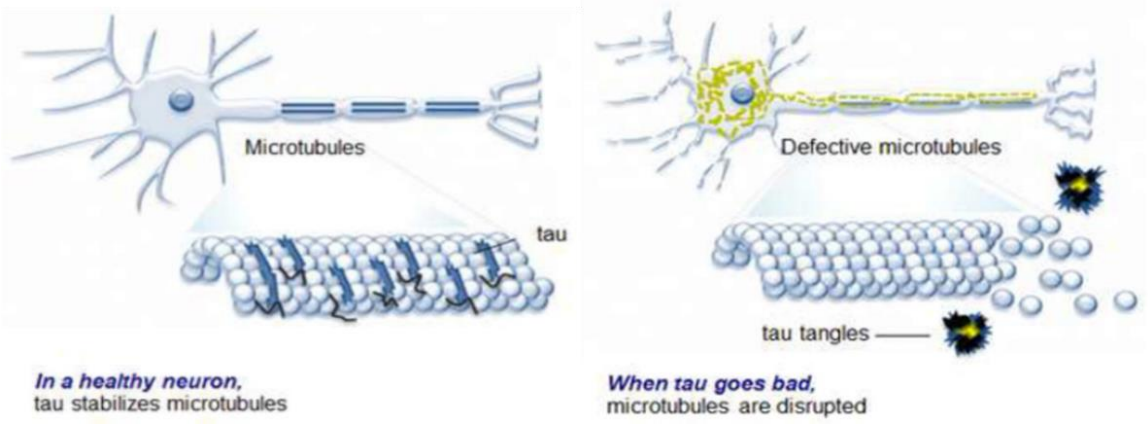


**Figure 1.5.** Function of tau proteins. In a healthy neuron (left), tau proteins stabilize microtubules supporting axonal transport. In contrast, in a diseased neuron (right) post-translational modifications such as hyperphosphorylation cause tau proteins to disassociate from microtubules resulting their disassembly, impaired axonal transport, and aggregations of tau, which ultimately contribute to neurodegeneration. Schematic modified from Lim et al., 2014.

## Challenges to therapeutic approaches of TBI and associated long-term disorders

Therapies in development target specific cellular pathways believed to contribute to injury progression (Kochanek et al., 2015; Xiong et al., 2015; Aertker et al., 2016). However, mechanisms once thought to be detrimental can also be beneficial, such as some inflammatory processes (Xu et al., 2011; Xiong et al., 2015; Tang and Le, 2016). Complications due the type of injury, severity of injury, age, gender, pre-existing diseases, other comorbidities, and small samples sizes in clinical studies are often unavoidable (Xiong et al., 2015). Candidate biomarkers serving as proxies for neuronal injury (neuron specific enolase and tau) and glial injury (glial fibrillary protein and S100β) have emerged (Zetterberg et al., 2013). The determination of biomarkers present in cerebrospinal fluid, blood, and/or urine could aid in rapid assessment of the temporal characteristics of injury profiles, and allow monitoring of the efficacy of therapeutic interventions (Adrian et al., 2016). In spite of considerable progress in identifying cellular pathologies following TBI and related long-term disorders, clinical breakthroughs in treatments and mitigation have been delayed. The heterogeneous nature of TBI and the limitations of transitioning experimental success in animal models into clinical practice remain a challenge in designing effective treatments (Menon, 2009).

**Summary of specific aims**

The objectives of this work were to evaluate the cellular changes in a previously validated rodent model of mild direct cranial blast and in human postmortem brains diagnosed with advanced stages of CTE to carry out the following three aims:

*1. Immunocytochemically evaluate neuronal and glial responses in the mouse hippocampus following acute (48 hour) and chronic (one month) exposure to a single and repeated mild blast pressures* (Chapter 2).

Vulnerability of the hippocampus following TBI has been widely documented (Royo et al., 2006; Sajja et al., 2014). The goal of this aim was to use neuronal and glial markers to evaluate cellular responses following acute (48 hours) and long-term (one month) exposure to single versus repeated blasts using a previously validated rodent model of blast injury (Kuehn et al., 2011).

Inflammation is a prevalent consequence following TBI. Several studies have cited the roles of astrocytes and microglia in eliciting immune responses following injury (Karve et al., 2016). In addition to inflammation, alterations in calcium ion homeostasis are prevalent consequences following TBI that have been implicated in apoptotic and necrotic cascades that result in cell death (Buritica et al., 2009; Weber, 2012; Karve et al., 2016). To evaluate glial response to injury

glial fibrillary acidic protein (GFAP) and ionized calcium binding adaptor molecule-1 (Iba-1) were used to label astrocytes and microglia, respectively. The calcium-binding proteins calretinin and parvalbumin were used to selectively label large populations of non-overlapping inhibitory cells.

*2. Establish whether astrocytes and microglia are similarly affected in the brain and retina following exposure to mild repetitive blast pressures* (Chapter 3).

As an accessible part of the central nervous system it has been speculated that the retina may provide insight into the central damage following injury. Although fiber degeneration has received considerable attention due to the DAI that is common following injury, less is known about the status of glia throughout the visual system. Thus, the goal of this aim was to compare glial morphologies in the retina and select brain regions essential for visual processing (the dorsal lateral geniculate nucleus, superior colliculus, and visual cortex) in a mouse model of blast-induced TBI following acute (48 hours) and long-term (one month) recovery to repetitive blasts.

*3. Immunocytochemically evaluate the extent of tau pathology in visual cortices and determine whether a specific sub-group of interneurons are structurally altered in advanced CTE* (Chapter 4).

No study to date has documented tau pathologies beyond the primary visual cortex, which is found to be spared except in the most severe cases (McKee et al., 2013). In addition, work exploring vulnerability of specific interneuronal populations in CTE is lacking. Thus, the goals of this aim were to determine the extent of tau pathology present in visual association areas and identify if a specific sub-class of GABAergic neurons containing the calcium-binding protein parvalbumin are affected in advanced stages of CTE.

# CHAPTER 2

Immunocytochemical evaluation of neuronal and glial responses in the mouse hippocampus following single and repeated blast exposures

## ABSTRACT

Hippocampal abnormalities resulting from TBI have been widely documented in several animal models. In this study immunocytochemistry was used to examine structural alterations in neurons containing the calcium-binding proteins calretinin and parvalbumin. Glial populations of interest were astrocytes and microglia. The time points evaluated were 48 hours (acute) and one month (chronic) following single and repeated blasts. Though statistically insignificant, results showed subtle, subthreshold, effects of blast within hippocampal interneurons. Of the different hippocampal regions surveyed, the stratum lacunosum moleculare and the outer molecular layer of the dentate gyrus showed statistically significant changes acutely following blast in both of the glial populations examined. Overall the findings from this study indicate a regional hippocampal vulnerability that may be transient. Future studies focused on the anatomical and functional responses to blast at more acute recovery time points (less than 48 hours) are clearly warranted.

# INTRODUCTION

## Anatomy of the hippocampus

The hippocampus is a bilateral structure integral to memory and spatial navigation (Strange et al., 2014). Technically, the hippocampus is part of a larger network called the hippocampal formation. Functionally, each part of the network has a distinct role in information processing. The hippocampal formation comprises the following adjacent regions: entorhinal cortex, parasubiculum, presubiculum, subiculum, dentate gyrus, and the hippocampus proper: cornu ammonis 1, 2, and 3 (Andersen, 2007). Each area differs in its cytoarchitecture, function, and projections. The seemingly simplistic allocortical (less than six layers) laminar organization and input from a diverse array of neocortical regions have rendered the hippocampal formation a widely studied network (Forster et al., 2006).

Hippocampal formations are somewhat grossly similar across several mammalian species. However, significant species specific differences exist in the number of cytoarchitectural sub-divisions, cell densities, neuroanatomy, and tissue volume(Andersen, 2007). Though works documenting hippocampal neuroanatomy in monkeys and humans exist, much of our understanding is based on rodents, specifically rats (Andersen, 2007). While mice offer unparalleled genetic manipulations, compared to rats, it is commonly assumed that the similarities between rodents outweighs the potential confounds due to species and strain

specific differences, although this belief is being challenged. However, this study focused on general hippocampal organization as it relates to rodents.

The rodent hippocampus is a curved, elongated, structure that runs longitudinally along a dorsoventral (or rostralcaudal) axis (Figure 2.1). Based on differences in cortical and subcortical connections and lesions studies, the dorsal hippocampus is implicated in spatial learning while the ventral hippocampus is believed to mediate emotional responses (Moser et al., 1993; Fanselow and Dong, 2010). It is worth noting that region-specific functional differences are not absolute nor a simple dichotomy but rather a complex and gradual functional spectrum along the longitudinal axis (Risold and Swanson, 1996).

Although the term ‘hippocampus’ is somewhat ambiguous and can differ based on context, it is commonly used as a reference for the cornu ammonis sub-fields described by the neuroanatomist Lorente de Nó (Andersen, 2007). However, in this work the term ‘hippocampus’ will be used to collectively denote the dentate gyrus (DG), cornu ammonis 3 ($CA_3$), and cornu ammonis 1 ($CA_1$) as the aforementioned are the hippocampal sub-fields that are the focus of the present work. Despite substantial controversy regarding the existence of cornu ammonis 2 ($CA_2$), evidence supporting its presence as distinct, yet narrow, sub-field located between $CA_1$ and $CA_3$, exists but it was not examined in this study.

**Neurons in the hippocampus**

The principle cell type in the hippocampus is a relatively homogenous population of pyramidal cells (granule cells in the dentate gyrus) (Klausberger and Somogyi, 2008). Non-principal inhibitory interneurons represent approximately 10–20% of the total neuronal population within the hippocampus (Chamberland and Topolnik, 2012). Although a small minority, interneurons have a significant role in coordinating cellular activity that affects the overall functionality of the hippocampus (Freund and Buzsaki, 1996). Spatially, interneurons are found scattered throughout all sub-fields and maintain local synaptic contact with principle cells in addition to other interneurons (Jones and Yakel, 1999).

The diversity of interneuron populations has been documented and is based on differences in electrophysiology, location, morphology, cell and molecular markers, and, more recently, single cell sequencing of ribonucleic acids (Zeisel et al., 2015). Given the sparse yet diverse interneuronal cell types exerting a powerful influence on the overall status of the hippocampus, this study examined whether two non-overlapping populations of interneurons, identified by the presence of the well-established calcium-binding proteins parvalbumin and calretinin, were affected following exposure to mild blasts.

## Hippocampal vulnerability to injury

The hippocampus is affected in several neurological conditions and disorders such as epilepsy (Huusko et al., 2015), seizures (Kovacs et al., 2014), Alzheimer's disease (Morrison and Hof, 2002), and chronic traumatic encephalopathy (McKee et al., 2013). Vulnerability of the hippocampus to damage following TBI (Royo et al., 2006; Atkins, 2011; Sajja et al., 2014) has been has been attributed to its anatomical position (Almeida-Suhett et al., 2015) and biochemical diversity (Geddes et al., 2003). However, most TBI studies employ invasive models of focal injury and/or moderate to severe blast models. Although most reports of structural hippocampal changes are based on results of moderate and severe forms of TBI, mild TBI accounts for over 80% of all injuries (Almeida-Suhett et al., 2015) and damage is often subtle and/or transient. In general, shifts in excitation and inhibition ratios, due to a loss of inhibition, and glial activation are two commonly cited mechanisms of injury within the hippocampus (Beamer et al., 2016).

## Study objectives

The main goals of this study were to use immunocytochemistry to characterize the extent of structural alterations in neurons containing calretinin and parvalbumin. The rationale for examining these neuronal populations was based on the prevalence of altered inhibition following TBI.

In addition to alterations in interneuronal populations, inflammation is a prevalent consequence of injury, as stated in Chapter 1. Several studies have cited the roles of astrocytes and microglia in eliciting immune responses following TBI (Karve et al., 2016). Thus, antisera directed against glial fibrillary acidic protein (GFAP) and ionized calcium binding adapter molecule-1 (Iba-1) were used to label astrocytes and microglia, respectively.

Both neuronal and glial populations were evaluated following exposures to single and repeated blasts using a previously established rodent model of direct cranial blast injury (Kuehn et al., 2011) at acute (48 hours) and long-term (one month) survival times. The choice to focus on the hippocampus was based on the prevalence of hippocampal vulnerability following TBI and the lack of studies focused on structural alterations in neurons and glia following exposure to blasts in the absence of anesthetics.

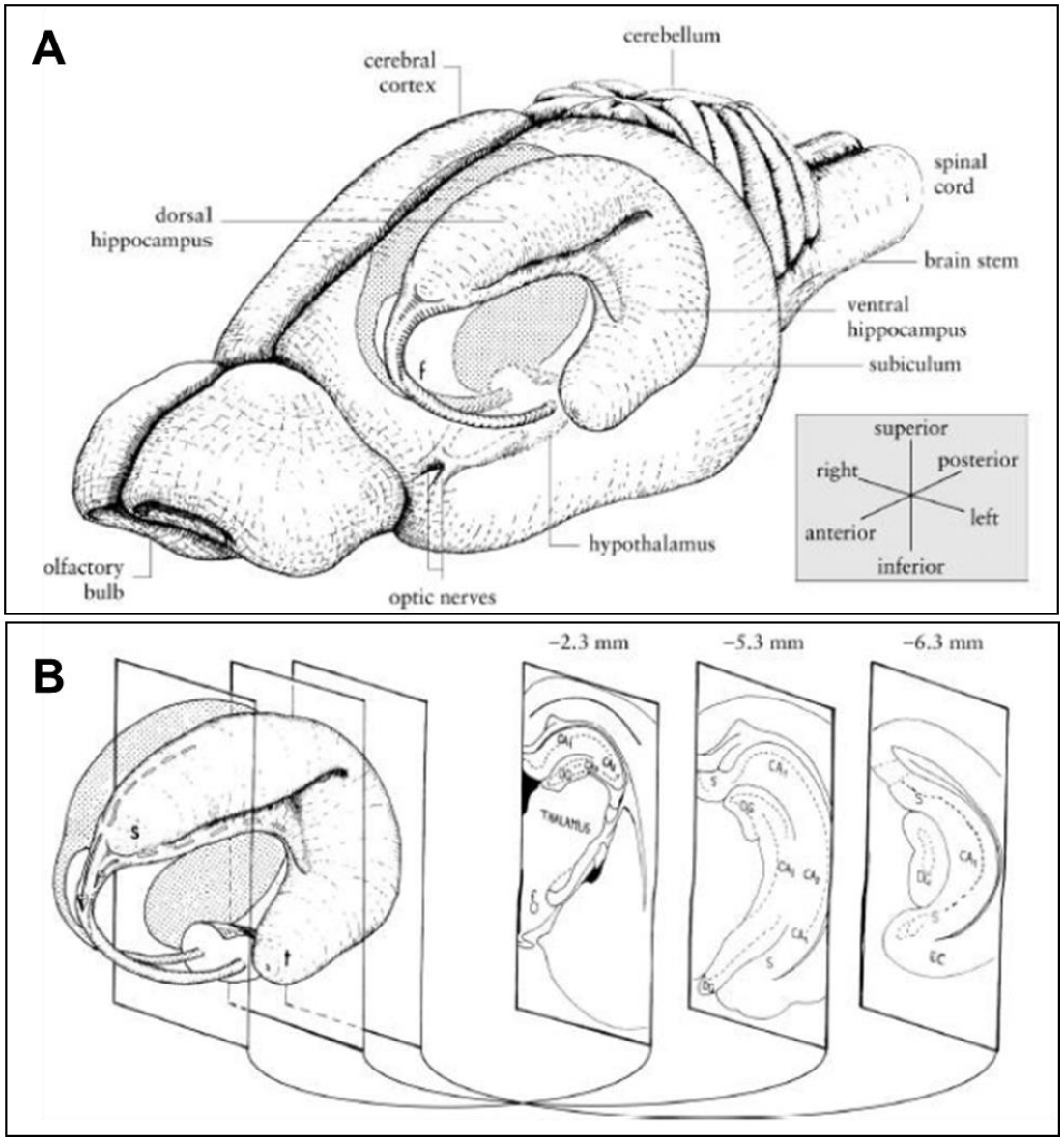


**Figure 2.1.** Rodent hippocampus. **(A)** General schematic of a rodent brain depicting the position of the hippocampus along its longitudinal dorsoventral axis relative to other brain regions. **(B)** Isolated hippocampi (left) and corresponding coronal sections (right). $CA_1$ = cornu ammonis 1. $CA_2$ = cornu ammonis 2. $CA_3$ = cornu ammonis 3. EC = entorhinal cortex. s=septal. S= subiculum. t=temporal. Schematic modified from Cheung et al., 2015.

## METHODS

### Blast Wave Measurements and Calibration

A precision dynamic high frequency piezoelectric pressure transducer (Model: 113B21 High Frequency ICP® pressure sensor, PCB Piezotronics, Inc., Depew, New York) was used to calibrate blast waves produced by the Cranium Only Blast Injury Apparatus (COBIA), (Figure 2.2A). The sensor was positioned where the head of the mouse would be inside the apparatus. A constant current supply (Model 5421, Columbia Research Laboratories, Inc., Woodlyn, PA) provided power to the transducer. Outputs were digitized using an analog to digital converter (Analog Devices, ADAS3022) before saving waveforms for offline analysis. The average blast overpressure was 1,034 kPa (Figure 2.2B).

### Blast procedure

All procedures were approved by the Institutional Animal Care and Use Committee at Boston University.

1. Adult C57BL/6 mice (2–6 months) were acclimated for 72 hours upon arrival to the Boston University animal facility where they were ear tagged while anesthetized with isofluorane. Mice were then acclimated for five days prior to experimentation to eliminate potential confounds from the presence of anesthesia.

2. The COBIA was used to generate blast overpressures as described and characterized previously (Kuehn et al., 2011). The central component of the COBIA was a .22 caliber, single-shot, powder-actuated tool (Ramset RS22; ITW Ramset, Glendale Heights, IL) modified by removing the piston that normally drove the fastener, causing it to function like a firearm allowing the blast wave to propagate un-dampened through the barrel. The tool was held vertically using a custom-fabricated stand, which also ensured its safe use. The blast was directed downwards into a blast dissipation chamber (BDC) that interfaced snugly with the muzzle of the tool (Figure 2.2A). The BDC was fabricated from polyvinyl chloride piping that directly delivered the blast overpressures onto the dorsal surface of the head. The blast wave was generated by firing a .22 caliber crimped brass cartridge (power hammer loads power level 4, yellow color coding, with 179 ± 5mg of smokeless powder).

All animals were weighed prior to experimental use. A mouse cylindrical restrainer (Stoelting Co. Wood Dale, IL) was used to immobilize the animals. Custom paper cones were fitted and wetted around the head to prevent potential quaternary damage from gunpowder during blasts. Once restrained, animals were inserted with the cranium positioned two (2) centimeters from the opening of the BDC. Blasts were directed between bregma and lambda. Sham animals represent mice treated identically to the blast exposed mice with the exception of exposure to injury.

As outlined in Figure 2.2C, the experimental timeline of this study centered

on evaluating neuronal and glial responses following acute (48 hours) and chronic (one month) exposures to a single blast and three blasts with 24 hour latencies.

**Tissue Preparation**

When the specified recovery time point was reached, mice were anesthetized with isofluorane (Butler Schein) prior to perfusion with heparinized saline (0.9% sodium chloride in distilled water) followed by 4% paraformaldehyde in 0.1 M phosphate buffer (PB, pH 7.4). Immediately after perfusion mice were decapitated, brains were harvested intact and immersed in 4% paraformaldehyde overnight at 4˚C.

After immersion fixation intact brains were cryoprotected in PB containing sucrose concentrations gradually increased from 5% to 30% overnight at 4˚C. Brains were dissected from bregma -0.94mm to -2.92mm using an adult mouse brain slicer matrix (BSMAS001-1, Zivic Instruments, Pittsburgh, PA). Serial coronal sections (40 µm) were obtained using a freezing sliding microtome (Reichert Jung) and stored in individual wells of a 96-well plate containing cryoprotectant (30% sucrose (Sigma), 30% ethylene glycol (Fisher), 1% polyvinylpyrrolidone (Sigma) in Tris-buffered saline pH 7.6 (0.4M Trizma HCl, Sigma, 0.01M Trizma base, Sigma, 0.15M Sodium Chloride, Fisher) at -20˚C prior to histology and immunostaining.

## Histology

To evaluate potential changes in cytoarchitecture, two coronal slices containing dorsal (bregma -1.46 to -1.70mm) and ventral (bregma -2.80 to -3.16mm) hippocampi were selected. Slices were matched according to Franklin and Paxinos, 2008. Sections were slide mounted, air-dried overnight and then defatted in chloroform:ethanol (1:1), rehydrated, and counterstained using 0.05% thionin (pH 4.8) to stain Nissl substance as previously described (Giannaris and Rosene, 2012).

## Immunocytochemistry

Three to five slices from each animal, spanning dorsal, bregma-1.46 to -1.70mm, (Franklin and Paxinos, 2008). Hippocampi were washed extensively in PB to remove residual cryoprotectant and then mounted and air-dried onto Colorfrost Plus subbed slides (ThermoFisher Scientific, Waltham, MA). Slices were rehydrated in PB and endogenous peroxidase was quenched using 3% hydrogen peroxide in PB before incubation in 5% normal donkey serum (Jackson ImmunoResearch Laboratory, Inc. West Grove, PA) diluted in PB-0.3% Triton X-100 (PBTx, Sigma) for one hour at room temperature. Following blocking, slices were incubated overnight at 4˚C in primary antisera directed against GFAP (GFAP 1:250, Clone No. N206 A/8, UC Davis/NIH NeuroMab Facility Cat# 75-240, RRID:AB_10672299) and Iba-1 (1:1000, Wako, Catalog No. 019-19741).

*Chromogenic detection*

After incubation in primary antisera slices were washed in PB and the appropriate biotinylated secondary antisera was applied (donkey anti-mouse (Jackson Immuno Research, Catalog No. 715-065-137) or donkey anti-rabbit (Jackson Immuno Research, catalog No. 711-065-152) both diluted to 1:500 in 0.3% PBTx) for one hour at room temperature. Following incubation in biotinylated secondary antisera, the tissues were incubated for 90 minutes in Neutravidin conjugated to horseradish peroxidase (diluted 1:250 in PBTx; ThermoFisher Scientific). Chromogenic detection was carried out using Metal-Enhanced 3'3'-diaminobenzidine (DAB) substrate (diluted 1:10 in stable peroxide buffer, Pierce Chemical Company, Rockford IL). DAB development was stopped by immersion in several changes of 0.1M PB. Slices were then rinsed in distilled water and coverslipped in Gelvatol (10% polyvinyl alcohol, Sigma; 20% glycerol, Sigma; 0.02% sodium azide, Fisher; 0.2M Tris, Amresco, pH 8.5).

*Fluorescence detection*

Following incubation in primary antisera, the sections were washed in PB and then incubated in the appropriate fluorescently conjugated secondary antisera (donkey anti-mouse Cy3 (Jackson Immuno Research, Catalog No. 715-165-150) or donkey anti-rabbit 647 (Jackson Immuno Research, Catalog No. 711-605-152), both

diluted to 1:500 in 0.3% PBTx) for two hours at room temperature. Slices were then coverslipped in Gelvatol and imaged within 24 hours.

During chromogenic and fluorescence immunostaining, some slices were stained without primary antisera to ensure antigen specificity. Slices not exposed to primary antisera were negative for immunoreactivity indicating that the signal observed was specific to the antigens probed. The specificity of these primary antisera in mice have been published previously (Jinno and Kosaka, 2002; Jinno et al., 2007).

**Imaging**

Fluorescently labeled hippocampal sections were imaged using the same laser and sensitivity settings on an Olympus BX61 spinning disk confocal (Olympus Corporation) using 10x and 40x water immersion, or a Nikon Eclipse motorized microscope (Nikon Instruments, Inc.) at 4x, 10x, and 20x.

**Analysis**

ImageJ software (U.S. National Institutes of Health, Bethesda, Maryland, USA) was used to analyze immunostained slices. CorelDraw (X6) was used to label and arrange images.

*Cell Counting*

Cells positive for calretinin and parvalbumin within cornu ammonis 1 ($CA_1$) and cornu ammonis 3 ($CA_3$) within a 20x field were manually counted in each hemisphere. Total cell counts were averaged by animal and then by condition.

*Densitometry*

To quantify potential differences in the density of neuronal process densitometry was performed. Signal intensities were matched across images. Fluorescent images were inverted such that signal appeared black. For calretinin immunostaining ROIs containing the inner molecular layer and granule cell layer were rotated to obtain vertical averages for each image using the plot profile feature in Image J (Figure 2.3 B). Grand averages were created from data obtained for each condition (sham versus blast). To assess parvalbumin positive immunoreactivity in the inner molecular layer of the dentate gyrus, ROIs containing processes only (Figure 2.4), were matched across images and the mean gray value was obtained. Values were averaged by animal and then by condition.

*Percent Area*

Four RGB (red, green, blue) multi-channel images within each ROI were obtained at 20x. All images were converted to single channel images. The channel with the

greatest signal to noise contrast (blue) was selected and used across all groups. All single channel (grayscale) images were made binary using a threshold overlay (Figure 2.5). The area fraction, defined as the percent coverage (percent area) of immunoreactivity within each ROI, was obtained for each binary image using the area fraction selection from the ImageJ "Measure" feature. It was hypothesized that hypertrophy due to glial activation would be reflected by a greater percent area. Values obtained for each ROI were averaged by animal and then by condition (sham versus blast).

*Semi-quantitation of Iba1 Phenotypes*

The total number of Iba-1 cells were categorized in based on three broad morphological groups: ramified, hypertrophic, and amoeboid (Karperien et al., 2013). Manual counts of Iba-1 positive cells were averaged for each animal and then averaged by group.

*Statistics*

An analysis of variance (ANOVA) with a Bonferroni *post hoc* correction was used (SPSS v24, IBM Corp.) to establish whether differences were present between sham and blast exposed mice ($p<0.05$).

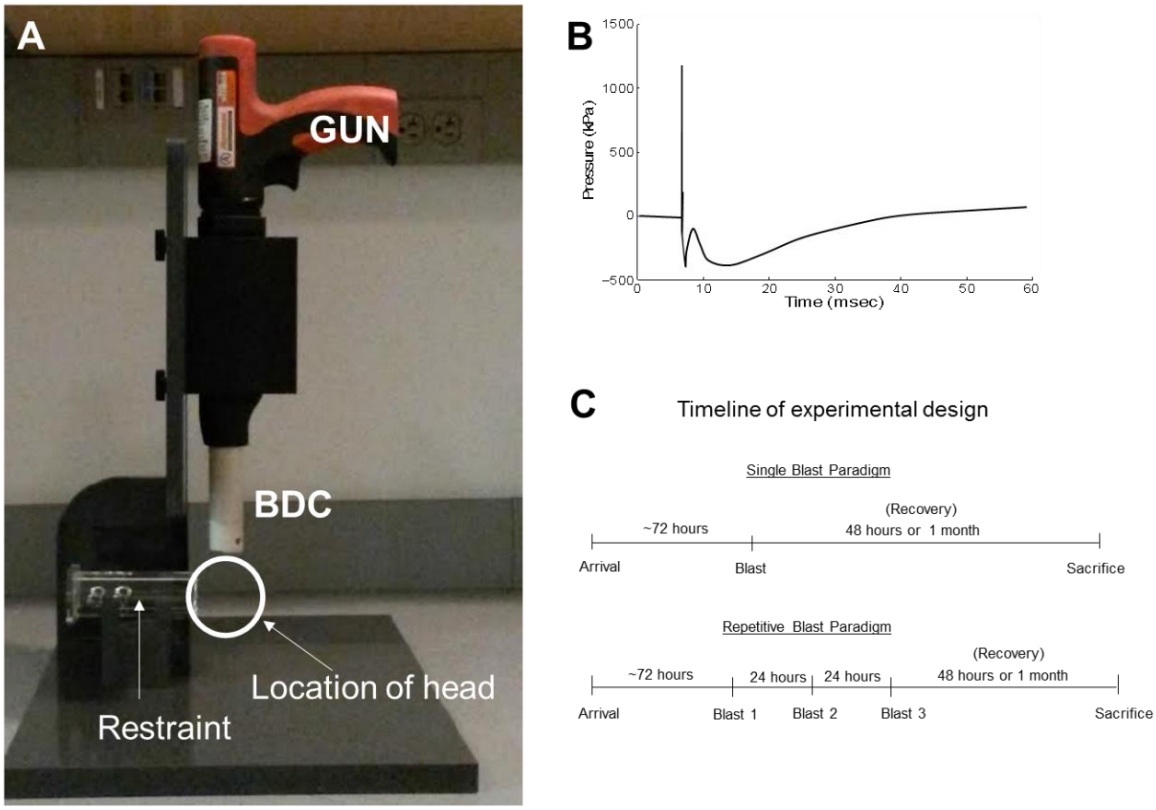


**Figure 2.2.** Experimental design. **(A)** The Cranium Only Blast Injury Apparatus (COBIA) used to generate blast overpressures. **(B)** Pressure waveform produced by the COBIA revealing average peak overpressure of 1,034 kPa. **(C)** Timeline of experimental paradigm. Animals were sacrificed after Blasts 1 (single blast paradigm) or Blast 3 (repetitive blast paradigm) following a 48 hour (acute) or one month (chronic) recovery. BDC = blast dissipation chamber.

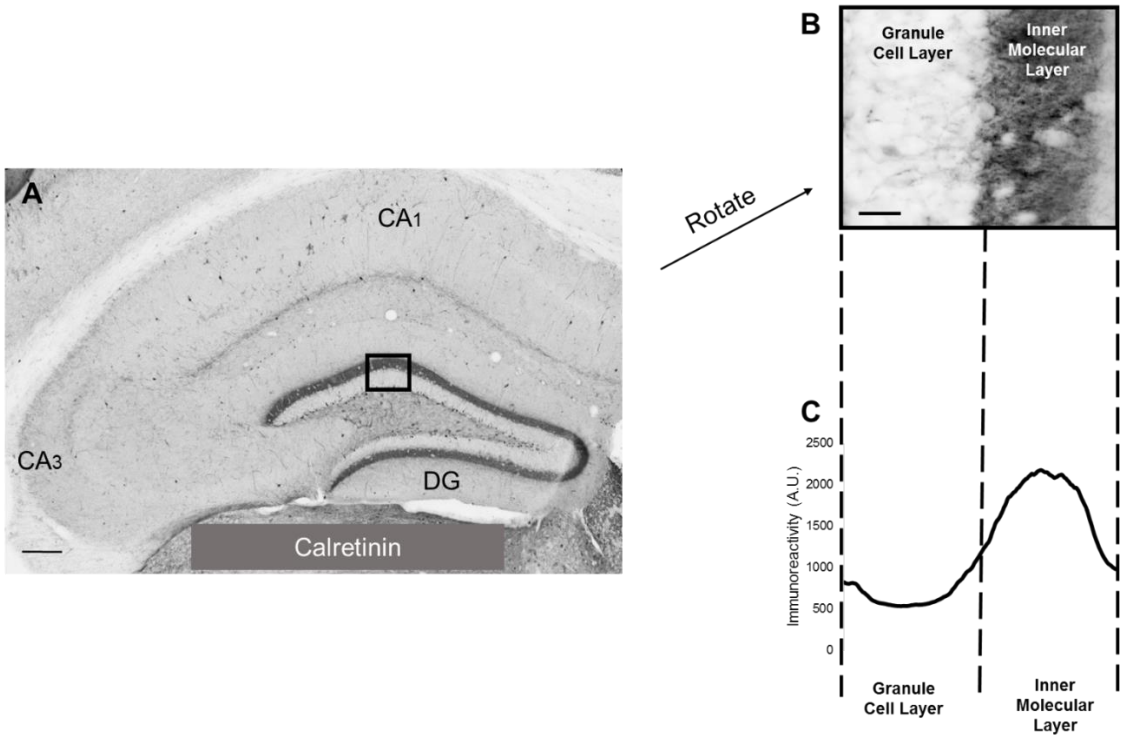


**Figure 2.3.** Calretinin immunoreactivity. **(A)** Representative low magnification image of calretinin immunostaining in the mouse hippocampus. The black box represents the sub-region sampled for vertical averaging, scale bar = 100 µm **(B)** Representative ROI from (A) rotated for vertical averaging of immunoreactivity, scale bar = 20µm **(C)** Vertical average of immunoreactivity detected in the granule cell layer and inner molecular delineated by vertical dashed lines. A.U. = arbitrary units. $CA_1$ = cornu ammonis 1. $CA_3$ = cornu ammonis 3. DG = dentate gyrus. ROI = region of interest.

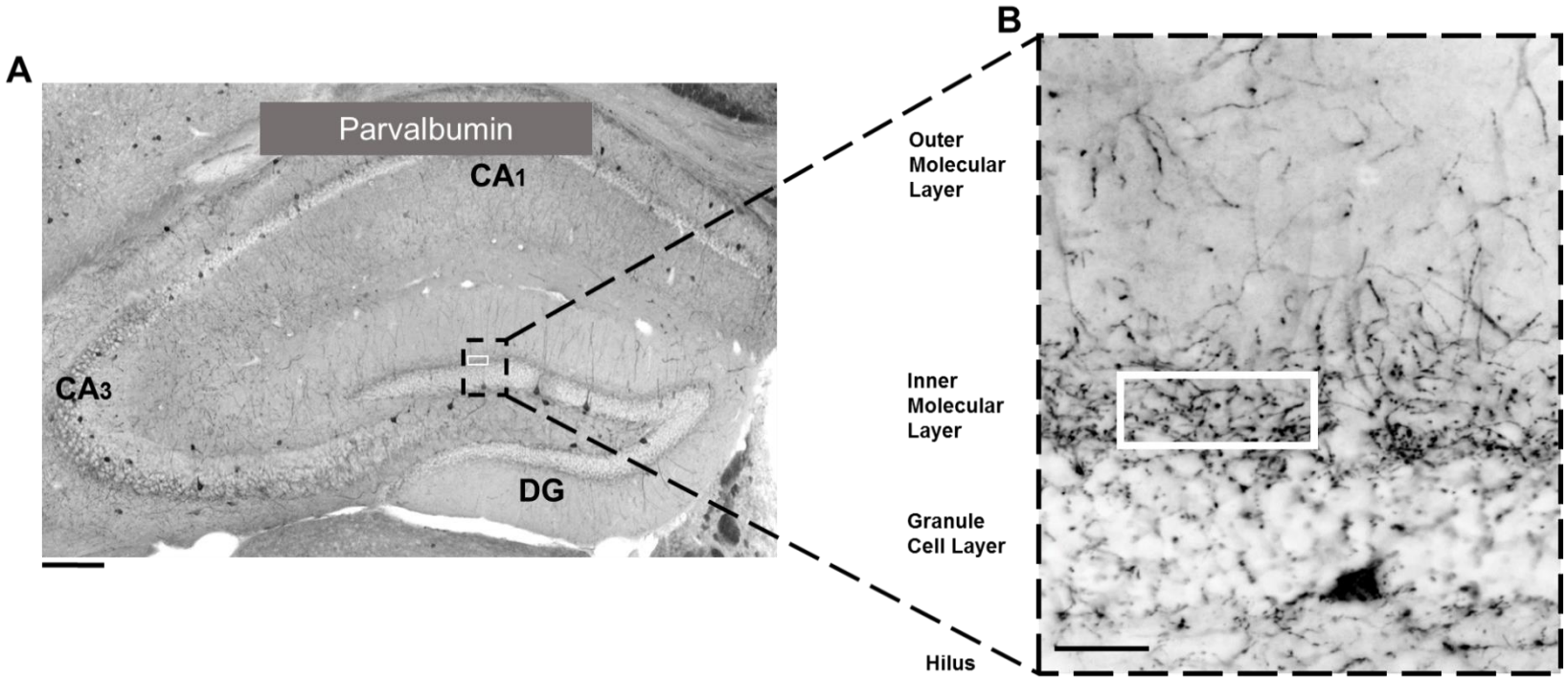


**Figure 2.4.** Parvalbumin immunoreactivity. **(A)** Representative low magnification image of parvalbumin immunostaining in the mouse hippocampus. Enclosure represents sub-region sampled for densitometry (white rectangle), scale bar = 100 µm. **(B)** Inset from (A) containing representative ROI (white rectangle) sampled, scale bar = 20µm. $CA_1$ = cornu ammonis 1. $CA_3$ = cornu ammonis 3. DG = dentate gyrus. ROI = region of interest.

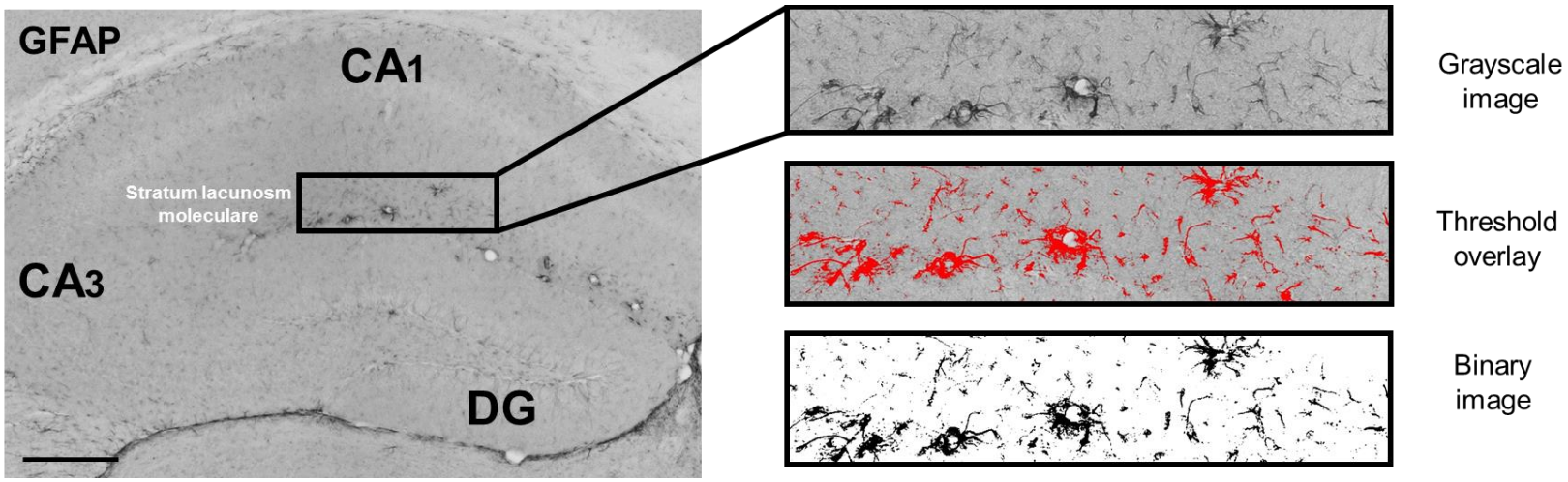


**Figure 2.5.** GFAP immunostaining. Grayscale image of GFAP immunostaining (left). Zoom of ROI analyzed (top right panel). Example threshold overlay (right middle panel) and resulting binary image (right bottom panel). $CA_1$ = cornu ammonis 1. $CA_3$ = cornu ammonis 3. DG = dentate gyrus. GFAP = glial fibrillary acidic protein. Scale bar = 250 µm. ROI = region of interest.

## RESULTS

### Hippocampal cytoarchitecture unaffected following blasts

A thionin stain was performed in order to determine if exposure to blast(s) affected cytoarchitecture. Hippocampi from sham and blast exposed mice were closely examined for gross differences in thionin staining. No apparent differences in the densities of cells or lamination of sub-fields were found. Lack of detectable differences in sham and blast exposed animals confirmed that acute and chronic recovery from a single blast as well as three consecutive blasts were insufficient to detectably alter cellular architecture (Figure 2.6).

### No significant difference in the average number of calretinin and parvalbumin positive neurons in $CA_1$ and $CA_3$ following exposure to blasts

The average number of calretinin and parvalbumin immunoreactive cells was not significantly affected following mild blasts. However, there were a number of noteworthy trends.

There was a slight increase in the average number of calretinin positive cells in $CA_1$ 48 hours following a single blast (Figure 2.7 B). Yet in $CA_3$ there was a noticeable decrease in calretinin positive cells 48 hours following 3 blasts relative to the pooled shams and the other post blast survivals (48 hours following single and repeated blasts and one month following three blasts) (Figure 2.8 B).

Interestingly, although the average number of parvalbumin positive cells in CA1 was the lowest one month following a single blast exposure, it most closely resembled the mean average of the pooled shams (Figure 2.9 B). Parvalbumin positive cells were noticeably reduced one month following a single blast in CA3 in comparison to the other recovery time points (48 hours following single and repeated blasts and one month following three blasts) as well as pooled shams (Figure 2.10 B).

The trends reported here indicate not only a differential effect that depends on the interneuronal cell type examined, but also the hippocampal sub-region and the recovery time point post blast (Figures 2.7 – 2.10).

**Densities of calretinin and parvalbumin positive processes in the inner molecular layer of the dentate gyrus unchanged following blasts**

Quantitative evaluation of immunostaining was used to determine whether exposure to blast affected synaptic processes within this region. The overlapping vertical averages of calretinin immunoreactivity in sham and blast exposed animals following a single insult (Figure 2.11 B, C) indicated that an isolated exposure did not significantly alter the density of calretinin positive processes. Although not as striking, the average density of parvalbumin positive processes one month following exposure to a single blast was slightly lower than sham (Figure 2.12, D).

It has not been established to what extent the observed increases or decreases are beneficial or detrimental. In the context of this study, there was no positive staining observed for markers implicated in cell death (caspase-3, FluoroJade C), therefore the functional implications of the trends reported remain unknown.

**Percent area of GFAP positive astrocytes significantly affected 48 hours following single and repeated exposure to blasts**

To evaluate whether structural differences in astrocytes were present, antisera against GFAP was used. Overall, GFAP labeled astrocytes were found throughout all hippocampal sub-regions with the lowest density in the pyramidal and granule cell layers matching published reports (Shimada et al., 1992; Jinno et al., 2007). The stratum lacunosm moleculare showed the strongest GFAP labeling of all hippocampal sub-regions (Figures 2.13 and 2.17) and was thus quantitatively compared between sham and blast exposed animals.

Acute recovery (48 hours) to a single blast (n=3) resulted in a significant increase in the average percent area of GFAP relative to pooled shams (Figure 2.13). In contrast, one month following exposure to a single blast a decrease was observed relative to pooled shams. Acute recovery to three consecutive blasts (n=3) showed a significant reduction in average percent area, similar to the blast exposed animals that recovered for one month after a single blast. However, one

month following three blasts (n=4) there was a slight increase compared to sham (Figure 2.13).

**Hypertrophic microglia present acutely following blast**

Iba1 was used to label and classify microglia based on established criteria (Jinno et al., 2007). There were significantly more hypertrophic Iba1 positive cells following acute recovery (48 hours) to single and repeated blasts (Figures 2.14–2.17). The amount of hypertrophic cells was restricted to the outer molecular layer of the dentate gyrus (Figure 2.16). No hypertrophic cells were detected one month following either a single or repeated blast (Figure 2.15). Furthermore, no differences were found in the average number of Iba1 positive cells across all recovery time points examined (data not included). The morphological differences in Iba1 positive cells present in sham versus blast exposed animals suggest that the microglia present locally, particularly following acute recovery where hypertrophic phenotypes were observed, were likely responding to the effect of blast within the microenvironment rather than migration of microglia.

As discussed in Chapter 1, Iba1 positive cells can assume a broad spectrum of morphologies from the dynamic ramified to the phagocytic amoeboid (Figure 1.4), although subtle and widely varied intermediate morphologies are prevalent (Karperien et al., 2013). Variations in morphology are contextual, based on signals present in the microenvironment. In an effort to identify potential factors

influencing Iba1 positive cells, immunocytochemistry was used to label several mediators such as tumor necrosis factor alpha, interleukin-1, and interleukin-6, however staining results were negative for all mediators probed (data not included).

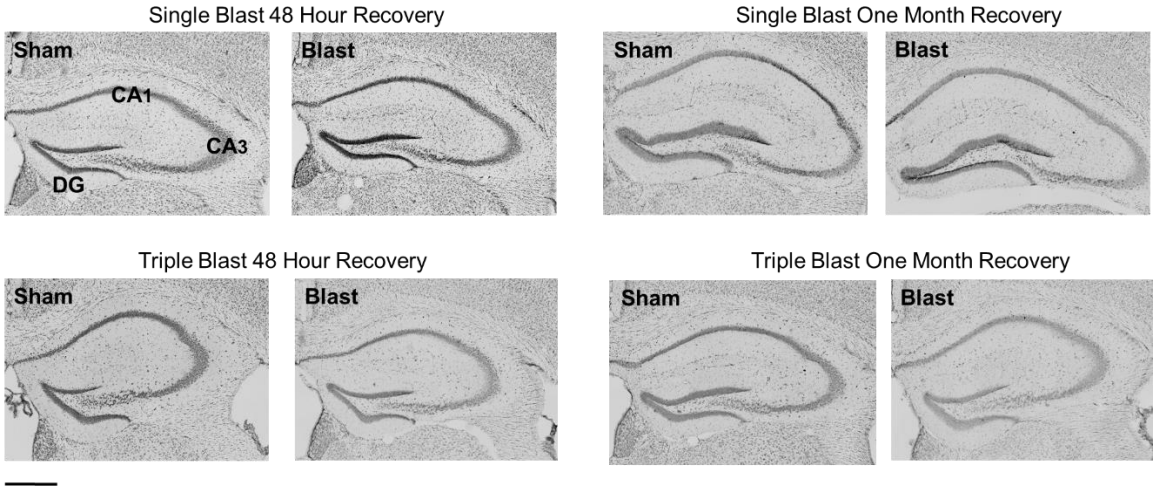


**Figure 2.6.** Cytoarchitecture unaffected following acute and chronic recovery to a single or repeated blast(s). Low magnification of thionin staining in the hippocampus in sham and blast animals. $CA_1$ = cornu ammonis 1. $CA_3$ = cornu ammonis 3. DG = dentate gyrus. Scale bar = 200 µm.

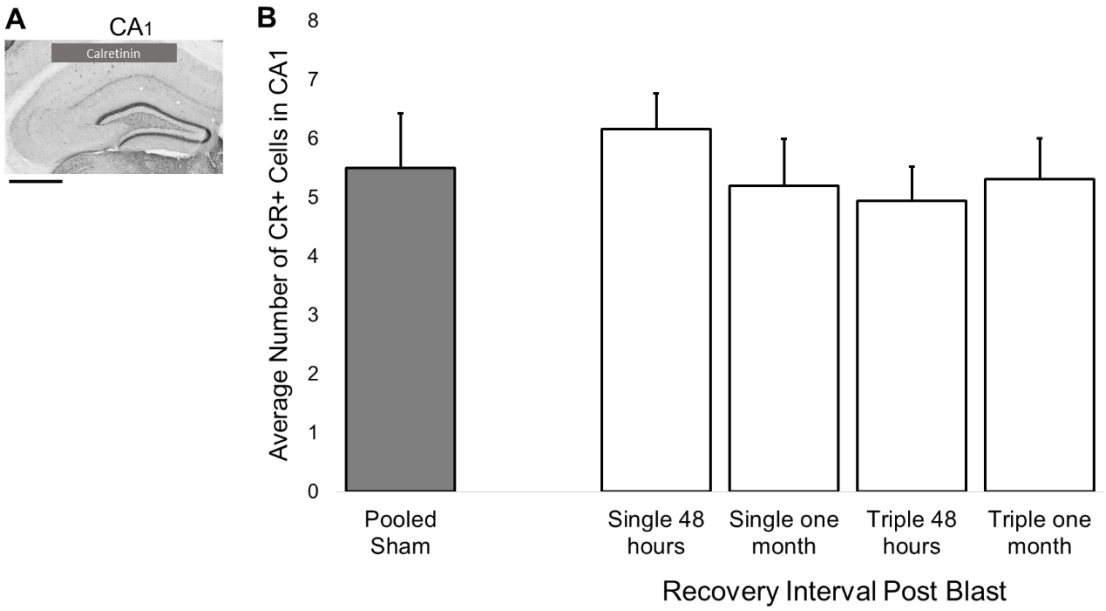


**Figure 2.7.** Average cell count of calretinin positive cells in CA1 unchanged following blast. **(A)** Representative calretinin immunostaining, scale bar = 500 µm. **(B)** Blast exposed animals (n=3 for single 48 hours, single one month, triple 48 hours; n=4 for triple one month) compared to pooled averages from sham animals (n=10) showed no significant difference in the average number of calretinin positive cells following blast. Error bars represent SD. CA1 = cornu ammonis 1. CR = calretinin.

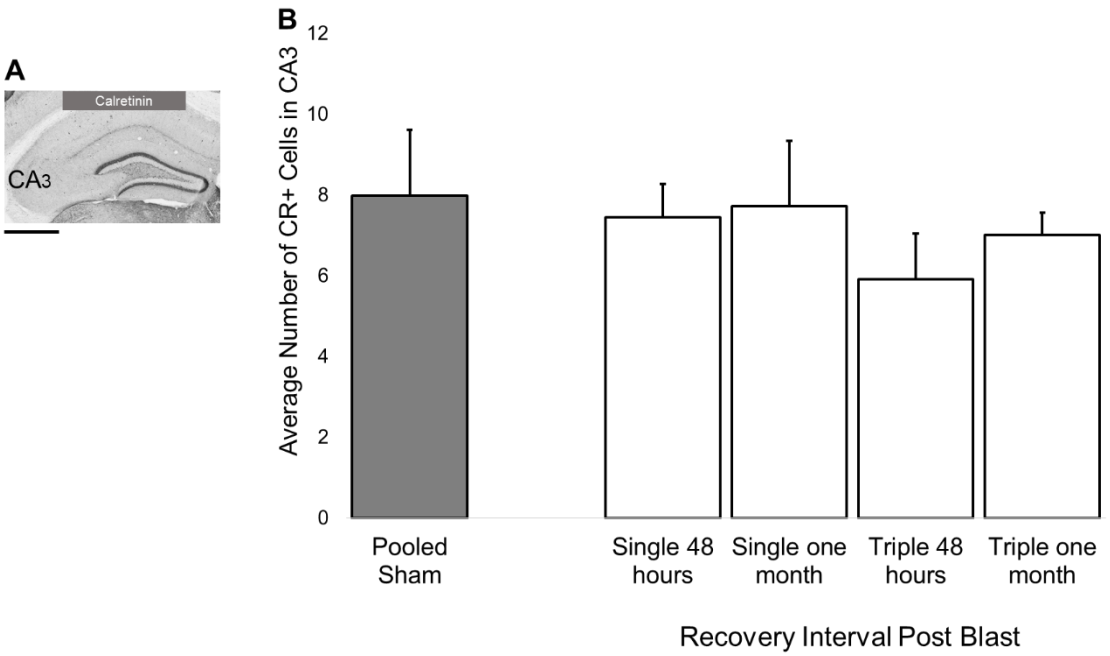


**Figure 2.8.** Average cell count of calretinin positive cells in CA3 unchanged following blast. **(A)** Representative calretinin immunostaining, scale bar = 500 µm. **(B)** Blast exposed animals (n=3 for single 48 hours, single one month, triple 48 hours; n=4 for triple one month) compared to pooled averages from sham animals (n=10) showed no significant difference in the average number of calretinin positive cells following blast. Error bars represent SD. CA3 = cornu ammonis 3. CR = calretinin.

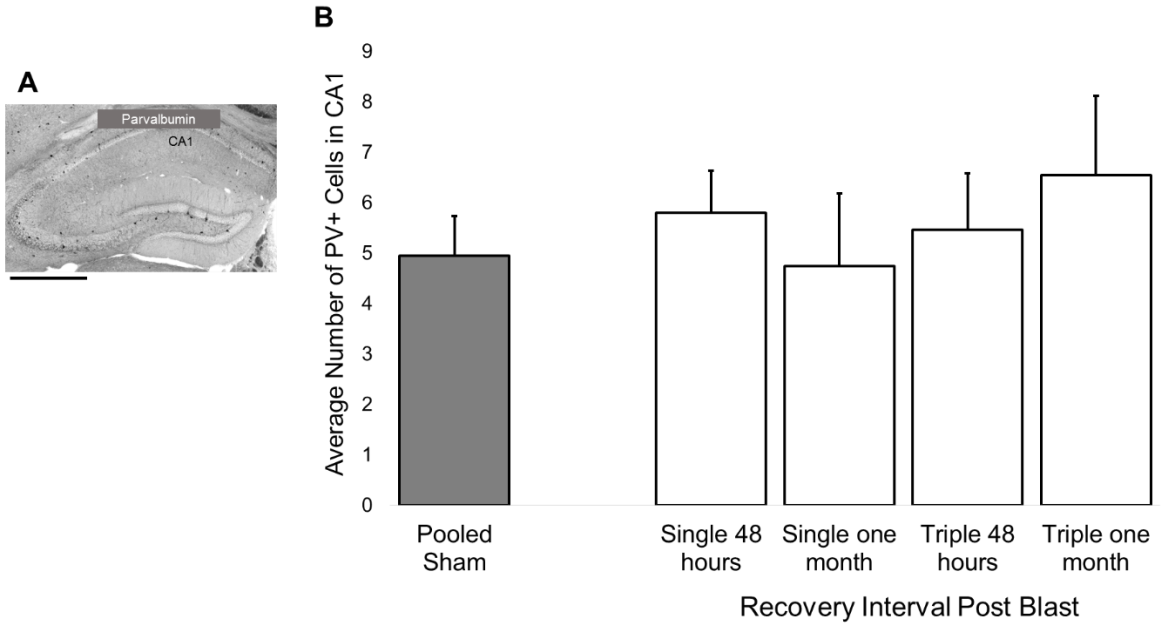


**Figure 2.9.** Average cell count of parvalbumin positive cells in $CA_1$ unchanged following blast **(A)** Representative parvalbumin immunostaining, scale bar = 500 µm. **(B)** Blast exposed animals (n=3 for single 48 hours, single one month, triple 48 hours; n=4 for triple one month) compared to pooled averages from sham animals (n=10) showed no significant difference in the average number of parvalbumin positive cells following blast. Error bars represent SD. $CA_1$ = cornu ammonis 1. PV = parvalbumin.

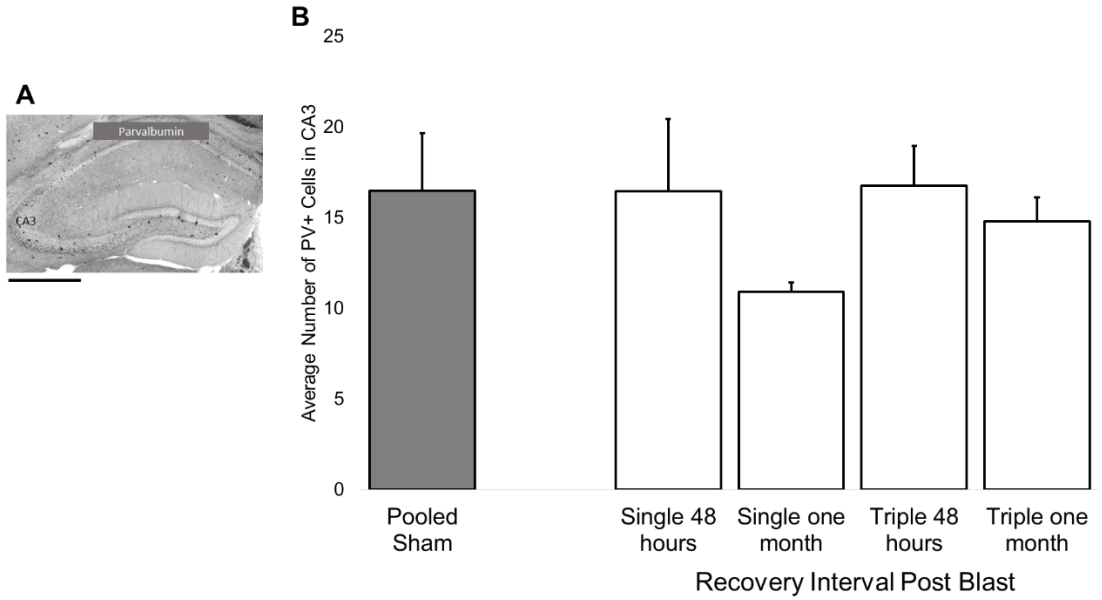


**Figure 2.10.** Average cell count of parvalbumin positive cells in CA3 unchanged following blast **(A)** Representative parvalbumin immunostaining, scale bar = 500 µm. **(B)** Blast exposed animals (n=3 for single 48 hours, single one month, triple 48 hours; n=4 for triple one month) compared to pooled averages from sham animals (n=10) showed no significant difference in the average number of parvalbumin positive cells following blast. Error bars represent SD. CA3 = cornu ammonis 3. PV = parvalbumin.

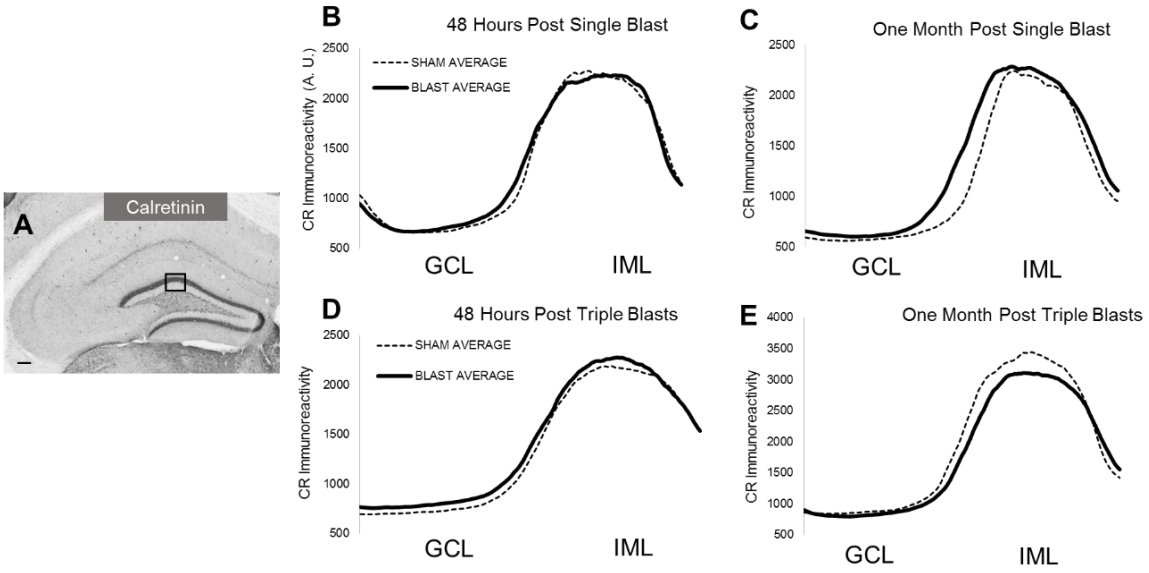


**Figure 2.11.** Density of calretinin positive processes in the inner molecular layer of the dentate gyrus remain unchanged following blast. **(A)** Representative CR positive immunostaining in the hippocampus, scale bar = 100 µm. Black box represents the ROI containing the GCL and IML. Vertical averages of CR positive processes in the IML shows no significant difference 48 hours following a single blast (sham n=2; blast n=3) **(B)**, one month following a single blast (sham n=2; blast n=3) **(C)**, and 48 hours (sham n=4; blast n=4) and one month (sham n=2; blast n=4) following triple blasts (**D** and **E**, respectively). A. U. = arbitrary units. CR = calretinin. GCL = granule cell layer. IML = inner molecular layer.

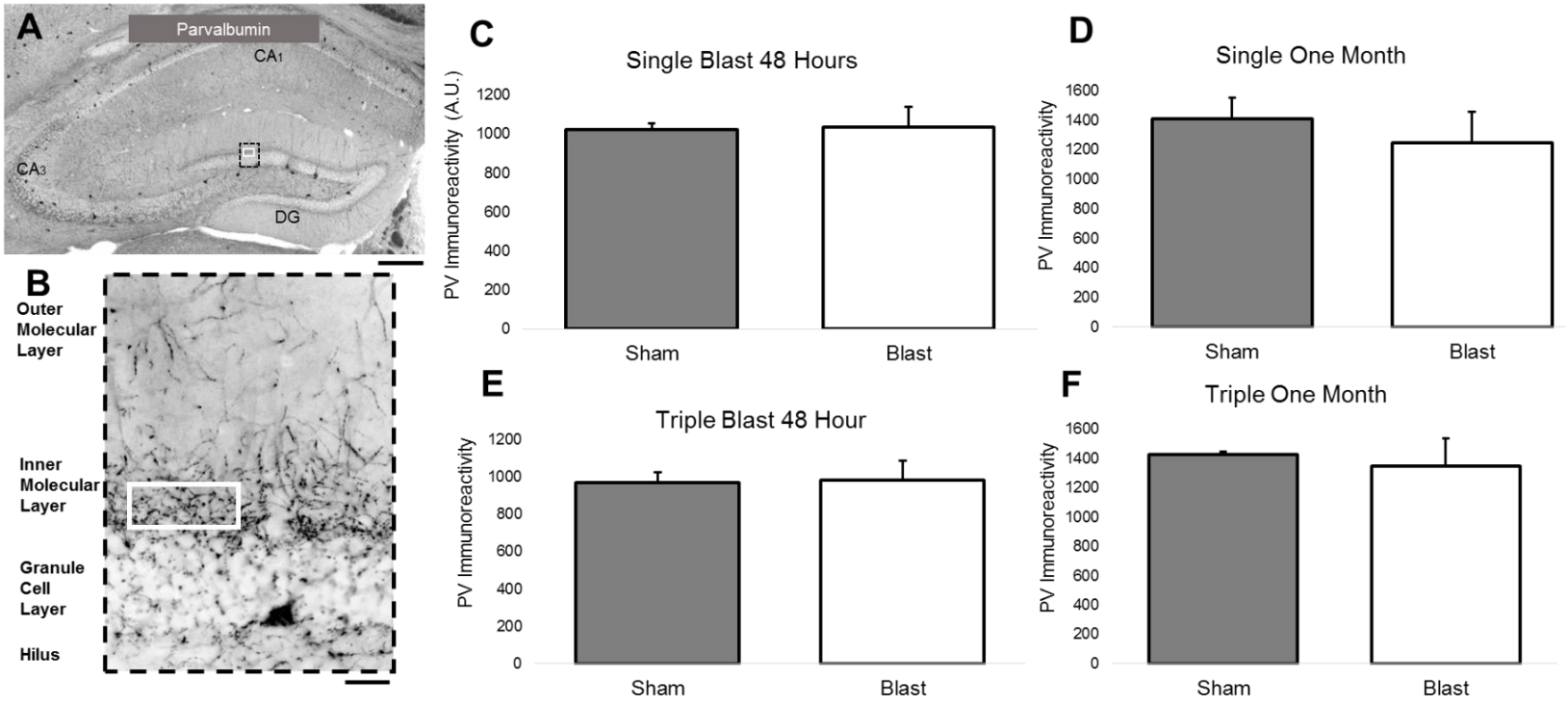


**Figure 2.12. (A)** Representative parvalbumin immunostaining in the hippocampus, scale bar = 100 µm. Dashed black box indicates the general region of hippocampus analyzed. **(B)** Zoom of the dashed black box in (A). White rectangle represents an example ROI sampled within the IML, scale bar = 20 µm. Density of PV positive processes did not differ significantly 48 hours following a single blast (sham n=2; blast n=3) **(C)**, one month following a single blast (sham n=2; blast n=3) **(D)**, and 48 hours (sham n=4; blast n=4) and one month (sham n=2; blast n=4) following triple blasts (**E** and **F**, respectively). Error bars (C-F) represent SEM. A. U. = arbitrary units. $CA_1$ = cornu ammonis 1. $CA_3$ = cornu ammonis 3. IML = inner molecular layer. PV = parvalbumin. ROI = region of interest. SEM = standard error of the mean.

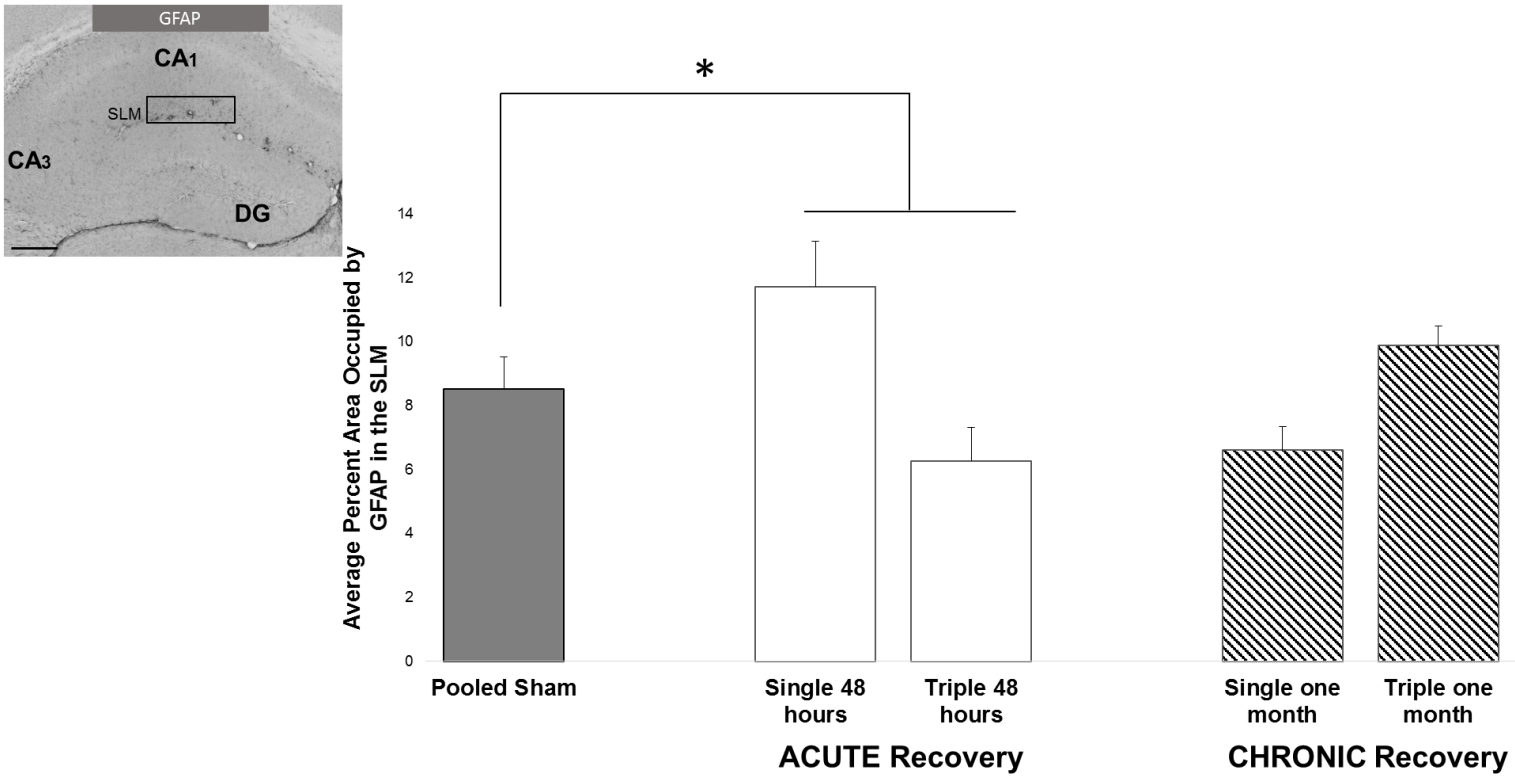


**Figure 2.13.** The percent area occupied by GFAP in the stratum lacunosum moleculare is significantly altered relative to sham acutely following blast. **(A)** Low magnification image of GFAP positive staining in the hippocampus, scale bar = 250µm. **(B)** Relative to pooled shams, a significant increase in the percent area occupied by GFAP was present 48 hours following exposure to a single blast (n=3) that decreased one month (n=3) and was significantly reduced 48 hours following three blasts (n=3) and increased one month after three blasts (n=4). Error bars represent SD. $CA_1$ = cornu ammonis 1. $CA_3$ = cornu ammonis 3. DG = dentate gyrus. GFAP = glial fibrillary acidic protein. SLM = stratum lacunosm moleculare.

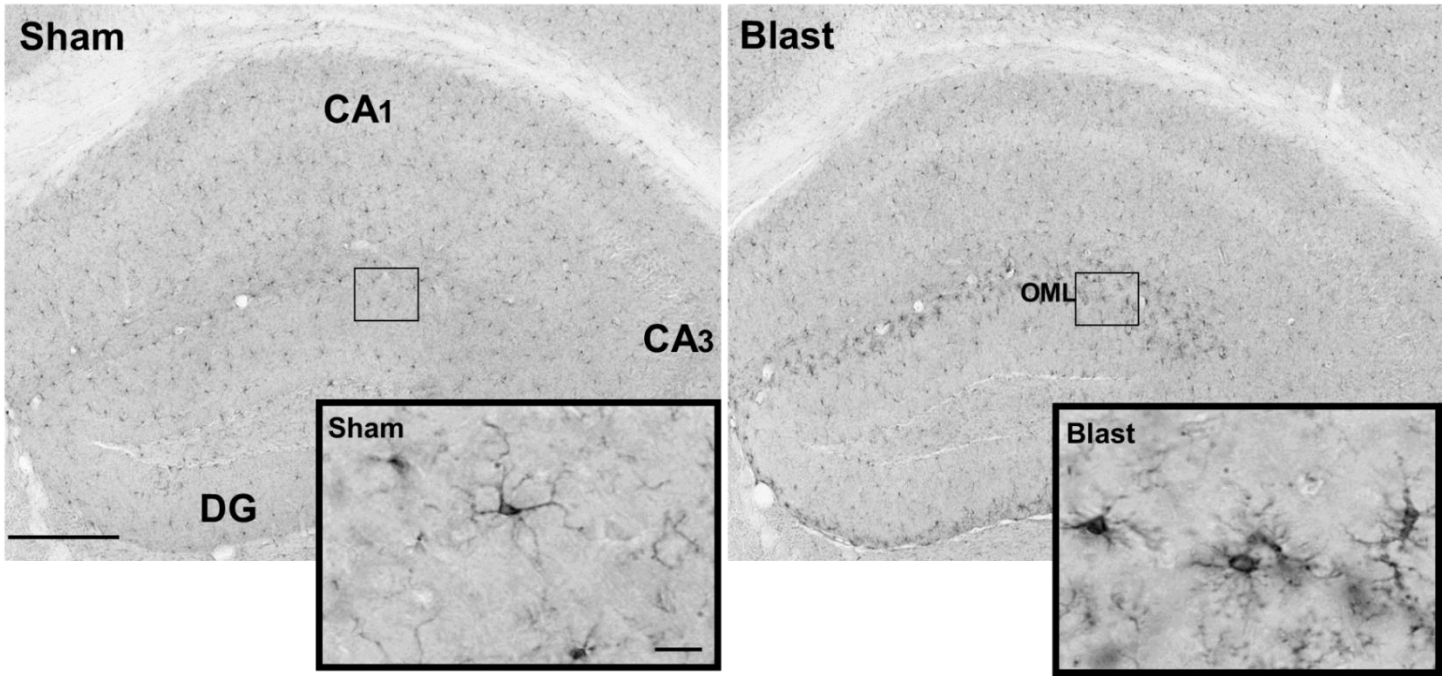


**Figure 2.14.** Hypertrophic microglia were restricted to the outer molecular layer of the dentate gyrus 48 hours following exposure to a single blast. Low magnification of Iba-1 immunostaining in a representative sham (left), scale bar = 250 µm. Inset reveals a ramified cell with thin, ramified processes, scale bar = 20 µm. In contrast, a low magnification image from a representative blast exposed animal (right) shows hypertrophic microglia limited to the OML. Inset reveals striking hypertrophic morphology of Iba-1 labeled cells. $CA_1$ = cornu ammonis 1. $CA_3$ = cornu ammonis 3. DG = dentate gyrus. Iba-1 = ionized calcium binding adapter molecule-1. OML = outer molecular layer.

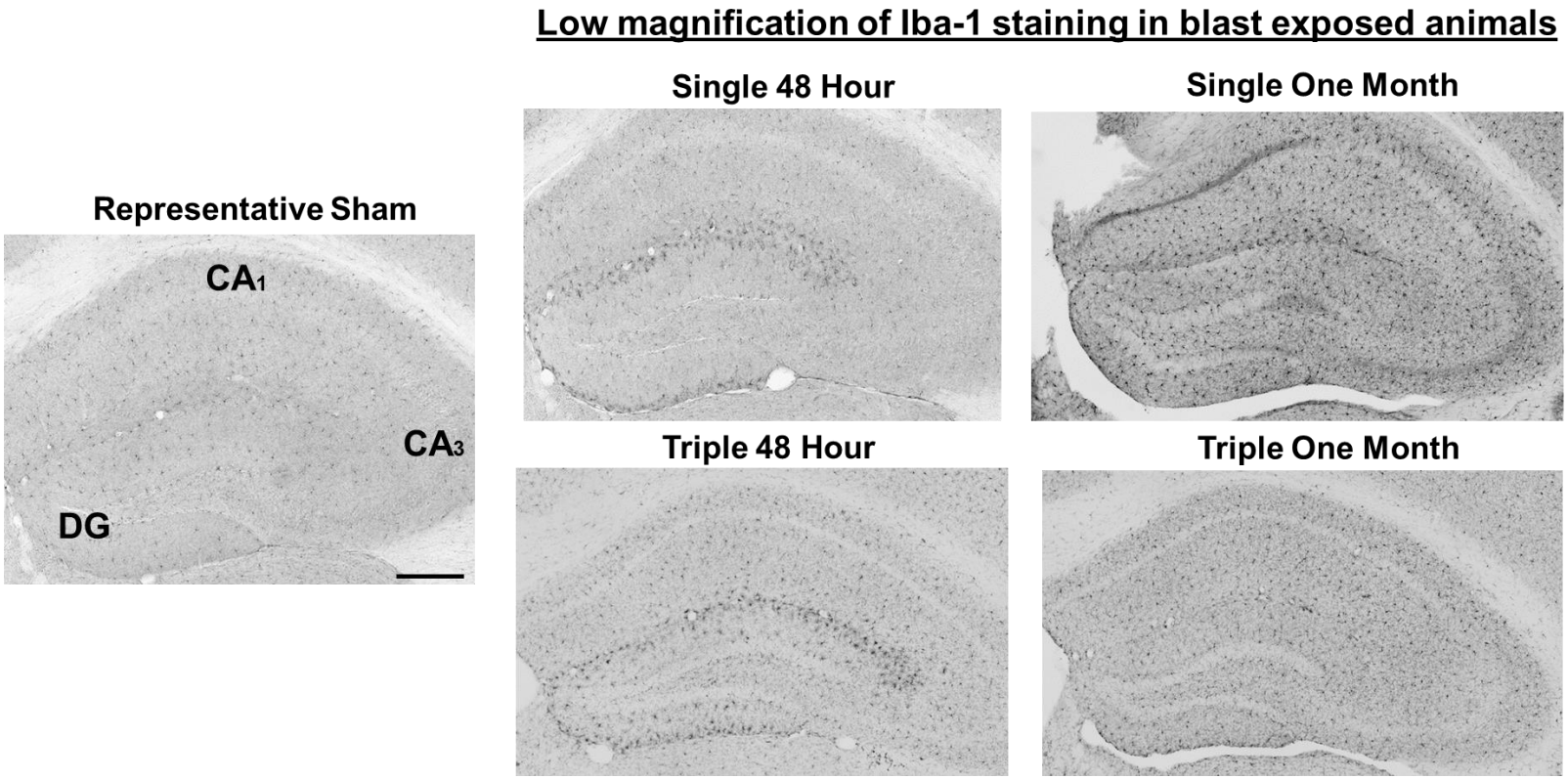


**Figure 2.15.** Hypertrophic microglia are restricted to the outer molecular layer of the dentate gyrus acutely following mild blast(s). $CA_1$ = cornu ammonis 1. $CA_3$ = cornu ammonis 3. DG = dentate gyrus. Iba-1 = ionized calcium binding adapter molecule-1. Scale bar = 250 µm.

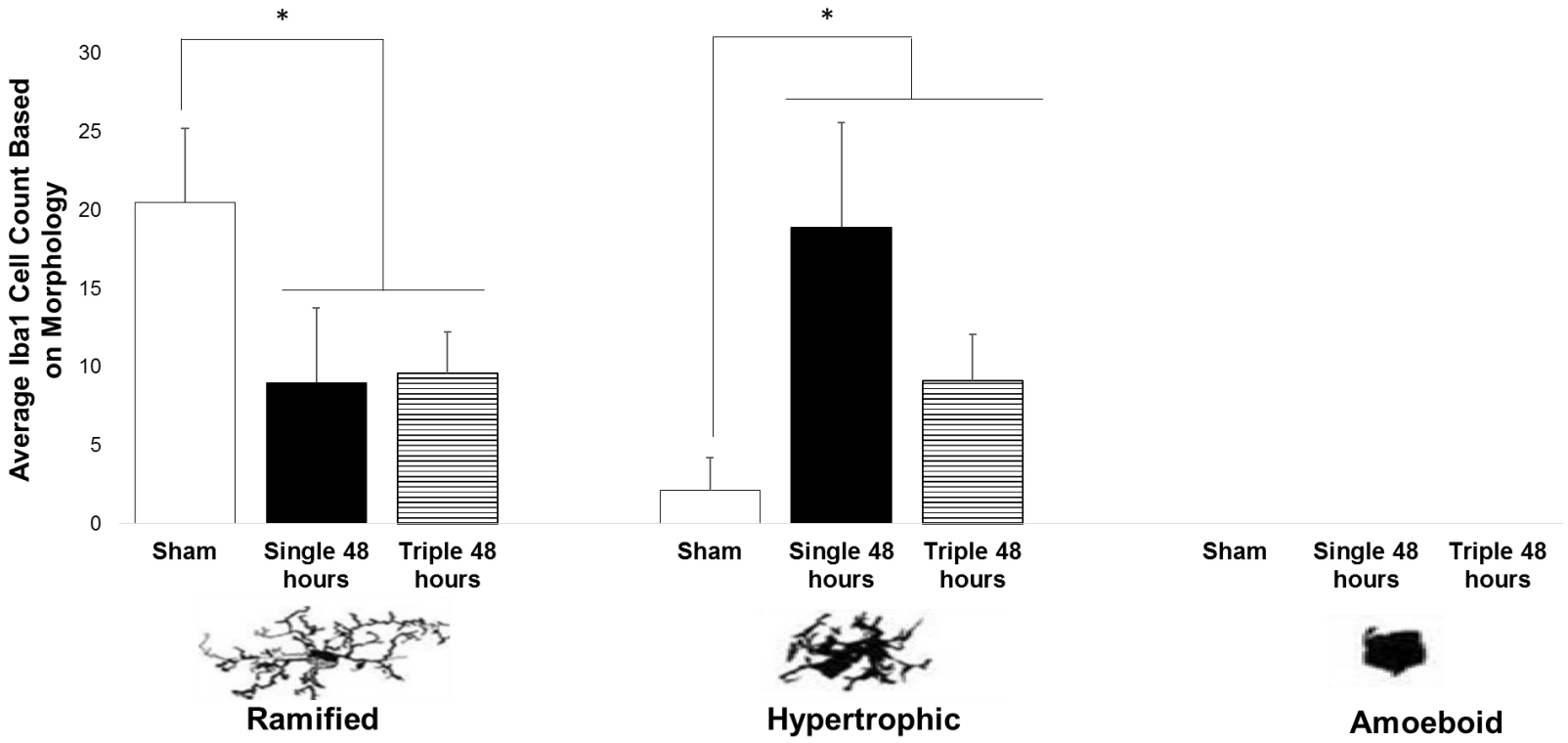


**Figure 2.16.** Significantly more hypertrophic microglia present in the outer molecular of the dentate gyrus 48 hours following blast(s) relative to sham. Average count of Iba-1 positive cells based on morphology (sham, n=5; single 48 hours blast n=3 triple 48 hours n = 4). Asterisks denote statistical significance between sham and both blast groups ($p<0.05$). Error bars represent SD. Schematics of microglia morphologies modified from Karperien et al., 2013. Iba-1 = ionized calcium binding adapter molecule-1.

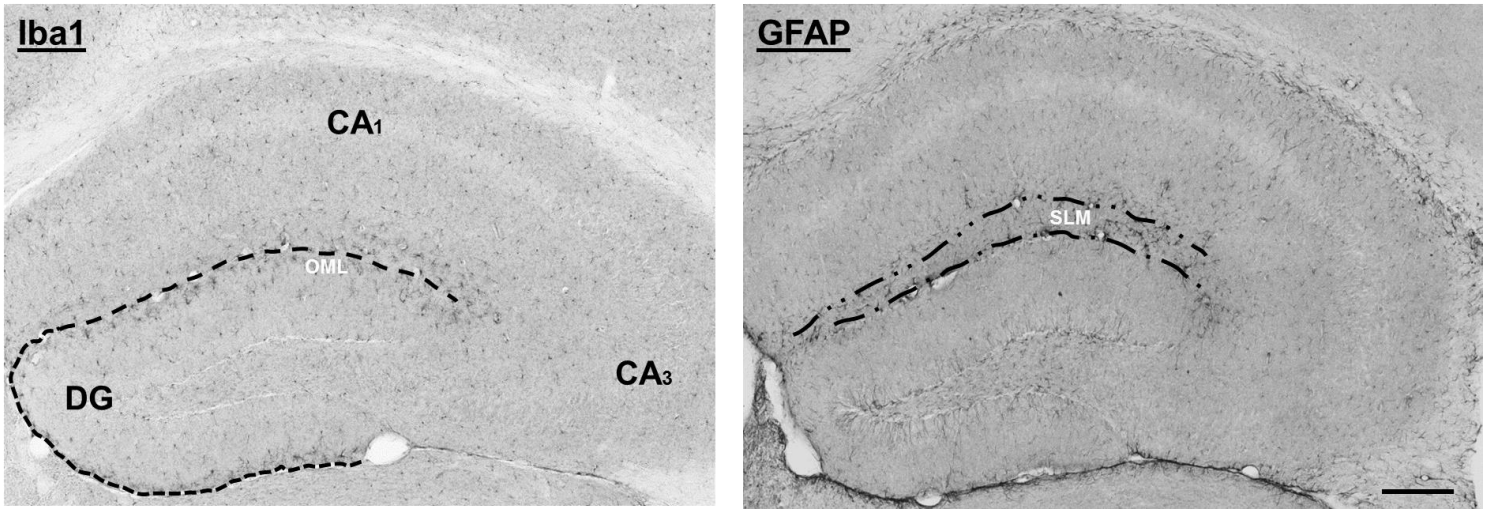


**Figure 2.17.** Mouse model of mild direct cranial blast reveals a region specific glial response in the hippocampus following acute recovery. Representative low magnification images of the mouse hippocampus. (Left) Dashed lines around the dentate gyrus delineate the outer molecular layer where hypertrophic microglia labeled with Iba-1 are prevalent. (Right) The region enclosed by dashed lines delineate the stratum lacunosm moleculare, where the GFAP immunoreactivity is strongest. $CA_1$ = cornu ammonis 1. $CA_3$ = cornu ammonis 3. DG = dentate gyrus. GFAP = glial fibrillary acidic protein. Iba-1 = ionized calcium binding adapter molecule-1. OML = outer molecular layer. SLM = stratum lacunosm moleculare. Scale bar = 250 µm.

## DISCUSSION

The first goal of this study was to evaluate whether exposure to single or repeated blasts altered two non-overlapping populations of interneurons containing calretinin or parvalbumin. The second objective was to identify the presence and extent of any activation of astrocytes and microglia within the hippocampus. The studies were performed following acute (48 hours) and chronic (one month) recovery from a single blast or three repetitive blasts spaced 24 hours apart in the absence of anesthetics.

A major limitation of this work is that immunocytochemistry can only convey static information regarding dynamic cellular processes. Because of this, it cannot be known if the interneurons examined were reversibly altered between the time points examined. This is an important limitation to be aware of because the localization of calcium-binding proteins can reversibly change spatially and temporally (Johansen et al., 1990). The non-stereological approach used for cell counting limits the rigor of the results obtained, although there are quantitative studies (Lawson et al., 1990; Savchenko et al., 2000) published without the use of stereological assessments. In spite of the aforementioned disadvantages, what can be concluded from the immunocytochemical evaluations presented here is a general overview regarding structural alterations following mild blast overpressures, a model that is not routinely used despite its clinical relevance.

**Immunocytochemical status of calretinin and parvalbumin following blast**

Hippocampal interneurons can be divided into three categories—perisomatic, dendritic, interneuronal—as defined, in part, by the spatial organization of their synaptic outputs (Somogyi and Klausberger, 2005; Toth and Magloczky, 2014). Calretinin positive neurons are reported to synapse onto the dendrites of other interneurons in addition to principle cell somata in the rat hippocampus (Gulyas et al., 1996). Parvalbumin has been reported to synapse perisomatically onto principle cells (Caliskan et al., 2016). The presence of calretinin and parvalbumin throughout each hippocampal sub-field allows inferences to be made regarding the effect of blast on these distinct interneuron populations.

In spite of the aforementioned limitations, the results of this study are similar to reports documenting histochemical changes in the expression of other calcium-binding proteins. One study evaluating short-term changes in parvalbumin immunoreactivity following cerebral ischemia in hippocampi of rats revealed a delayed decrease that was reversible, despite lack of detectable changes two days following insult (Johansen et al., 1990). It was hypothesized that reduced parvalbumin immunoreactivity could be the result of reduced synthesis, increased degradation, as well as changes in the amount of calcium ions present in the cytoplasm.

Selective sparing of interneurons containing calcium-binding proteins following injury have been reported previously, however spared cell populations

have been shown to exhibit morphologies indicative of degeneration in human cases of epilepsy (Toth and Magloczky, 2014). Although the morphological features of parvalbumin and calretinin positive neurons were not assessed in detail, in general there were no obvious differences in blast versus sham. However, the slight differences in the density of dendritic arborizations suggest some differences in the intracellular localization of the antigens or anatomical alterations within the arborizations.

Overall there are certain inconsistencies in the literature regarding the status of calretinin and parvalbumin. For example, one group reported greater vulnerability of perisomatic versus dendritic interneurons following TBI (Huusko et al., 2015), while another group found dendritic interneurons containing the neuropeptides somatostatin and neuropeptide-Y to be highly vulnerable (Toth et al., 2010). These differences may be due, in part, to the dynamic nature of cellular responses and the species under evaluation. Additional factors to consider include differences in time points examined and experimental design as several of the previously discussed studies focused on epilepsy (Toth and Magloczky, 2014), cerebral ischemia (Johansen et al., 1990), and focal TBI resulting from FPI (Huusko et al., 2015).

**Status of astrocytes and microglia following blast exposure**

The complex relationship between astrocytes and microglia in the hippocampus has been the focus of several studies (Savchenko et al., 2000; Jinno et al., 2007; Pascual et al., 2012). Results of this study demonstrated significant differences in the percent areas of GFAP in the stratum lacunosum moleculare and in Iba1 in the outer molecular layer of the dentate gyrus.

GFAP percent coverage in the stratum lacunosum moleculare showed a significantly acute increase 48 hours after one blast. However, a dramatic decrease at one month following one blast was also present 48 hours following three blasts. The combination of blasts directed between bregma and lambda and full head mobility could underlie the changes reported in the GFAP immunoreactivity in the stratum lacunosum moleculare. There are also several physiological explanations to account for the differences the percent area, three of which will be highlighted.

The first plausible explanation relates to the inputs and outputs to the stratum lacunosum moleculare. Direct input to the dendrites of pyramidal cells within the stratum moleculare is from glutamatergic cells in layer 3 of the entorhinal cortex (Maccaferri, 2011) with additional thalamic input from the nucleus reuniens (Andersen, 2007). Previously, increases in GFAP within the stratum lacunosum moleculare have been documented in an animal model of epilepsy (Dalby et al., 1995). Increased GFAP immunoreactivity was attributed to the previously reported

increased neuronal activity (Steward et al., 1991). Thus the changes observed in GFAP at the blast time points, relative to control, in this study could result from cellular changes due to blast in distal regions such as the entorhinal cortex.

The stratum lacunosm moleculare also contains a high density of blood vessels and has been reported to possess a high energy metabolism (Shimada et al., 1992). Astrocytes have a significant role in maintaining vascular networks that supply neurons with glucose from the bloodstream (Lund-Andersen, 1979; Pardridge, 1983). In this study, the GFAP immunoreactivity was intensely associated with vasculature (Figure 2.5). Thus the second, and perhaps more probable, explanation pertains to the effect of blast on vasculature. It is not unreasonable that the mild blasts in this study affected the integrity of the vessels and/or the astrocytes within this region. A number of TBI and related studies have documented the link between astrocytic changes, vascular alterations, oxidative changes, and inflammation (Ogundele et al., 2014; Karve et al., 2016). The increase in percent area of astrocytes observed 48 hours after a single blast was expected and can be readily confirmed by studies reporting elevations in GFAP immunoreactivity following injury. One study examined blood brain barrier integrity hours (2–6 hours) and days (1–7) following controlled cortical impact (Baskaya et al., 1997). Results showed a biphasic response to injury with an increase in membrane permeability 24 hours following injury and then again 3 days later (Baskaya et al., 1997) similar to a previously reported increase following ischemic insult (Hatashita and Hoff, 1990). As it relates to blast-induced injury, one study

found evidence of cerebrovascular inflammation and oxidative stress 6 to 24 hours following exposure to single and repeated blasts (Abdul-Muneer et al., 2013).

Third, given the nature of the detection method it is possible there was a loss of immunoreactivity due to altered antigenicity. The decreases observed one month following a single blast and 48 hours following three blasts were initially unexpected. However, review of the literature does show evidence to support a decrease in GFAP immunoreactivity following injury. One study examining the effect of lateral fluid percussion injury reported a significant loss of GFAP 30 minutes following injury that remained progressive up to 24 hours (Zhao et al., 2003). It was hypothesized that diminished immunoreactivity was due to dismemberment of intermediate filaments present in astrocytes due to alterations in protein function. Another study attributed diminished GFAP labeled astrocytes to an increase in fibroblast growth factor signaling (Kang and Song, 2010). While the structural variation in GFAP following acute (48 hour) and chronic (one month) recovery to the blast paradigm in this study are of interest and have been supported in the literature, the interpretation from this work is limited because the molecular identity of the glial phenotypes are unknown. As indicated in Chapter 1, astrocytes have a role in neurotrophic and cytotoxic responses. The heterogeneity of astrocytic responses following insults has motivated the use of multiple assays to fully characterize molecular changes in glia (Anderson et al., 2014) and would be of great benefit in the present study.

Similar to astrocytes, microglia are commonly documented in pathological conditions however, their role is also not a simple dichotomy. Under a variety of conditions microglia can undergo subtle or dramatic changes in morphology (Karve et al., 2016). As discussed in Chapter 1, microglia can infer beneficial neuroprotective effects (M2 microglia) or promote injury cascades (M1 microglia). It is unclear whether the structural changes observed at the 48-hour time point in this study are beneficial or detrimental. It could be that the hypertrophic cells in the outer molecular layer represent a lesion of microglia that is a newly formed scar or presence of a resolving lesion. Regardless, the spatially restricted hypertrophic phenotype in the outer molecular layer of the dentate gyrus suggests that this region could be susceptible to blast-related insults.

In animal models of TBI, hypertrophic microglia are either diffuse throughout the hippocampus, or diffuse within a specific sub-field. Interestingly, a mouse model of Alzheimer's disease documented amyloid beta pathology that was restricted to the outer molecular layer of the dentate gyrus in transgenic mice (Schenk et al., 1999). However, no hypothesis to account for the regional susceptibility to pathology was provided. Indication of a similarly striking spatially restricted glial response was lacking. In spite of this, based on established reports of microglial dynamics (Schwartz et al., 2006; Karperien et al., 2013; Karve et al., 2016), it is highly unlikely that the observed hypertrophy is spurious. What is most probable is the detection of a region specific microglial response that may be transient. The outer molecular layer of the dentate gyrus receives inputs from the

entorhinal cortex (Forster et al., 2006). Thus, similar to the unique differences in GFAP immunoreactivity, the neuronal activity within this specific hippocampal sub-region, the complexities of microglial interactions with adjacent neurons and glia could contribute to the observed phenotypes. Use of assays to identify changes in levels of relevant ions/neurotransmitters or gene expression, which are more sensitive than the histological method employed here, could provide greater insight regarding subtle changes following exposure to mild blasts. The benefit in a more detail characterization of the functional phenotypes (cytotoxic M1 versus reparative M2) would aid insight into the cellular response within the hippocampus to mild blast and, potentially, how such changes compare with other models of TBI.

# CHAPTER 3

Immunocytochemical examination of glial morphologies following exposures to mild repetitive blasts in the mouse brain and retina

## ABSTRACT

As an accessible part of the central nervous system (CNS), the retina has become an integral focus in evaluating visual pathologies following blast injury. Recognition of the retina's potential to extrapolate central damage is due, in part, to the similarities in brain and retinal pathology following other CNS insults. The goal of this study was to evaluate whether glial morphologies in the retina were similar to central visual pathways (lateral geniculate nucleus, superior colliculus, and visual cortex) in a mouse model of mild repetitive blast injury. The time points examined were 48 hours and one month following multiple blasts. Results demonstrated no morphological alterations in astrocytes or microglia following exposures. The absence of structural alterations in glia at the time points examined could be attributed to the rapid and reversible properties of glia. Additional efforts to identify potential functional alterations, in absence of anatomical changes, are warranted.

# INTRODUCTION

## Vertebrate visual system

Despite its peripheral location, the retina originates from the developing diencephalon and is thus part of the central nervous system. The capture of light by photosensitive cells within the retina is the first stage of visual processing. The retina is stratified by the somata of the photoreceptors (rods and cones), bipolar cells, horizontal cells, amacrine cells, ganglion cells and the plexiform layers containing the synaptic contacts of each cell type (Hoon et al., 2014). In addition to retinal neurons there are three glial cell types in the retina, Müller cells, astrocytes, and microglia. Müller cells span the width of the retina and guide neuronal development. In addition, Müller cells provide structural support (Vecino et al., 2016). Astrocytes extend end feet that help form the blood retinal barrier and are prevalent within the inner retina, most commonly associated with ganglion cell axons (Seoane et al., 1999). Microglia are dynamic sentinel cells scattered throughout the retinal layers that continuously survey the microenvironment and phagocytose debris (Karlstetter et al., 2015; Horstmann et al., 2016).

Ganglion cell axons form the major output from the retina to central brain regions responsible for higher order visual processing (London et al., 2013). Although the retina projects to over 30 different brain regions (Morin and Studholme, 2014), the dorsal lateral geniculate nucleus, superior colliculus, and

visual cortex are the most widely documented central regions involved in visual processing and were the regions evaluated in this study.

The dorsal lateral geniculate nucleus (DLG) is the main thalamic relay in mammals for visual information from the retina. Approximately 70–80% of neurons within the DLG process input from retinal ganglion cells before projecting information to regions responsible for behaviors such as pupil dilation and reflexive eye movements (Huberman and Niell, 2011; Leist et al., 2016). The primary visual cortex is an essential cortical region that receives direct input from the DLG before projecting to visual association areas responsible for the perception and recognition of complex visual features such as motion and depth (Huberman and Niell, 2011).

In addition to the DLG, the superior colliculus (SC) is another major recipient of information from retinal ganglion cells. The SC is a mammalian midbrain region that is the equivalent of the optic tectum in non-mammalian vertebrates (Kandel, 2013). The SC is recognized for its essential role in regulating head and eye movement in response to visual stimuli (Byun et al., 2016), although it is also implicated in an array of species-specific behaviors such as limb direction toward targets and threat perception (May, 2006). Although the SC is highly laminated it is often simply divided into superficial and intermediate layers based on structural and functional distinctions (Ghose et al., 2014; Byun et al., 2016). The superficial layers receive direct visual input from the retina and are believed to have a significant role that is exclusive to visual integration (Langer and Lund, 1974). By

contrast, deeper layers are associated with integration of several sensory and motor systems (Sparks and Hartwich-Young, 1989).

**Visual system pathology following blast**

Blast injuries can impair vision at different stages of the afferent visual pathway from the retina to higher visual centers in the brain, or even the efferent pathways (Cockerham et al., 2009). While ocular trauma in the form of ruptured globes and penetrating injuries have been documented, less overt eye injuries may pose an increasing cause for concern because visual impairments in the absence of physical injury to the eye have also been reported (Lemke et al., 2013). Such impairments include problems with accommodation, saccades and pursuits, vergence, integrity of the visual field, and photophobia (Kapoor and Ciuffreda, 2002; Suh et al., 2006; Goodrich et al., 2007; Stelmack et al., 2009; Alvarez et al., 2012; Bulson et al., 2012; Capo-Aponte et al., 2012; Cockerham et al., 2013; Walsh et al., 2015) which suggests that visual system pathology has contributions from the brain, as well as the eye.

Reports of similar brain and retinal pathology following blast injury have motivated efforts to examine the utility of the retina as a surrogate for central damage. Ganglion cell damage in rodents following blast is similar to that seen in humans, indicating that the rodent visual system can provide information that may eventually be useful diagnostically and therapeutically (Wang et al., 2014). A

widely cited animal study conducted by Petras et al. (1997) compared brain and retina pathology following a range of sub-lethal blast overpressures delivered perpendicularly to the side of rats using a shock tube. In accordance with other animal studies supporting similar pathologies in the brain and retina following blast, axonal degeneration in the optic nerve, superior colliculus, diencephalon and thalamus mirrored retinal injuries (Petras et al., 1997; Mohan et al., 2013; Bricker-Anthony et al., 2014; Dutca et al., 2014). Similarly, work from Koliatsos et al. (2011) that comprehensively documented pathology in the retina and brain of mice following blast exposure found axonal degeneration in retinal ganglion cells (RGCs) and axonal tracts in brain including the optic and corticospinal tracts.

**Study objectives**

Although fiber degeneration receives considerable attention, due to the extensive projections from the retina to thalamus, midbrain and cortex, less is known about the status of glia throughout the visual pathway following blast. Therefore the goals of this study were to immunocytochemically identify whether gliosis was present in the retina, DLG, SC, and visual cortex (Figure 3.1) following exposure to mild repetitive blasts.

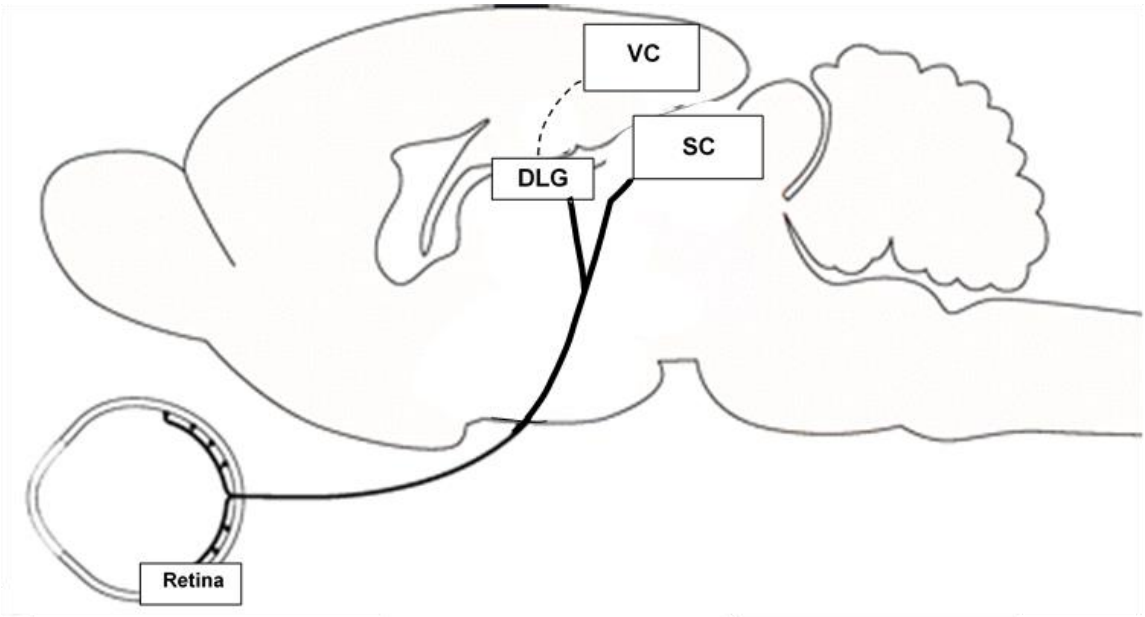


**Figure 3.1.** General schematic of the rodent visual pathway from retina to selected brain regions involved in visual processing. DLG = dorsal lateral geniculate SC = superior colliculus VC = visual cortex. Schematic modified from Do and Yau, 2010.

## METHODS

### Blast Wave Measurements and Calibration

A precision dynamic high frequency piezoelectric pressure transducer (Model: 113B21 High Frequency ICP® pressure sensor, PCB Piezotronics, Inc., Depew, New York) was used to calibrate blast waves produced by the Cranium Only Blast Injury Apparatus (COBIA), (Figure 3.2A). The sensor was positioned where the head of the mouse would be inside the apparatus. A constant current supply (Model 5421, Columbia Research Laboratories, Inc., Woodlyn, PA) provided power to the transducer. Outputs were digitized using an analog to digital converter (Analog Devices, ADAS3022) before saving waveforms for offline analysis. The average blast overpressure was 1,034 kPa (Figure 3.2B).

### Blast procedure

All procedures were approved by the Institutional Animal Care and Use Committee at Boston University.

1. Adult C57BL/6 mice (2–6 months) were acclimated for 72 hours upon arrival to the Boston University animal facility where they were ear tagged while anesthetized with isofluorane. Mice were then acclimated for five days prior to experimentation in order to eliminate potential confounds from the presence of anesthesia.

2. The COBIA was used to generate blast overpressures as described and characterized previously (Kuehn et al., 2011). The central component of the COBIA was a .22 caliber, single-shot, powder-actuated tool (Ramset RS22; ITW Ramset, Glendale Heights, IL) modified by removing the piston that normally drove the fastener, causing it to function like a firearm allowing the blast wave to propagate un-dampened through the barrel. The tool was held vertically using a custom-fabricated stand, which also ensured its safe use. The blast was directed downwards into a blast dissipation chamber (BDC) that interfaced snugly with the muzzle of the tool (Figure 3.2A). The BDC was fabricated from polyvinyl chloride piping that directly delivered the blast overpressures onto the dorsal surface of the head. The blast wave was generated by firing a .22 caliber crimped brass cartridge (power hammer loads power level 4, yellow color coding, with 179 ± 5mg of smokeless powder).

All animals were weighed prior to experimental use. A mouse cylindrical restrainer (Stoelting Co. Wood Dale, IL) was used to immobilize animals. Custom paper cones were fitted and wetted around the head to prevent potential quaternary damage from gunpowder during blasts. Once restrained, animals were inserted with the cranium positioned two centimeters from the opening of the BDC. Blasts were directed between bregma and lambda. Sham animals represent mice treated identically to the blast exposed mice with the exception of exposure to blast.

Glial responses were evaluated 48 hours and one month following exposure to three consecutive blasts spaced 24 hours apart (Figure 3.2C).

**Tissue Preparation**

Following recovery from repeated blasts, mice were deeply anesthetized with isofluorane (Butler Schein) prior to perfusion with heparinized saline (0.9% sodium chloride in distilled water) followed by 4% paraformaldehyde in 0.1 M phosphate buffer (PB, pH 7.4). Immediately after perfusion the mice were decapitated, their brains were harvested intact, and eyecups were created from each enucleated eye by cutting along the corneo-sclera divide to allow removal of the cornea, lens, and vitreous. All tissues were immersed in 4% paraformaldehyde in PB overnight at 4˚C.

After immersion fixation the eyecups and intact brains were cryoprotected in PB containing sucrose concentrations gradually increased from 5% to 30% overnight at 4˚C. Brains were dissected from bregma -0.94mm to -2.92mm using an adult mouse brain slicer matrix (BSMAS001-1, Zivic Instruments, Pittsburgh, PA). Serial coronal sections (40 µm) were obtained using a freezing sliding microtome (Reichert Jung). All cryoprotected tissues were stored at -20˚C in cryoprotectant (30% sucrose (Sigma S0389), 30% ethylene glycol (Fisher BP230-1), 1% polyvinylpyrrolidone (BP431-500) in Tris-buffered saline pH 7.6 (0.4M

Trizma HCl, Sigma T-3253, 0.01M Trizma base, Sigma T-1503, 0.15M Sodium Chloride, Fisher BP358-212) prior to immunostaining.

## Immunocytochemistry

### *Retinal Wholemounts*

Eyecups were washed with several changes of PB for one week to remove residual cryoprotectant. To thoroughly document glial morphology retinal wholemounts were created based on modifications to previously published protocols (Claybon and Bishop, 2011; Ivanova et al., 2013; Tual-Chalot et al., 2013). In short, retinas were isolated intact following four perpendicular cuts from the peripheral retina half-way toward the optic nerve head. Wholemounts were washed in PB for two days prior to quenching of endogenous peroxidase (3% hydrogen peroxide in PB) free floating on a rotator for 30 minutes at room temperature. Non-specific labeling was blocked using 5% normal donkey serum (Jackson ImmunoResearch Laboratory, Inc. West Grove, PA) diluted in 0.5% Triton-X 100 in PB (PBTx, Sigma) overnight at 4°C on rotator. Following blocking, the wholemounts were individually incubated in either mouse anti-glial fibrillary acidic protein (GFAP 1:250, Clone No. N206 A/8, UC Davis/NIH NeuroMab Facility Cat# 75-240, RRID:AB_10672299) or rabbit anti-Iba1 (1:1000, Wako, Catalog No. 019-19741), for 72 hours at 4°C on a rotator.

*Brain Slices*

Brain slices (bregma -3.08 to -3.40mm) containing the dorsal lateral geniculate nucleus, visual cortex, and the superior colliculus (Figure 3.3) were selected (Franklin and Paxinos, 2008). Free floating sections were washed extensively in PB to remove residual cryoprotectant and then mounted and air-dried onto Colorfrost Plus subbed slides (ThermoFisher Scientific, Waltham, MA). Following rehydration in PB the slices were incubated in 95°C sodium citrate buffer (10mM sodium citrate, 0.05% Tween 20, pH 6.0) for twenty minutes. Following antigen retrieval slices were allowed to cool to room temperature and washed several times in PB. Endogenous peroxidase was quenched using 3% hydrogen peroxide before incubation in 5% normal donkey serum (Jackson ImmunoResearch Laboratory, Inc. West Grove, PA) diluted in 0.3% PBTx for one hour at room temperature. Following blocking, slices were incubated overnight at 4˚C in primary antisera directed against either GFAP (GFAP 1:250, Clone No. N206 A/8, UC Davis/NIH NeuroMab Facility Cat# 75-240, RRID:AB_10672299) or Iba-1 (1:1000, Wako, Catalog No. 019-19741).

The specificity of these antisera in mice has been previously demonstrated (Ramirez et al., 2010; Karlstetter et al., 2015). For retinal wholemounts and coronal brain slices, some tissues were incubated without primary antisera to ensure that the signal observed was specific to the antigens probed.

*Chromogenic detection*

After incubation in primary antisera, tissues were incubated in the appropriate biotinylated secondary antisera, either donkey anti-mouse (Jackson Immuno Research, Catalog No. 715-065-137) or donkey anti-rabbit (Jackson Immuno Research, catalog No. 711-065-152) diluted 1:500 in 0.3% PBTx (brains) or 0.5% PBTx (wholemounts) for one hour at room temperature. Following incubation in biotinylated secondary antisera, tissues were incubated for 90 minutes in Neutravidin conjugated to horseradish peroxidase (diluted 1:250 in 0.3% PBTx; ThermoFisher Scientific). Chromogenic detection was carried out using Metal-Enhanced 3'3'-diaminobenzidine (DAB) substrate (diluted 1:10 in stable peroxide buffer, Pierce Chemical Company, Rockford IL). DAB development was stopped by immersion in several changes of PB. Brain slices were rinsed in distilled water and coverslipped in Gelvatol (10% polyvinyl alcohol, Sigma P8136, 20% glycerol, Sigma G-9012, 0.02% sodium azide, Fisher s-227-100, 0.2M Tris, Amresco 0497, pH 8.5) prior to imaging. Retinal wholemounts were dried onto Colorfrost slides and coverslipped using Gelvatol.

**Imaging**

Brain slices and retinal wholemounts were imaged on a Nikon Eclipse motorized microscope (Nikon Instruments, Inc.) at 4x, 10x and 20x.

## Analysis

### *Retinal Wholemounts*

ImageJ software (U.S. National Institutes of Health, Bethesda, Maryland, USA) was used for quantitative analysis. Regions of interest (ROI) delineating the central, mid-central, and peripheral retina were created in Image J and applied to the grayscale images. The location of the optic nerve was used to center the ROIs (Figure 3.4). The size of each ROI was matched across all wholemounts captured at 4x.

Four RGB (red, green, blue) multi-channel images within each ROI were obtained at 20x. All images were converted to single wavelength channel images. The channel with the greatest signal to noise contrast (blue) was selected and used across all groups. Two cells within each image were selected for analyses. All single channel (grayscale) images were made binary using a threshold overlay. An ROI large enough to enclose a single cell was used for all analyses. The area fraction, defined as the percent coverage (percent area) of immunoreactivity within each ROI, was obtained for each binary image using the area fraction selection from the ImageJ "Measure" feature. It was expected that hypertrophy, due to glial activation, would be reflected as a greater percent area because the cells would be larger in size and therefore occupy a greater percentage of the ROI.

Values for percent area were obtained for each cell within each ROI. Results were averaged by region (central, mid-central, peripheral) for every animal

and then averaged by condition (sham versus blast). To determine if significant differences in the percent areas of sham and blast exposed animals were present across central, mid-central, and peripheral retinas, a two-way analysis of variance was used (SPSS v24, IBM Corp.). Significance was set at $p<0.05$.

*Brain slices*

Similar to retinal wholemounts, RGB images were obtained and converted to single channel images for all subsequent analyses.

Regionally matched ROIs were used to determine percent area following the same procedure outlined previously for retinal wholemounts. An analysis of variance (ANOVA), was used (SPSS v24, IBM Corp.) to determine if significant differences in the percent area of GFAP labeled astrocytes were present in acute versus chronic recovery post blasts. Significance was set at $p<0.05$.

To determine if differences in both the number and morphology of Iba-1 labeled microglia existed among sham and blast exposed mice, manual counts were performed by an observer blinded to condition. Counts of Iba-1 positive cells were averaged for each animal and then averaged by group. Iba-1 cells were categorized in based on three broad morphological groups: ramified, hypertrophic, and amoeboid (Karperien et al., 2013). A two-way analysis of variance (ANOVA) was used (SPSS v24, IBM Corp.) to establish whether differences in the average number of cells based on morphology was significant ($p<0.05$).

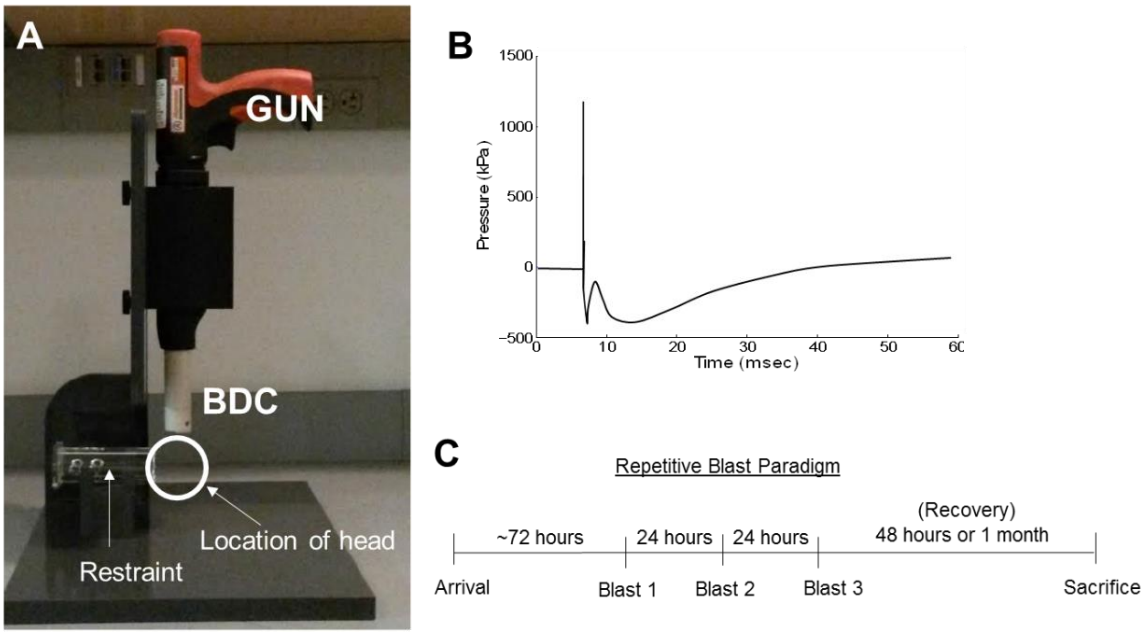


**Figure 3.2. (A)** The Cranium Only Blast Injury Apparatus (COBIA) used to generate blast overpressures. **(B)** Pressure waveform produced by the COBIA revealing maximum overpressure of 1,034 kPa. **(C)** Repetitive blast paradigm of acute (48 hours) and chronic (one month) recovery following three consecutive blasts with 24 hour latencies. BDC = blast dissipation chamber.

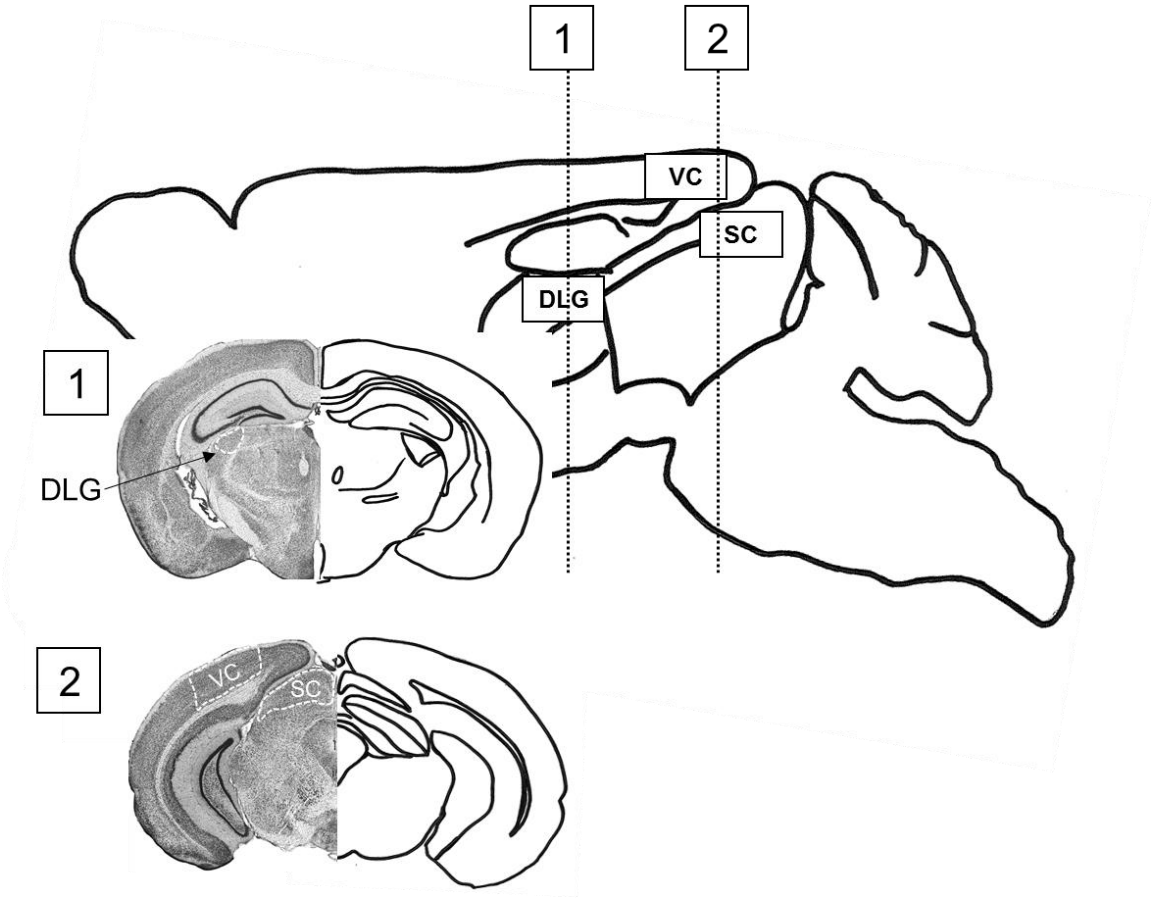


**Figure 3.3.** General schematic of selected brain regions involved in visual processing. Dashed vertical lines and corresponding numbers represent coronal brain slices containing regions of interest (Left, Nissl stain; Right, Corresponding line drawing). DLG = dorsal lateral geniculate SC = superior colliculus VC = visual cortex. Nissl stained coronal images modified from Franklin and Paxinos, 2008.

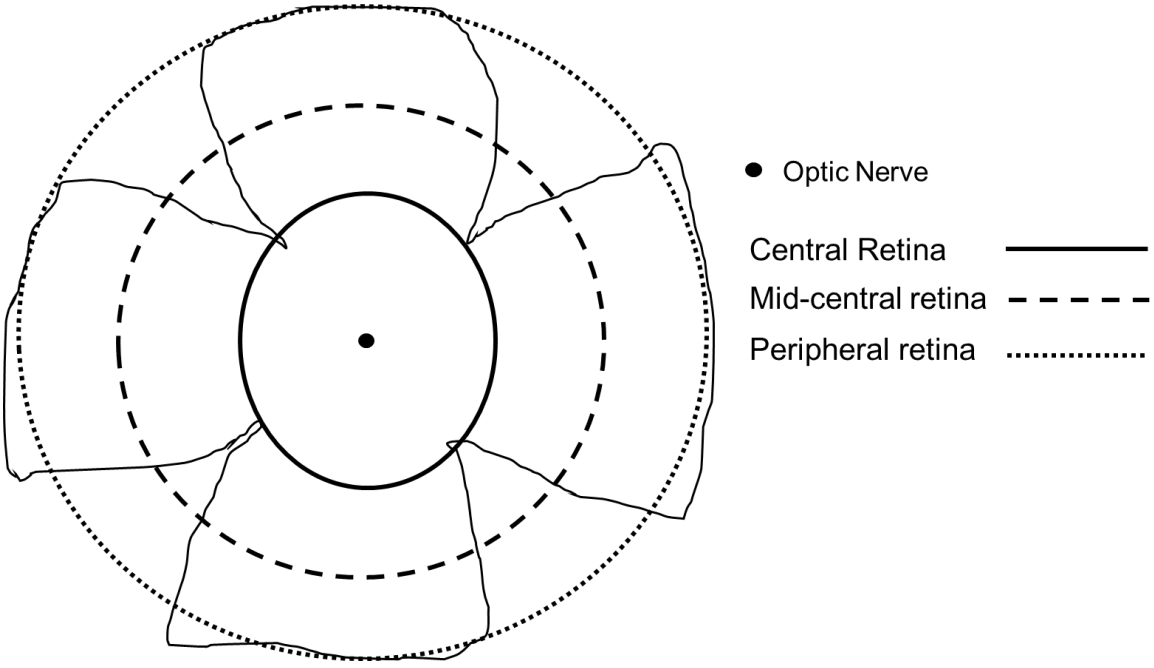


**Figure 3.4.** Delineation of central, mid-central, and peripheral retina based on location of the optic nerve.

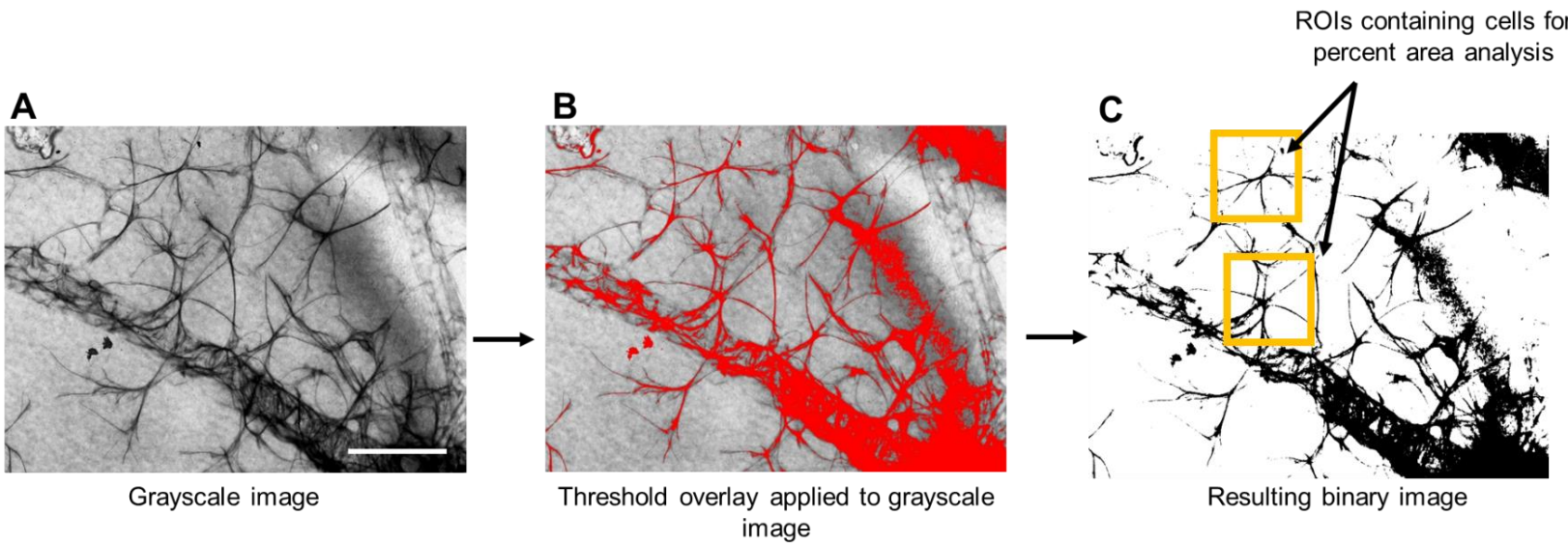


**Figure 3.5.** Evaluation of the percent area occupied by GFAP. **(A)** Single channel (grayscale) image of GFAP staining in a retinal wholemount, scale bar = 100µm. **(B)** Representative threshold overlay applied to GFAP labeling present in grayscale image in (A). **(C)** Resulting binary image. GFAP = glial fibrillary acidic protein.

## RESULTS

### No hypertrophic glia were present in the retina following multiple blasts

Astrocytes with GFAP immunoreactivity showed no indication of hypertrophy throughout the retina 48 hours and one month following three consecutive blasts (Figures 3.6 and 3.7). Quantitative analyses were not performed to assess whether differences were present in astrocytes and microglia. However during microscopic observation, all of the cells (somata and processes) had the same appearance. Processes from all of the GFAP labeled cells within the central, mid-central, and peripheral retina possessed a thin ramified appearance (Figures 3.6 and 3.7). Similarly, there were no differences in the percent area of individual Iba-1 positive cells from sham and blast exposed animals (Figure 3.8). Similar to astrocytes, the processes of Iba-1 cells revealed no hypertrophy.

### No structural alterations in DLG following repeated blasts

The Iba1 positive microglia that tiled the DLG in a non-overlapping fashion contained thin ramified processes with no difference in the average number of Iba1 positive cells present, although there was considerable variability in the average number of Iba1 positive cells in animals allowed to recover 48 hours following three blasts (Figure 3.9). Minimal GFAP immunostaining was present within the DLG for both sham and blast animals (data not included).

**No significant gliosis present in the SC and Visual cortex following repeated blasts**

A slight increase in the percent area occupied by GFAP was observed 48 hours following repeated blast exposure in both the SC and visual cortex relative to control (Figures 3.10 and 3.11). The GFAP labeling in the SC at the 48-hour time point was diffuse throughout the colliculi whereas in the sham and one month recovery the staining was focal (Figure 3.10). Similarly, a slight decrease was observed one month following consecutive blasts in both brain regions (Figures 3.10 A and 3.11 A). It is of note that the superficial layers in the visual cortex had the greatest GFAP immunoreactivity (Figure 3.11 B–D).

Although not significant, the percent area occupied by GFAP labeled astrocytes showed a similar pattern in the SC and visual cortex (Figures 3.10 and 3.11). Overall there was no change in the average number of microglia present in the visual cortex. A small number of hypertrophic cells were observed 48 hours following three blasts, however the morphology of most cells were ramified at the 48 hour time point and all of the cells assessed in the sham groups and one month recovery cohort were ramified (Figure 3.12). Similarly, no hypertrophic cells were observed in the SC (data not included).

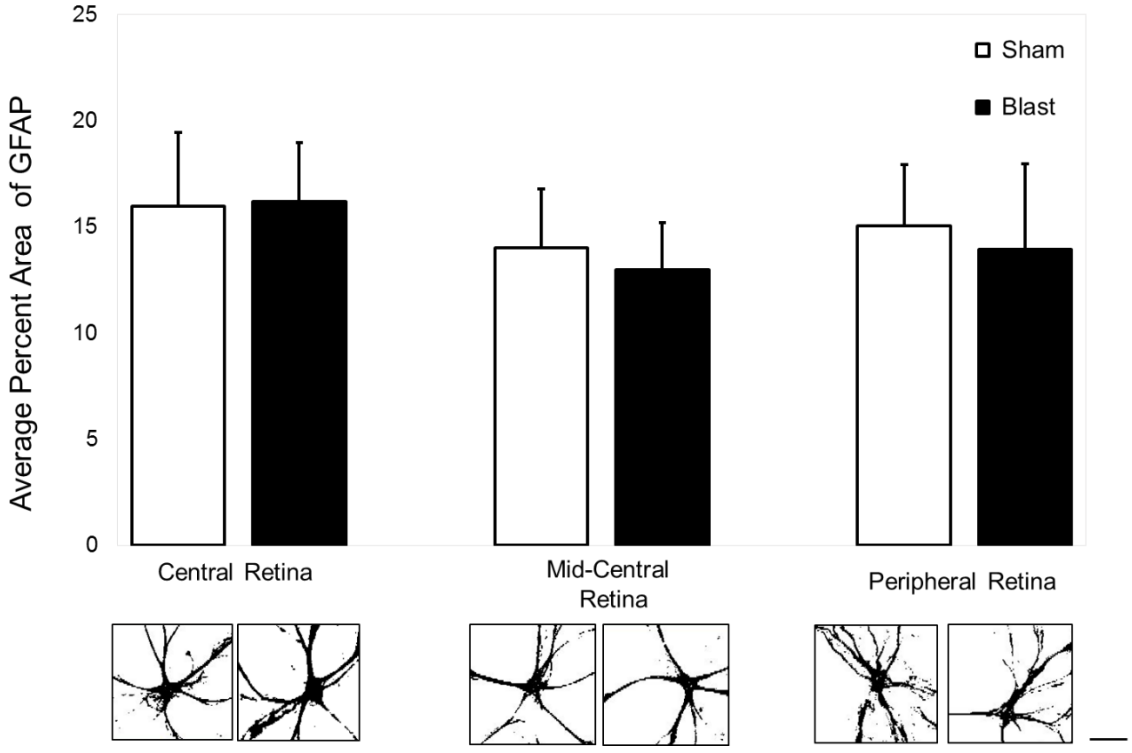


**Figure 3.6.** There was no difference in the average percent area occupied by GFAP labeled astrocytes 48 hours following three consecutive blasts. Error bars represent SD (n=3 for each group). Binary images below each bar are representative binary images of astrocytes observed within each region of retina evaluated (central, mid-central, and peripheral). GFAP = glial fibrillary acidic protein. Scale bar = 20µm.

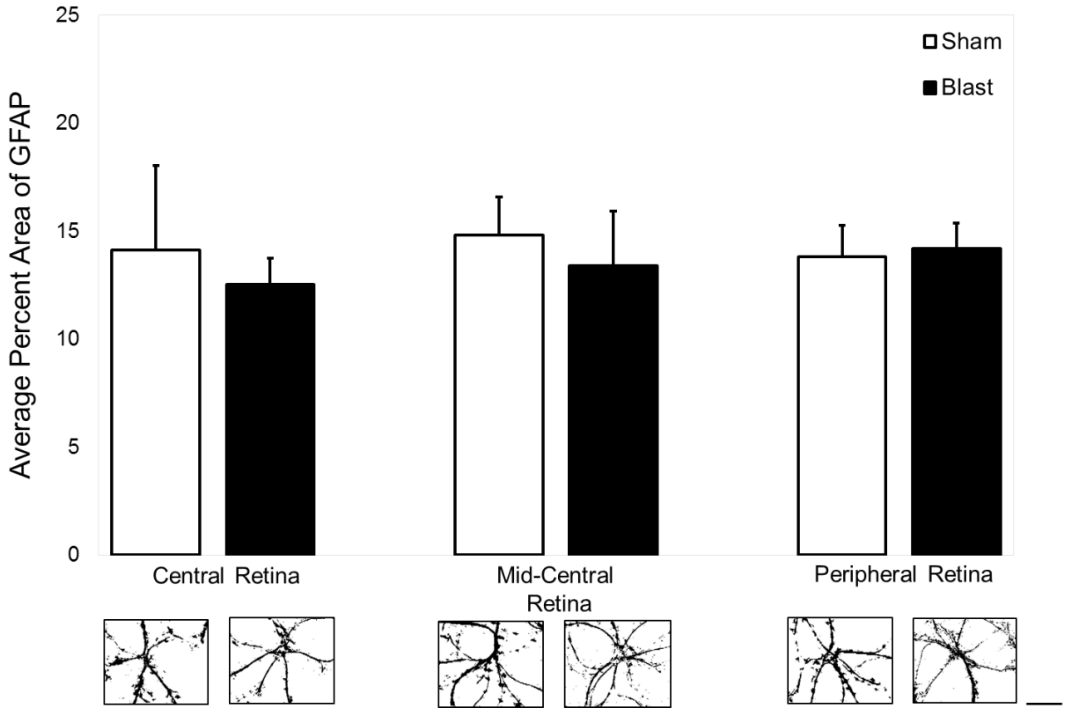


**Figure 3.7.** There was no difference in the average percent area occupied by GFAP labeled astrocytes one month following three consecutive blasts. Error bars represent SD (n=3 in each group). Binary images below each bar are representative binary images of astrocytes analyzed within each region of retina evaluated (central, mid-central, and peripheral). GFAP = glial fibrillary acidic protein. Scale bar = 20µm.

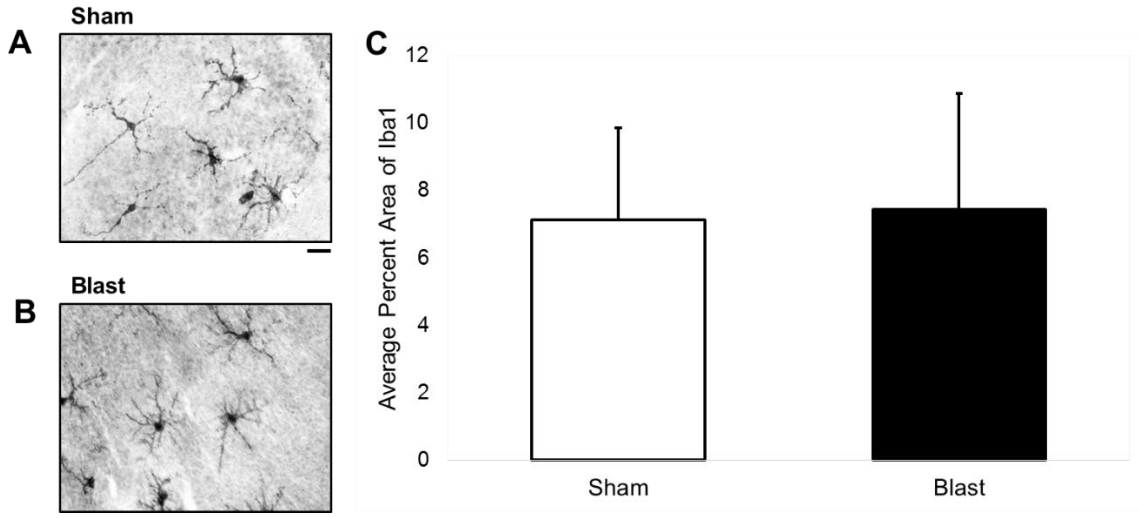


**Figure 3.8.** There were no hypertrophic microglia in the retina 48 hours following repeated blast exposures. Representative microglia morphologies in sham **(A)** and blast exposed mice **(B)** No difference in the average percent area occupied by Iba-1 positive microglia (sham n=4, blast n=5), error bars represent SD **(C)**. Iba-1 = ionized calcium-binding adapter molecule-1. Scale bar = 30µm.

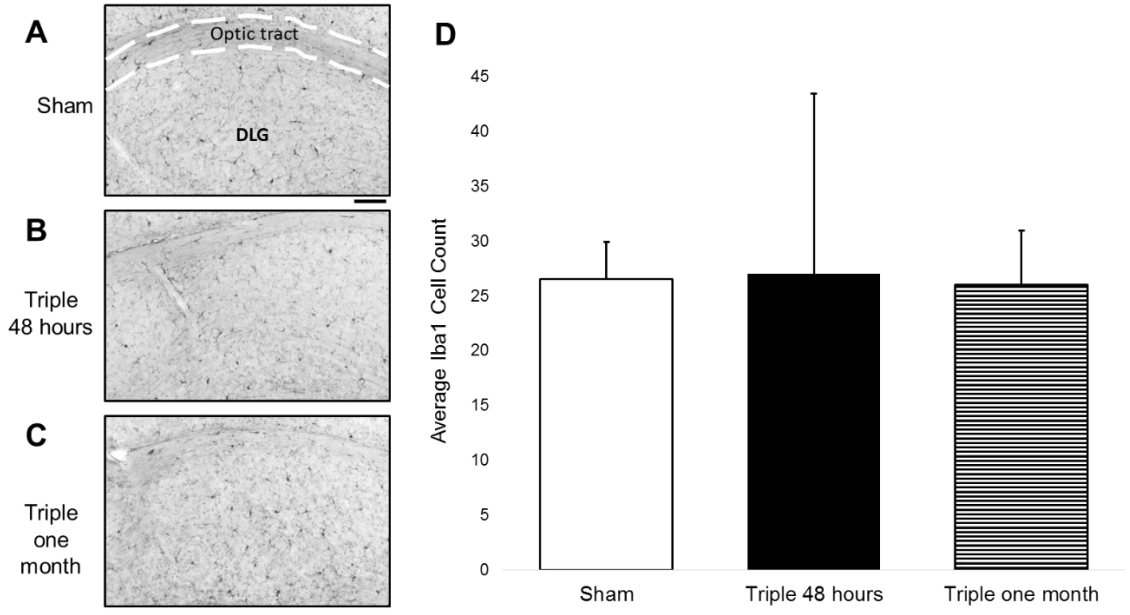


**Figure 3.9.** Hypertrophic microglia were not observed in the dorsal lateral geniculate nucleus following repeated blasts. **(A–C)** Representative Iba-1 immunostaining revealing tiled, non-overlapping ramified microglia. **(D)** There was no difference in average counts of Iba1 positive cells (n=3 in each group), error bars represent SD. Iba1 = ionized calcium binding adapter molecule-1. Scale bar = 100µm.

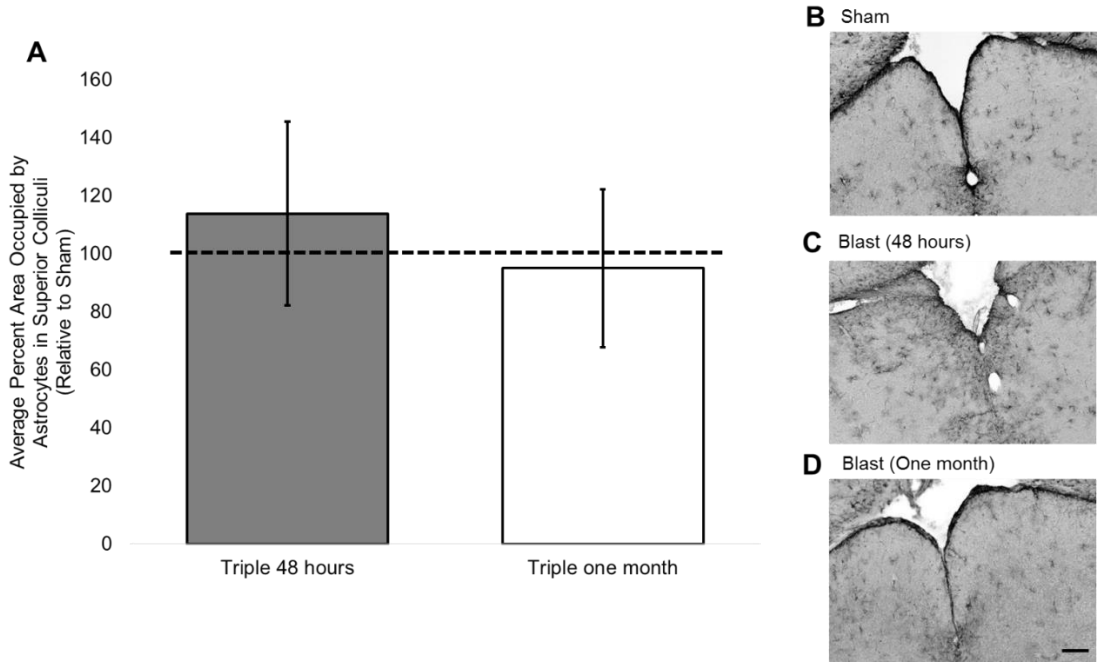


**Figure 3.10.** GFAP labeled astrocytes in the superior colliculi following exposure to repeated blasts. **(A)** Relative to sham (dashed horizontal line) there was a slight increase in the average percent area occupied by astrocytes 48 hours following three blasts (n=3) while a slight decrease in the average percent area occupied by astrocytes was detected one month (n=3) following repeated blasts. Representative sham **(B)** and blast exposed mice 48 hours **(C)** and one month **(D)** following three blasts. Error bars represent SD. GFAP = glial fibrillary acidic protein. GFAP = glial fibrillary acidic protein. Scale bar = 100 µm.

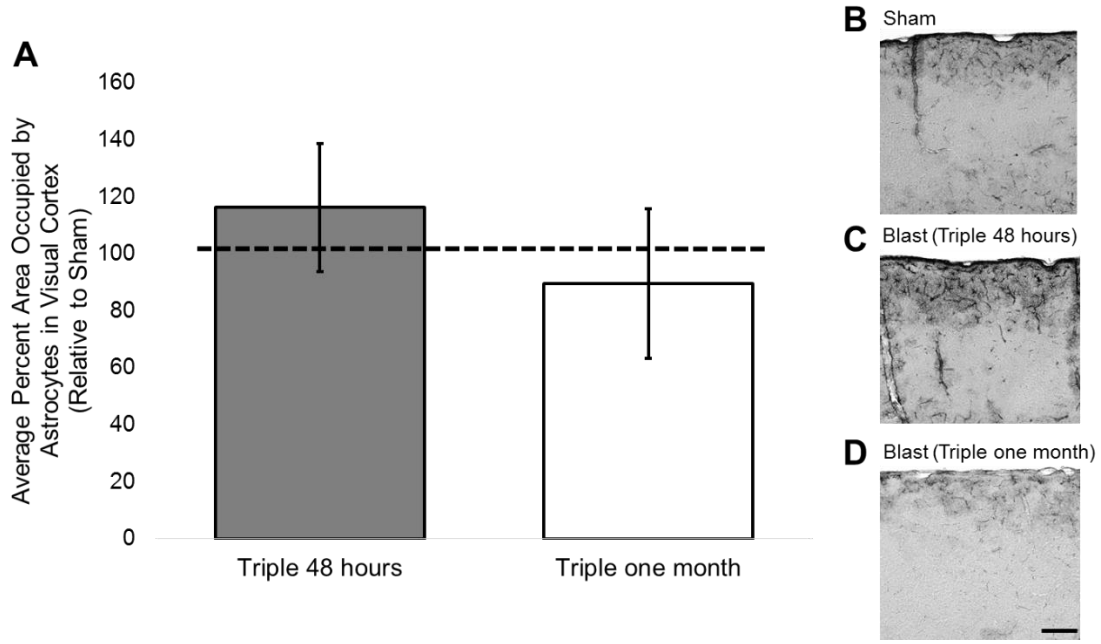


**Figure 3.11.** GFAP labeled astrocytes in the visual cortex following exposure to repeated blasts. **(A)** Relative to sham (dashed horizontal line), there was an increase in the average percent area occupied by astrocytes at 48 hours post repeated blast (n=3), while there was a decrease in the average percent area occupied by astrocytes at one month (n=3) following repeated exposures. Representative sham **(B)** and blast exposed mice 48 hours **(C)** and one month **(D)** following three blasts. Error bars represent SD. GFAP = glial fibrillary acidic protein. Scale bar = 100 µm.

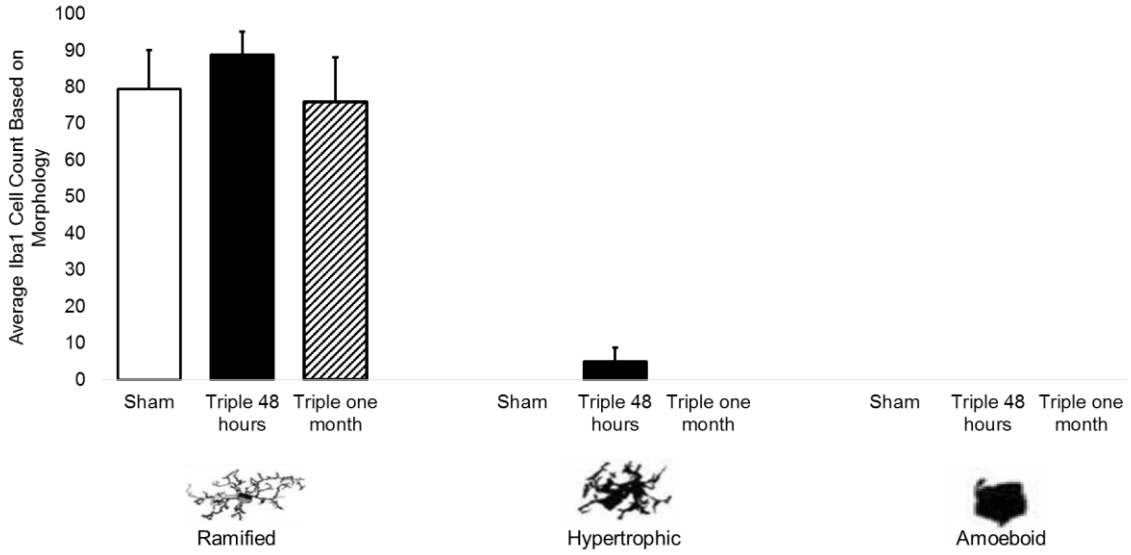


**Figure 3.12.** There was no significant difference in the average number of Iba-1 labeled cells in the visual cortex following three consecutive blasts. Hypertrophic microglia were largely absent in the visual cortex following three consecutive blasts, although a small number of hypertrophic microglia were observed 48 hours following three blasts. Iba-1 = ionized calcium binding adapter molecule-1. Schematic of microglia morphologies modified from Karperien et al., 2013.

## DISCUSSION

The absence of structural alterations detected in glial morphologies at the time points evaluated suggests that the regions of the visual system examined—retina, DLG, SC, and visual cortex may have been structurally spared from the diffuse injury that is common following blast. However, it is possible that transient alterations in glial phenotypes occurred along a more acute (less than 48 hours) time scale as morphological alterations in glia can be rapid and reversible (Karve et al., 2016). In light of this, it is possible that transient hypertrophy in one or both of the glial populations could have occurred. The intermediate filament (GFAP) and microglial calcium-binding protein (Iba1) are commonly used markers to identify injury status. However, use of glial markers to label Müller cells within the retina and myelin outside of the retina within the optic nerve and tracts, may reveal the existence of alterations in more subtle histopathology following the mild blasts used in this study.

Alternatively, it may be that the blast overpressures applied onto the dorsal surface of the head in this study were too low to produce the visual pathology commonly seen following blasts. However, an important consideration is the orientation of the animals with respect to blast. Several studies (Mohan et al., 2013; Bricker-Anthony et al., 2014; Bricker-Anthony and Rex, 2015; DeMar et al., 2016) highlight the importance of blast wave directionality in rodents. For example one study (Guley et al., 2016) in mice evaluating visual system deficits found that a single blast directed unilaterally onto a small portion of the cranium produced

noticeable axonal damage. Another rodent study (DeMar et al., 2016) using electroretinograms (ERGs) and histology found retinal pathology to be absent when blasts were directed to the front of the head rather than unilaterally (to one side of the animal). This finding demonstrates that orientation with respect to the direction of blast waves can affect the pathological outcome, which may account for the lack of glial alterations in this study.

While differences in percent area between control and experimental groups are commonly used within the IHC field, this form of analysis cannot adequately detect subtle morphological differences. Morphometric studies using Sholl analysis in neurons and fractal dimension in microglia (Karperien et al., 2013; Williams et al., 2013) have revealed subtle differences in glia from control and experimental groups. Regardless, although use of structural changes as a proof of concept in injury models is prevalent, functional alterations in the absence of anatomical pathology have been reported (Wang et al., 2013) and could be a feature of the model employed. While most reports center on neuronal functionality, functional assessments of glia using markers to label channels such as glutamate transporters (Maguire et al., 1998) could offer additional insight into the potentially subtle and transient glial changes following mild blasts.

The increased motivation to accurately identify and eventually treat TBI-related pathologies during life has prompted work focused on the evaluation of functional integrity within the central nervous system following injury. For example, non-invasive assessments of the retina include optical coherence tomography

(OCT) (Schuman, 2008; Spaide et al., 2008), which produces high resolution *in vivo* cross-sections of the retinal microstructure, and ERGs which measure the electrical activity in the retina following stimulation with light (Gouras, 1970). Although OCT, ERGs and their derivatives are used in humans, they have been adapted for use in animals and provide critical information on visual system integrity. For example, diminished functional integrity of the retina and optic nerves following acute and chronic blast exposure in mice, have resulted in significant reductions in pattern-electroretinograms (Porciatti, 2007; Azarmina, 2013), a modified ERG used to evaluate RGC integrity by summing the depolarization of RGCs in response to light stimulation (Mohan et al., 2013). Modifications to non-invasive techniques such as positron emission tomography (Muzaffar et al., 2013) and magnetic resonance imaging, (Townsend et al., 2008) used to assess integrity of soft tissue organs such as the brain have been applied to the retina (Cheng et al., 2006). While OCT and ERGs allow valuable insight into retinal function, visually evoked potentials (VEP) provide rapid, reproducible, and objective insight into overall integrity of afferent visual pathways (Kolappan et al., 2009). VEPs are electrical signals produced in the primary visual cortex in response to a time-locked visual stimulus (Sokol, 1976; Yadav and Ciuffreda, 2013). The ability of VEPs to aid in the cortical evaluation of different deficits in the retina and brain gives it considerable advantage in identifying visual impairments that extend beyond the retina.

# CHAPTER 4

Immunocytochemical evaluation of tau pathology and parvalbumin in visual cortices of advanced chronic traumatic encephalopathy in human postmortem brains

## ABSTRACT

Chronic traumatic encephalopathy (CTE) is a devastating progressive neurodegenerative tauopathy that is widely associated with mild repetitive head injury. Although visual deficits are reported in CTE, the primary visual cortex is often spared. In this study, immunocytochemistry was used to determine whether lateral visual association (extrastriate) areas were susceptible to the tau pathology that is common in CTE. In addition, a sub-class of inhibitory interneurons containing the calcium-binding protein parvalbumin was assessed using un-biased stereology to evaluate a potential cell specific vulnerability. Results showed progressive tau pathology in extrastriate cortices that was largely absent from the primary visual cortex. No change was observed in the number of parvalbumin positive cells. The results of this work provide valuable insight regarding the extent of tau pathology in visual association cortices and the potential cell-specific resistance despite advanced CTE pathology.

## INTRODUCTION

### What is chronic traumatic encephalopathy?

Chronic traumatic encephalopathy (CTE) is a distinct neurodegenerative disorder associated with mild repetitive brain injuries (McKee et al., 2013). Historically, CTE was first described in 1928 by pathologist Dr. Harrison Martland, who observed the late onset of behavioral and cellular pathology in boxers (Martland, 1928). Around the time of Martland's account terms such as 'punch drunk', 'dementia pugilistica' and 'psychopathic deterioration of pugilists' were used to describe the outward display of CTE symptoms that were associated with boxing (Yi et al., 2013). Although early reports of CTE were mainly in boxers, clear evidence to support the association of CTE in other sports such as football, hockey, rugby, wrestling, and soccer led to the broadly encompassing term 'progressive traumatic encephalopathy' now currently defined as CTE (Gavett et al., 2011). In addition to repetitive head injury in sports, damages sustained from repeated exposure to blast explosions, as seen in veterans and civilians, and concussive injuries from persistent head banging and physical abuse are now widely recognized risk factors (McKee et al., 2013).

## Clinical features and diagnosis of CTE

The distressing manifestations of CTE usually present 8–10 years following repeated injury and include: progressive rage, impairments in memory, and visuospatial abnormalities (Gavett et al., 2011; McKee et al., 2013; McKee and Robinson, 2014). The pathology of CTE is defined by neurofibrillary tangles that are immunoreactive for abnormally hyperphosphorylated tau located around blood vessels and in an irregular pattern that is prevalent within the depths of sulci (McKee et al., 2016). Four clinical stages (depicted in Figure 4.1 and summarized in Table 4.1) have been established to characterize the progression of tau's pathological accumulation in CTE (McKee et al., 2013). Although histological consensus exists among leading neuropathologists, definitive diagnoses can only be obtained from postmortem examination (McKee et al., 2016). Efforts to diagnose CTE during life and elucidate cellular mechanisms that contribute to injury progression are earnestly underway.

## Cellular mechanisms underlying CTE pathology

Axonal injury is believed to underlie the pathology of CTE (Gavett et al., 2011; Giza and Hovda, 2014). Specifically, alterations in membrane permeability and concentrations of ions such as calcium that can promote release of caspases and calpains have been reported to initiate the misfolding, truncation, phosphorylation, and/or aggregation of tau proteins (Gavett et al., 2011). As detailed in Chapter 1,

tau proteins normally bind and stabilize microtubules (Figure 1.5) thereby aiding in neurite growth, axonal transport, and overall neuronal integrity (Johnson and Stoothoff, 2004; Ballatore et al., 2007; Wolfe, 2012). In addition tau has been reported to interact, directly and indirectly, with actin, the plasma membrane and the nucleus, as well as influencing the activity of proteins such as the scaffolding protein 14-3-3 and the membrane associated enzyme phospholipase Cɣ which ultimately affects signal transduction (Gendron and Petrucelli, 2009). With such extensive interactions among a variety of cellular components, disruption to tau homeostasis can result in devastating pathologies.

The tau protein, encoded by the MAPT gene located on chromosome 17, can be alternatively spliced into six isoforms (Gendron and Petrucelli, 2009). Figure 4.2 depicts a basic schematic of the six isoforms of the tau protein. Two distinguishing features include the presence or absence of N-terminal acidic inserts as well as the number of C-terminal tubulin binding repeats (Ballatore et al., 2007). Post-translational modifications to tau are extensive and have been reported to include: acetylation, deamination, glycation, glycosylation, nitration, oxidation, phosphorylation, and ubiquitination (Avila et al., 2004). Despite such widespread modifications the most widely studied tau modification is phosphorylation. Several kinases and phosphatases are responsible for tau's dynamic interaction with microtubules. Mutations, physical trauma, or alterations in signaling cascades that affect the rate of phosphorylation and dephosphorylation are reported to contribute to tau pathology (Ballatore et al., 2007; Gendron and

Petrucelli, 2009). The commonly cited pathological mechanisms include the toxic loss of function, due to tau's inability to bind and stabilize microtubules when hyperphosphorylated, and the toxic gain of function due to tau's ability to self-aggregate and bind other proteins (Gendron and Petrucelli, 2009). The increased phosphorylation resulting in aggregation of tau proteins can interfere with intracellular trafficking culminating in degeneration as the efficient clearance of protein aggregates decline over time (Guo and Lee, 2014).

Although tau proteins are normally intracellular there are reports of extracellular tau (Frost et al., 2009). Tau protein aggregates released from dying neurons are believed to account for extracellular tau (Hanger et al., 2014). In addition diffusion through membranes, release from synaptic vesicles and ruptured exosomes have also been speculated to contribute to extracellular tau (Wang and Mandelkow, 2016). The presence of extracellular tau can initiate glial activation. The over activation of glia can worsen over time as cellular cascades elicited from inflammatory mediators negatively affect surrounding neurons (Guo and Lee, 2014).

One hypothesis to explain the spatial and temporal progression of tau from discrete focal entities to wide-spread lesions involving many brain regions is trans-synaptic propagation between neurons in anatomically connected regions (Wang and Mandelkow, 2016). Studies using cell cultures and intracerebral injections showing tau pathology in connected neural networks provide convincing evidence to support trans-synaptic spreading of tau pathology (Liu et al., 2012).

Another prevalent hypothesis to account for the spreading of tau is based on prion-like propagation (Costanzo and Zurzolo, 2013; Woerman et al., 2016). Pathological tau in CTE shares similarities with prion protein plaques in Creutzfeldt-Jakob disease, alpha-synuclein Parkinson's disease, and amyloid-beta and tau in Alzheimer's disease, (Guo and Lee, 2014). In a seminal study conducted by Dr. Stanley Pruisner's group cell cultures infected with pathological tau, obtained from diagnosed cases of CTE and other neurodegenerative diseases, showed evidence of tau propagation in a prion-like manner (Woerman et al., 2016). In addition, animal models have shown that pathological tau can stability maintain specific conformations when introduced to different cell types and brain regions (Sanders et al., 2014). The implications from studies characterizing the cellular mechanisms that underlie CTE pathology will undoubtedly help in studies aimed at delaying the progression of neurodegeneration.

**Rationale for examining visual cortices in advanced CTE**

It has been estimated that 60% of those suffering from CTE show visual impairments ranging from blurred vision to complete vision loss (McKee, 2016). However, previous work indicates the relative absence of tau pathology in the primary visual cortex (Brodmann area (BA) 17) except in the most severe cases (McKee et al., 2013). It is believed that such sparing is due to the medial location of BA17 rendering it less vulnerable to physical trauma and thus cellular damage

that is a hallmark of CTE. Although BA17 is relatively spared in CTE, visual association cortices (extrastriate cortex), such as BA 18 and 19, are vulnerable to tau pathology in neurodegenerative disorders such as AD (McKee et al., 2006). The highly complex connectivity, vascular, and metabolic features are believed to underlie neurodegeneration in extrastriate areas (Tong, 2003; McKee et al., 2006; Pikkarainen et al., 2009).

Understandably pathologies involving tau and glia have received considerable attention in the CTE field (McKee et al., 2013; Cherry et al., 2016; Kanaan et al., 2016). However, few studies have explored whether tau preferentially accumulates in excitatory glutamatergic cells or in inhibitory GABAergic neurons (gamma-amino butyric acid, GABA). Morphologically, tau inclusions (neurofibrillary tangles) appear to affect pyramidal cells in CTE. In light of the axonal pathology that is believed to underlie CTE, it is likely that projection neurons such as pyramidal cells would be a vulnerable population. However, vulnerability of GABAergic neurons has been reported in AD, animal models of brain injury, and human postmortem examinations following TBI (Leuba et al., 1998; Buritica et al., 2009). Based on the similarities between CTE and AD, it is advantageous to determine whether GABAergic neurons are affected in CTE.

## Study objectives

The first goal in this study was to characterize tau pathologies in visual cortices (BA17-19) in advanced (stages 3 and 4) CTE. The second goal was to determine whether a specific sub-class of GABAergic interneurons containing the calcium-binding protein parvalbumin, was affected in advanced (stages 3 and 4) CTE.

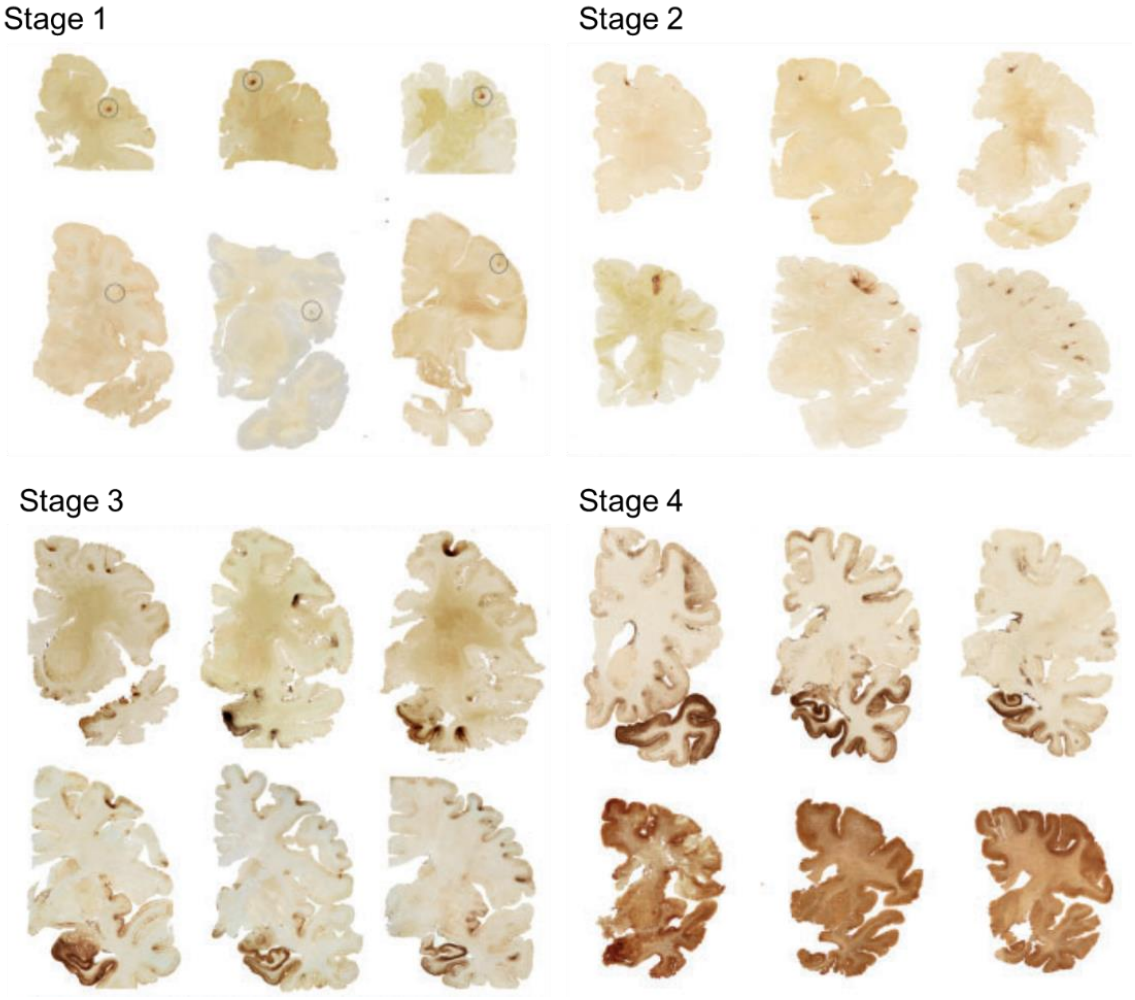


**Figure 4.1.** Four clinical stages of CTE based on the progression of neurofibrillary tau pathology described in Table 4.1. Circles in Stage 1 indicate discrete, focal, clusters of phosphorylated tau labeled with CP13 antibody located primarily within the fundus of the sulcus. The prevalence of tau pathology in the depths of sulci increase (Stage 2) and spread to the superficial cortices of surrounding regions becoming increasing widespread in later stages (3 and 4). Figure modified from McKee et al., 2013.

**Table 4.1.** Description of the four clinical stages* of CTE

| Stage | Pathological description | Affected brain regions |
|---|---|---|
| 1 | Discrete, focal clusters of phosphorylated tau in sulci depths and surrounding vasculature | Superior, dorsolateral, lateral frontal corties |
| 2 | Multiple focal clusters of phosphorylated tau in the depths of sulci | Superficial cortical layers of adjacent cortices in Stage 1 |
| 3 | Widespread phosphorylated tau | Frontal, insular, temporal, parietal, amygdala, hippocampus, entorhinal cortices |
| 4 | Widespread, severe phosphorylated tau | Medial temporal lobe and most brain regions (primary visual cortex largely spared) |

*As described in McKee et al., 2013 and McKee et al., 2016

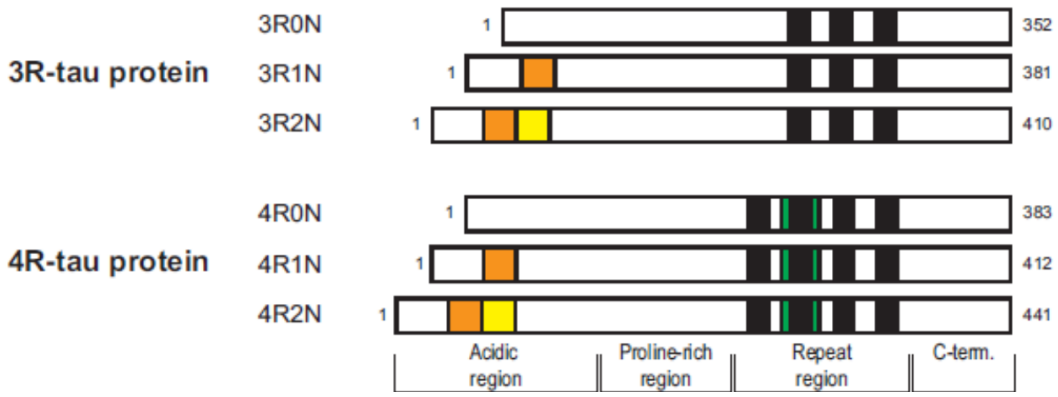


**Figure 4.2.** Schematic of the six isoforms of tau protein. Black boxes represent the presence of repeat regions (3R, 4R). Orange and red boxes represent N-terminal inserts. Numbers flanking each isoform indicate the number of amino acids present. Schematic modified from Gendron and Petrucelli, 2009.

## METHODS

### Subjects

Coronal slabs of occipital lobes from fifteen subjects (7 controls, 4 stage 3 CTE, 4 stage 4 CTE) were received from the Boston University Alzheimer Disease Center (BU-ADC) and Center for the Study of Traumatic Encephalopathy (CSTE) at Boston University School of Medicine. Tables 4.2a and 4.2b summarize general information on subjects evaluated in this study.

### Tissue preparation

Occipital lobes were cryoprotected in progressive glycerol solutions as previously described (Rosene et al., 1986) and then dissected into smaller blocks (approximately 2 x 3 centimeters). Each dissected block contained multiple sulci and gyri for detailed histological characterization (Figure 4.3). The primary visual cortex (BA 17) was identified grossly by the stria of Gennari, a myelinated band of axons in layer 4. A distal extrastriate region located laterally within the occipital lobe, opposite the stria of Gennari, was selected from each subject to evaluate differences in the medial versus lateral visual cortices. Dissected tissue blocks were quickly frozen in 2-methylbutane at -80°C as previously described (Rosene et al., 1986).

Both regions of the visual cortices were cut into 40 µm thick slices using a freezing sliding microtome (Reichert Jung). Slices were collected in 15% glycerol in 0.1M PB in 16 uninterrupted series. Sections from each subject were maintained at -80°C until tissue from all subjects could be immunostained at the same time to avoid technical and procedural variability.

**Immunocytochemistry and histology**

For each antibody one uninterrupted series from striate and extrastriate regions from each subject were thawed overnight at 4°C and then brought to room temperature. Slices were processed free-floating with agitation. Prior to immunostaining sections were thoroughly rinsed in Tris Buffered Saline (TBS, pH 7.6) (20mM Trizma base, 0.14M sodium chloride). To retrieve antigens masked during fixation, slices were first incubated in sodium citrate buffer (10mM sodium citrate, 0.05% Tween 20, pH 6.0) for twenty minutes at room temperature and then heated to 40°C using 550 Watts for 25 minutes with alternating 5 minute rest/heat cycles. Following heat-induced antigen retrieval slices were incubated at room temperature for 20 minutes in sodium citrate buffer and then rinsed in TBS. Endogenous peroxidase was quenched for 30 minutes at room temperature using 3% hydrogen peroxide. Slices were incubated for one hour at room temperature in Superblock Blocking Buffer (Thermo Fisher, cat# 37515) to minimize non-specific binding. Following blocking sections were incubated in primary antisera (mouse

anti-CP13 1:500, gift from Dr. Peter Davies; rabbit anti-parvalbumin, Novus Biologicals, cat# NB120-11427) diluted in TBS containing 0.5% Superblock Blocking Buffer and 0.3% Triton-X100 for 48 hours at 4°C. Slices from a randomly chosen subject were processed simultaneously without the addition of primary antisera to ensure specificity of staining.

Following incubation in primary antisera, the tissues were washed in TBS and incubated in the appropriate secondary antisera (VectorLabs biotinylated goat anti-mouse (BA-9200) and biotinylated goat anti rabbit (BA-1000), both diluted to 1:500 in TBS containing 0.3% Trition-X100) for one hour at room temperature. Slices were rinsed in TBS prior to incubation in avidin-biotinylated horseradish peroxidase (Vectastain Elite HRP Kit, cat# PK-6100, 1:500) for one hour at room temperature. Following TBS washes slices were simultaneously developed in 0.05% 3,3-diaminobenzidine tetrahydrochloride (DAB) diluted in TBS and 0.005% hydrogen peroxide and rinsed in TBS. Free-floating sections were mounted and dried onto gelatin-subbed slides. Slide mounted slices were dehydrated in increasing alcohol solutions, cleared in xylene, and coverslipped in Permount (Fisher, cat# SP15). A subset of slides from each subject were defatted in chloroform:ethanol (1:1), rehydrated, and counterstained using 0.05% thionin (pH 4.8) to stain Nissl substance as previously described (Giannaris and Rosene, 2012).

## Antibody Characterization

The phosphorylation of several amino acid residues have been implicated in tau pathology (Figure 4.6). In this study, CP13, a monoclonal antibody (a generous gift from Dr. Peter Davies at Albert Einstein College of Medicine), that recognizes tau phosphorylated at serine 202 was used to characterize tau pathology. CP13 is one of three supported antibodies in the diagnosis of CTE (McKee et al., 2016). Additional studies supporting the specificity of CP13 have been published previously (Goldstein et al., 2012; McKee et al., 2013).

A commercially obtained rabbit polyclonal parvalbumin antibody was used in this study to label a specific sub-class of GABAergic interneurons. Comparison of the staining quality and distribution of parvalbumin was analogous to previously published parvalbumin immunoreactivity in human striate and extrastriate cortices (Leuba et al., 1998; Buritica et al., 2009).

## Analysis

### *Extrastriate identification*

The abrupt termination of the grossly visible stria of Gennari, in parvalbumin and thionin stained slices, was identified as the transition from BA 17 into BA 18 (Figure 4.7). The extrastriate region opposite the calcrine sulcus was identified as BA 19

based on location and the laminar distributions of previously published cytoarchitectonic studies (Amunts et al., 2000; Amunts and Zilles, 2015).

*Semi-quantitative evaluation of CP13 phosphorylated tau*

Figure 4.4 depicts an example of the neuroanatomical regions-gyral crests and sulcal fundi-surveyed. Sulci and gyri with the greatest CP13 immunoreactivity in three to five slices from BA 17, 18, and 19 from each subject were analyzed. The four phosphorylated tau phenotypes of interest included: neurofibrillary tangles (NFTs), plaques, threads, as well as tau pathology associated with vasculature. Table 4.3 and Figure 4.5 detail the four pathological tau phenotypes evaluated. Characterization of NFTs and plaques were based on a previously described semi-quantitative scoring system (McKee et al., 2006). Vasculature associated tau pathology was evaluated by calculating the ratio of vessels associated with tau pathology to the total number of vessels in a 10x field. Tau positive processes (threads) were scored based on the density within a 10x field. All coded subjects were re-coded to avoid bias and analyzed by a single experimenter blinded to the condition.

*Design-based stereology*

The optical fractionator probe was used to obtain unbiased stereological estimates of parvalbumin positive cells in sulci and gyri in BA 17 and BA 19. Regions of interests were outlined using a 2x Nikon Plan objective using StereoInvestigator software (version 8.21.7, MBD Bioscience, Williston, VT). Table 4.4 summarizes stereological parameters used. All coded subjects were re-coded to avoid bias. Counts were performed at 20x by a single experimenter blinded to the conditions.

The Gunderson coefficient of error (CE), was used to identify the precision (<0.1) of stereological estimates (Gundersen et al., 1999). The mean CE for BA 19 Was 0.07 and 0.08 for sulci and gyri, respectively; for BA 17 the mean CE was 0.07 for both sulci and gyri. With the exception of one outlier in BA 17 (CE = 0.14) CE values for each subject ranged from 0.04 to 0.09.

*Statistics*

A one-way analysis of variance and Pearson's correlation were used to evaluate whether significant differences ($p<0.05$) were present among subjects (SPSS v24, IBM Corp.). Based on sample sizes less than 5 (for CTE stages 3 and 4), and the non-normal distribution, a Friedman test was used to evaluate differences in tau pathologies within advanced CTE groups across the three visual cortical areas.

**Imaging**

Brain slices were imaged on a Nikon Eclipse motorized microscope (Nikon Instruments, Inc.) at 4x, 10x and 20x. ImageJ software (U.S. National Institutes of Health, Bethesda, Maryland, USA) was used to process the images.

**Table 4.2a.** Subject demographics

| Subject | Group | Gender | COD | Repetitive trauma | Symptom Duration* | Age of Symptom Onset |
|---|---|---|---|---|---|---|
| 1 | Control | Female | | | | |
| 2 | Control | Male | | | | |
| 3 | Control | Male | | | | |
| 4 | Control | Female | | | | |
| 5 | Control | Male | | | | |
| 6 | Control | Female | | | | |
| 7 | Control | Female | | | | |
| 8 | CTE Stage 3 | Male | Cerebrovascular disease | Professional Football | 4 | 80 |
| 9 | CTE Stage 3 | Male | Dementia | Professional Football | 8 | 63 |
| 10 | CTE Stage 3 | Male | Cancer | Professional Football | 23 | 48 |
| 11 | CTE Stage 3 | Male | Cardiovascular disease | Professional Football | 58 | 27 |
| 12 | CTE Stage 4 | Male | Dementia | College Football | 10 | 56 |
| 13 | CTE Stage 4 | Male | Dementia | Professional Football | 5 | 64 |
| 14 | CTE Stage 4 | Male | Dementia | College Football | 11 | 66 |
| 15 | CTE Stage 4 | Male | Dementia | College Football | 15 | 50 |

Abbreviation: COD = Cause of death

* Duration determined by the difference between age at death and age of onset

**Table 4.2b.** Subject demographics (continued)

| Subject | Group | Hemisphere | Brain Weight | Age | PMI (hours) | Fixation duration | Fixation Type |
|---|---|---|---|---|---|---|---|
| 1 | Control | Right | 1170 | 87 | Unknown | 0.5 months | Formalin then PLP |
| 2 | Control | Right | 1290 | 91 | 22.0 | 6 months | PLP |
| 3 | Control | Right | 1600 | 91 | 2.5 | 6 months | PLP |
| 4 | Control | Right | 940 | 83 | 6.5 | 4 months | PLP |
| 5 | Control | Right | 1290 | 70 | 48.0 | 4.5 months | PLP |
| 6 | Control | Right | 1080 | 87 | 12.8 | 4.5 months | PLP |
| 7 | Control | Right | 1079 | 95 | 15.5 | 0.5 months | PLP |
| 8 | CTE Stage 3 | Left | 1400 | 84 | 46.0 | 5.5 months | Formalin then PLP |
| 9 | CTE Stage 3 | Right | 1219 | 71 | 17.0 | 4.5 months | Formalin then PLP |
| 10 | CTE Stage 3 | Right | 1510 | 71 | 12.0 | unknown | Formalin then PLP |
| 11 | CTE Stage 3 | Right | 1060 | 79 | 120.0 | 5.5 months | Formalin then PLP |
| 12 | CTE Stage 4 | Right | 1275 | 66 | 9.0 | 4 months | Formalin then PLP |
| 13 | CTE Stage 4 | Left | 1390 | 69 | 36.0 | 7 months | Formalin then PLP |
| 14 | CTE Stage 4 | Left | 1244 | 77 | 15.5 | 6 months | Formalin then PLP |
| 15 | CTE Stage 4 | Right | 1265 | 65 | 30.5 | 3.5 months | PLP |

Abbreviations: PMI = Postmortem Interval, PLP = Paraformaldehyde/Lysine/Periodate

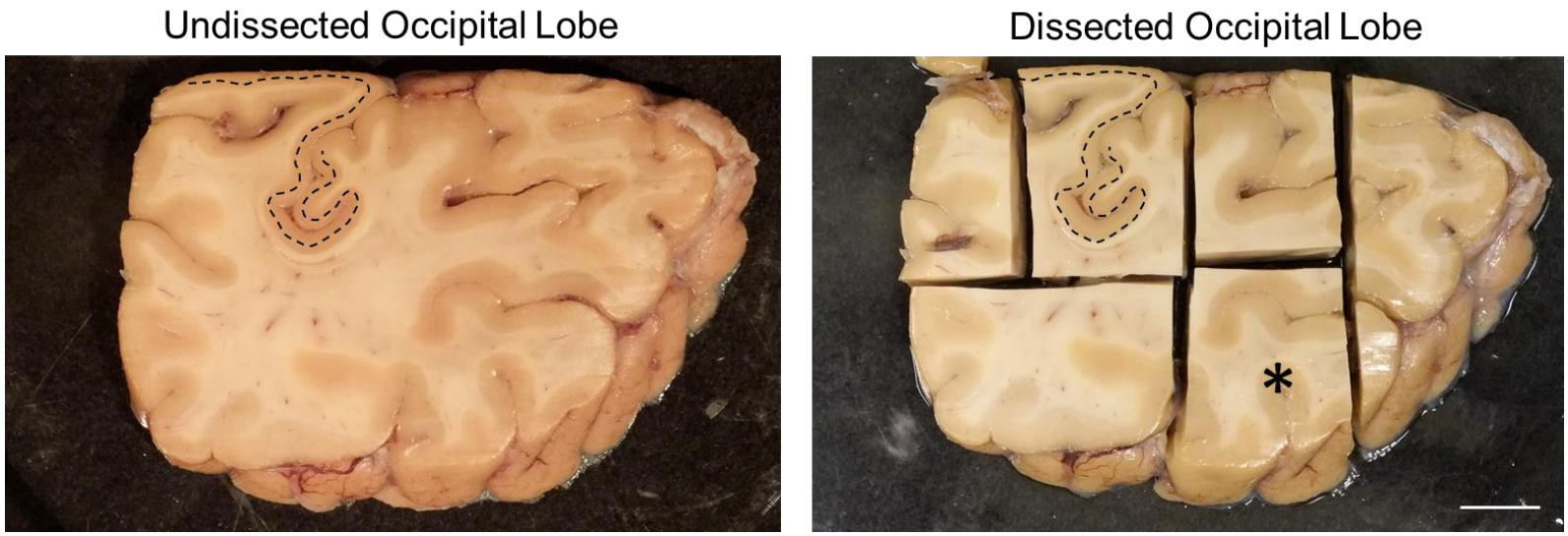


**Figure 4.3.** An example of a dissected and undissected occipital slab. The dashed black line indicates the location of the grossly visible stria of Gennari. Asterisk indicates the distal extrastriate area located opposite primary visual cortex that was chosen for comparative analyses. Scale bar = 10mm.

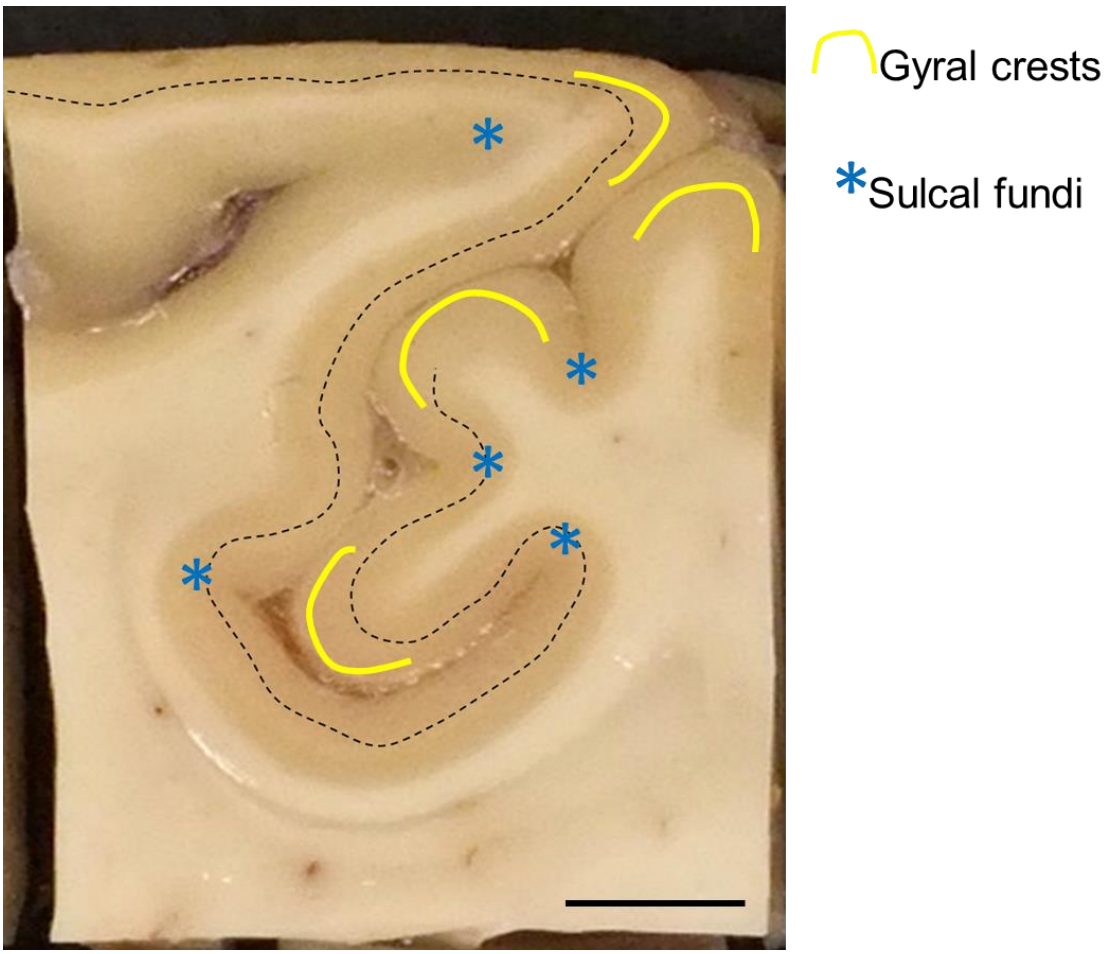


**Figure 4.4.** Neuroanatomical regions of interest. An example of a dissected tissue block depicting the regions of interest sulcal fundi (asterisks) and gyral crests (demi-circles) immunocytochemically evaluated. Dashed line indicates the location of the stria of Gennari. Scale bar = 5mm.

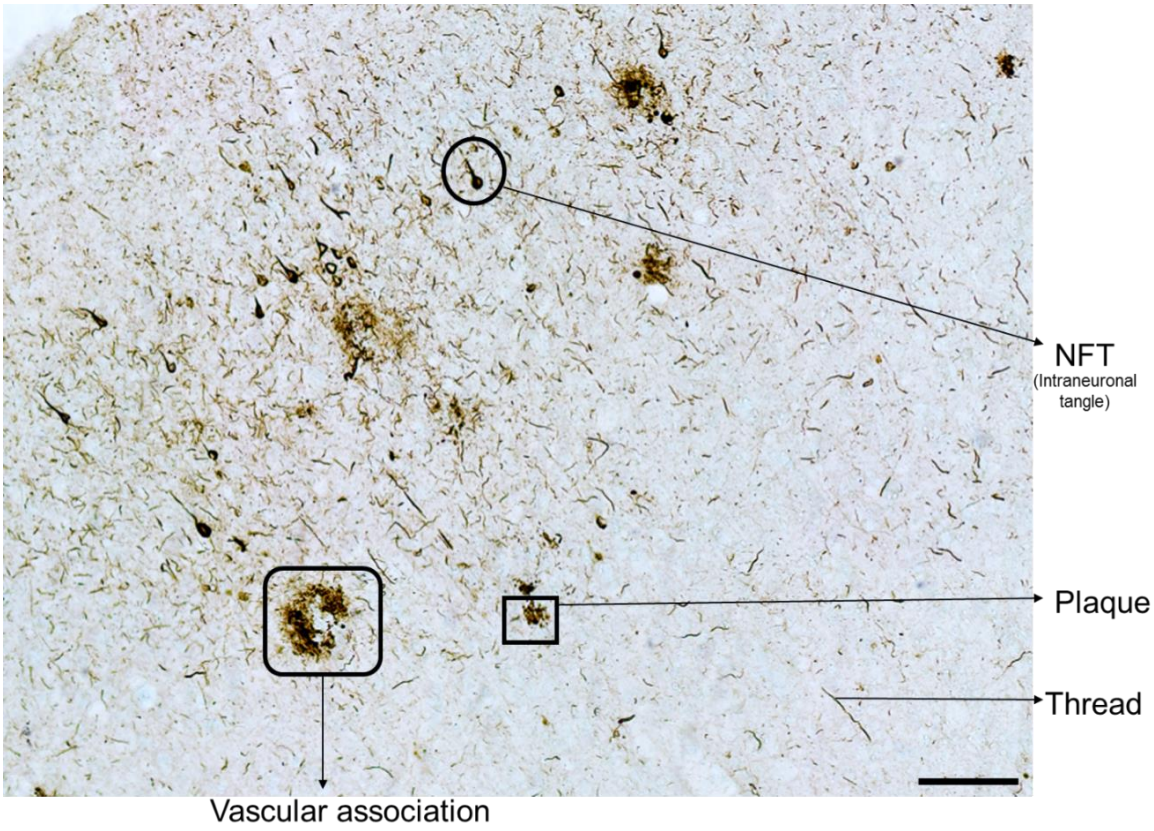


**Figure 4.5.** Section immunostained for CP13 indicating the four phenotypes of tau pathology semi-quantitatively evaluated. The CP13 antibody used was provided as a generous gift from Dr. Peter Davies. NFT = neurofibrillary tangle. Scale bar = 100µm.

**Table 4.3.** Tau pathology evaluated

| CP13 Phenotype | Description | Evaluation |
|---|---|---|
| Neurofibrillary tangle (NFT)* | Pre-tangles, intraneuronal tangles, extraneuronal tangles | 0 (Absent); 1+(1/10x field); 2+ (2-5/10x field); 3+ (6-9/10x field); 4+ (≥10/10x field) |
| Plaque* | Aggregated tau | 0 (Absent); 1+(1-9/10x field); 2+(10-19/10x field); 3+(20-32/10x field); 4+(≥33/10x field) |
| Threads* | Tau positive processes | 0 (Absent); 1+ (Sparse); 2+ (Moderate); 3+ (Dense) |
| Vascular Association | Clusters of NFTs, plaques, and threads apposed to vasculature cross sections | Comparison of the ratio of vessels associated with phosphorylated tau |

*Semi-quantitative scoring stratification modified from McKee et al., 2006

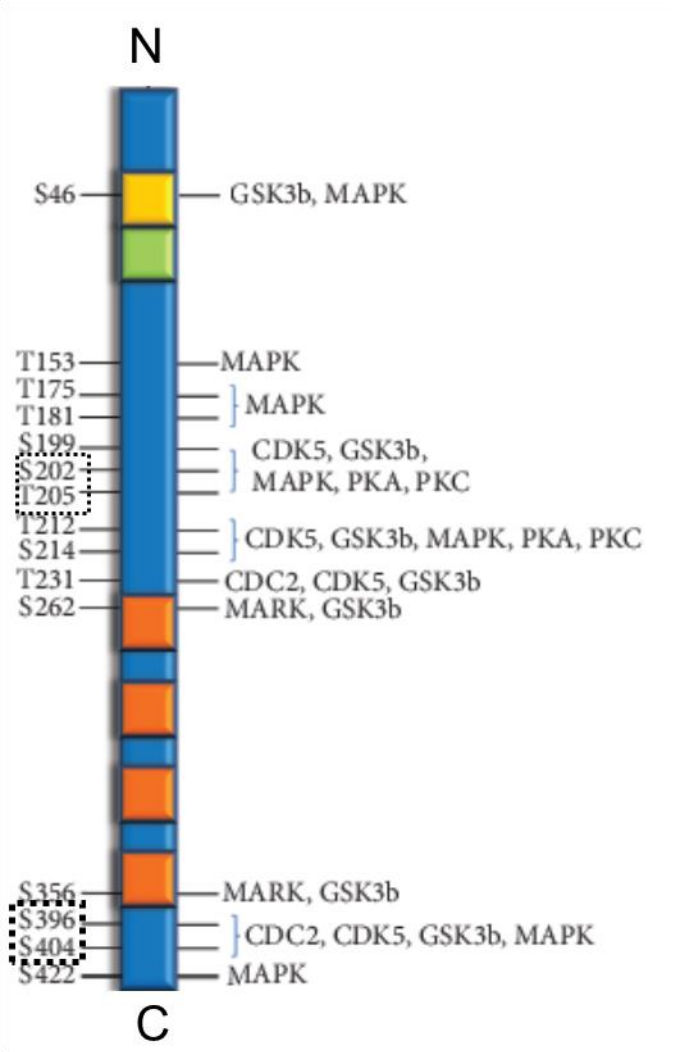


**Figure 4.6.** Schematic representation of key phosphorylation sites (left) in an arbitrary isoform of tau with the associated kinases (right). C = C terminal. CDK5 = cyclin dependent kinase 5. GSK3b = glycogen synthase 3 beta. MAPK = mitogen-activated protein kinase. MARK = Microtubule affinity-regulating kinase. N = N terminal. PKA = protein kinase A. PKC = protein kinase C. S = serine. T = threonine. Schematic adapted from Wolfe, 2012.

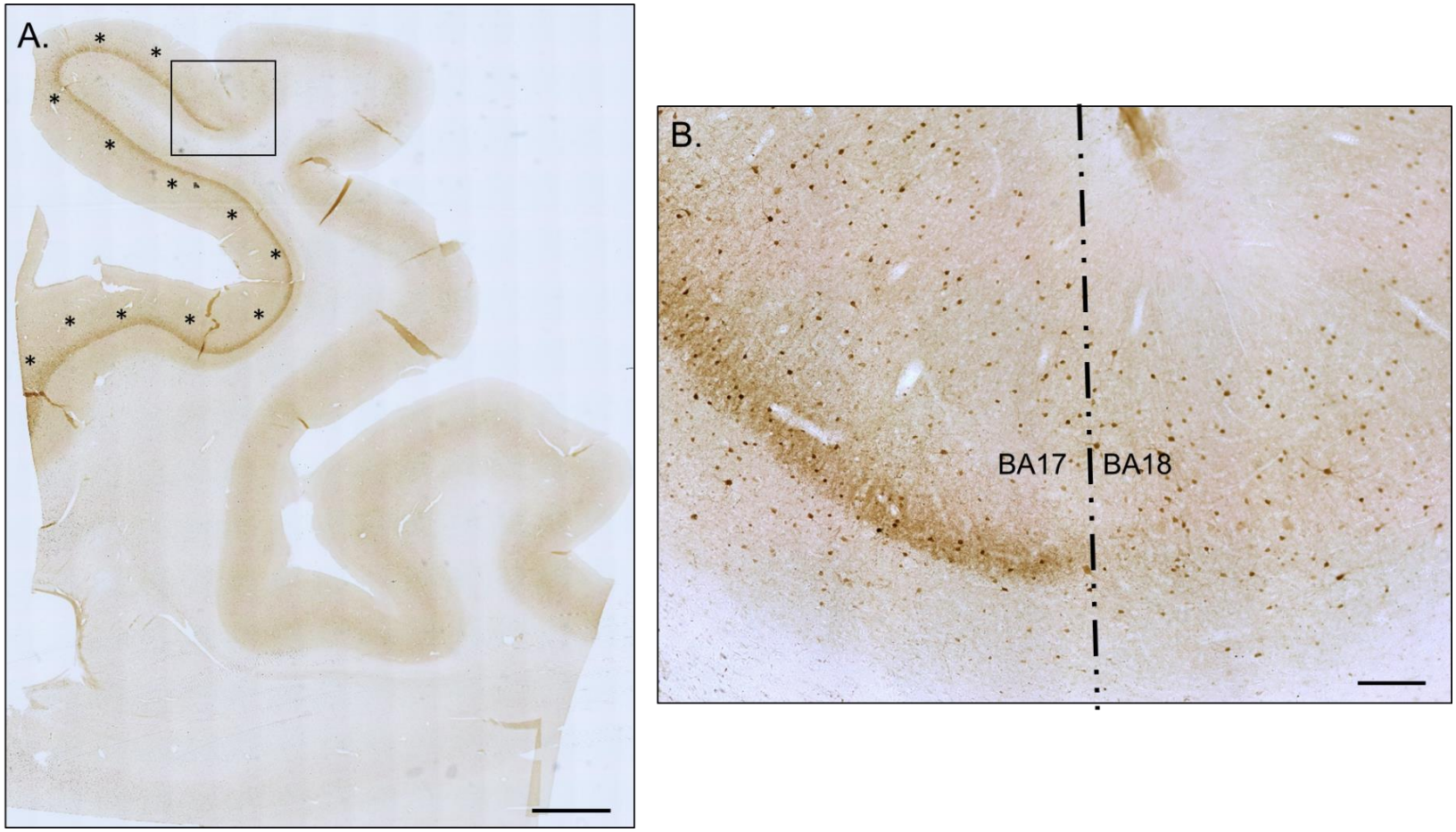


**Figure 4.7. A.** Low magnification of parvalbumin stained brain slice depicting the prominent stria of Gennari (asterisks), scale bar = 3mm **B.** Inset from (A) revealing the abrupt termination of the densely immunoreactive band unique to the primary visual cortex (BA 17), scale bar = 100µm. The dashed vertical line represents the border between BA17 and the adjacent BA18. BA = Brodmann area.

**Table 4.4.** Stereology parameters

| | |
|---|---|
| Counting Frame Area (XY) (µm²) | 14400.0 |
| Disector Height (Z) (µm) | 18.0 |
| Disector Volume (XYZ) (µm³) | 259200.0 |
| Guard Zone Distance (µm) | 2.0 |
| Counting Frame Width (X) (µm) | 120.0 |
| Counting Frame Height (Y) (µm) | 120.0 |
| Sampling Grid (X) (µm) | 838.0 |
| Sampling Grid (Y) (µm) | 666.0 |
| Sampling Grid Area (XY) (µm²) | 558108.0 |
| Section Evaluation Interval | 16 |

## RESULTS

### Effect of subject parameters

Parameters such as age, brain weight, and postmortem interval were evaluated on all 15 subjects to determine whether significant differences existed. The average age and standard deviation (SD) of control (n=7), stage 3 (n=4), and stage 4 (n=4) groups were 86 (SD 8.13), 76 (SD 6.39) and 69 (SD 5.43), respectively. There was a statistical difference in the average age of control versus stage 4 subjects ($F(2,12)=7.705$, $p=0.007$, Bonferroni post hoc analysis). Although a slight variation in brain weights existed, there were no statistically relevant correlations between brain weights and age ($R=-.190$, $n=15$, $p=.498$), health status ($F(2,12)=.433$, $p=.658$), postmortem interval ($R=-.210$, $n=14$, $p=.471$), or fixation duration ($R=.477$,$n=14$,$p=.084$) (Figure 4.6). Although one stage 3 subject had a substantially higher postmortem interval (120 hours), removal of this subject did not affect the correlation of brain weight and postmortem interval. Similarly, removal of the two outliers with fixation durations of 2 weeks did not result in a significant correlation between brain weight and fixation duration. The differences in postmortem interval did not differ significantly among groups ($F(2,11)=1.456$, $p=.275$) and were not correlated with the duration of fixation ($R=.212$, $n=13$, $p=.487$).

All of the CTE subjects were male and experienced repetitive head trauma from football. Interestingly, the overall duration of CTE symptoms were greater

among the stage 3 cohort compared to stage 4, (23.25 and 10.25 respectively) however the variation in symptom duration was greater among stage 3 (SD = 24.6) than the stage 4 (SD = 4.1). Of note is the fact that all of the stage 3 subjects played professional football whereas three of the four stage 4 subjects played college football and shared the same cause of death (dementia) (Table 4.2a).

**Tau pathology was present in visual association cortices despite sparing of the primary visual cortex**

The four phenotypes of tau pathology included: neurofibrillary tangles (NFTs), threads, plaques, and vascular association. Heat maps in Tables 4.5 and 4.6 summarize the four tau phenotypes in sulci (Table 4.5) and gyri (Table 4.6). With the exception of one control subject, whose health status was unknown, all four phenotypes of tau pathology were absent in sulci and gyri of control subjects. Overall there was an increase in tau pathology in BA 18 and BA 19. No tau pathology was observed in BA 17 for any of the subjects diagnosed with stage 3 CTE in either the sulci or gyri. However, 50% of the stage 4 CTE subjects had evidence of some tau pathology in both the sulci and gyri in BA 17. In BA 18, plaques, NFTs, and threads, were present in 75% of stage 4 subjects whereas only 25% of stage 3 cases showed evidence of pathology. In BA 19 all of the stage 4 CTE subjects had ≥ 10 tangles per 10x field whereas the scores for tangles present in the gyri in BA 19 varied from 1+ to 3+. The presence of vascular

associated pathology in BA 18 and BA 19 was in general highly varied in both stage 3 and stage 4 subjects. Vascular association of tau was present in 50% of the stage 4 cases to the same extent in both sulci and gyri.

**Average number of parvalbumin cells unaffected in advanced CTE**

No significance difference was observed in the mean density (cell count/$mm^3$) of cells immunocytochemically labeled for the calcium-binding protein parvalbumin (Figure 4.9) within sulci and gyri of the primary visual cortex (sulci, $F(2,11)=.896$, $n=14$, $p=.436$; gyri $F(2,11)=.757$, $n=14$, $p=.492$) or extrastriate cortex (sulci, $F(2,11)=.888$, $n=14$, $p=.439$; gyri $F(2,11)= 3.008$, $n=14$, $p=.091$) of control, stage 3 and stage 4 subjects (Figure 4.10).

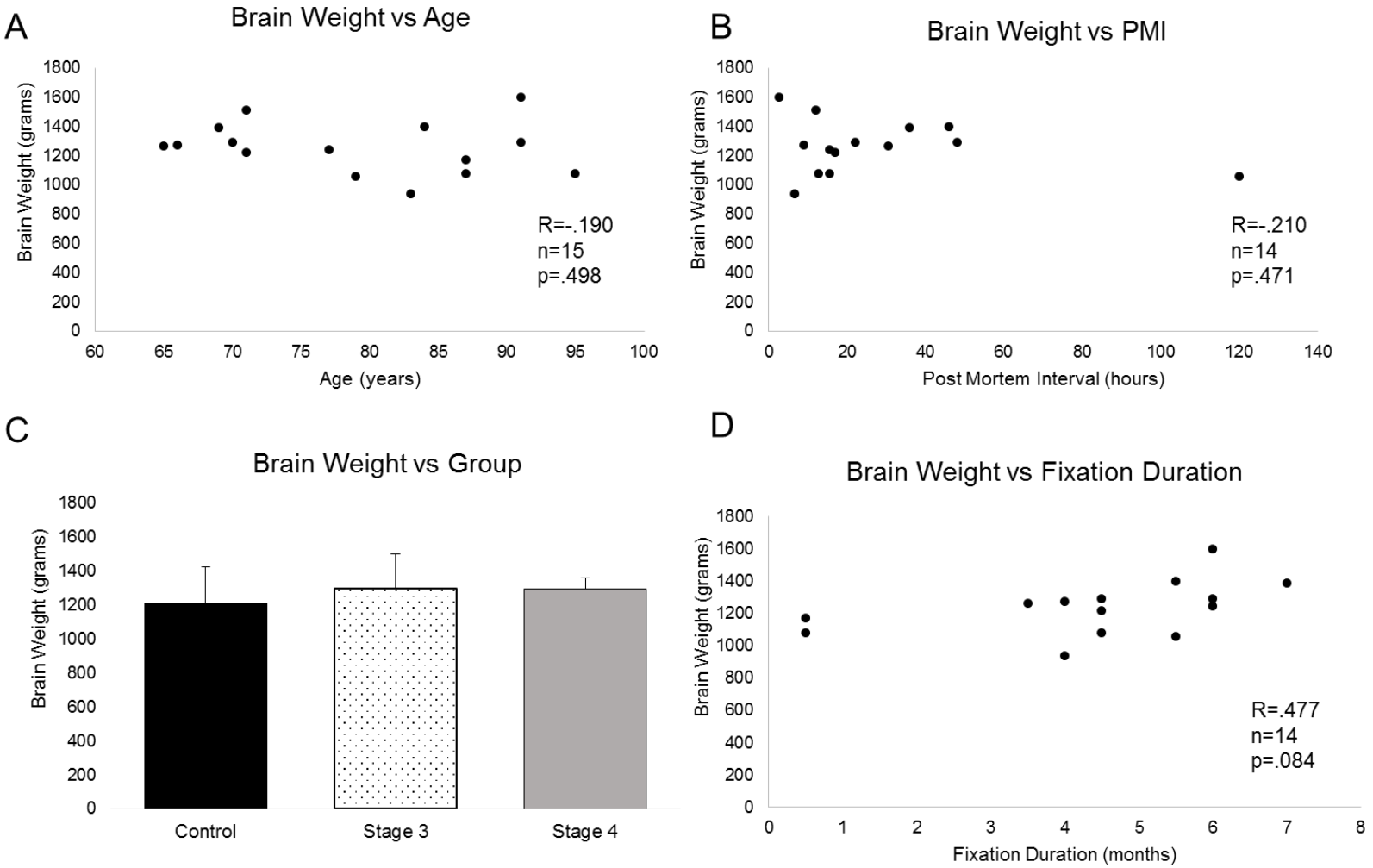


**Figure 4.8.** Differences in brain weights were not correlated with age (**A**), PMI (**B**), group (**C**), or duration of fixation (**D**). Error bars in (**C**) represent SD (control = 7, stage 3 = 4, stage 4 = 4). PMI = postmortem interval.

**Table 4.5** Heat map of phosphorylated tau pathology within the depths of sulci across brain regions

| | | Plaques | | | NFTs | | | Threads | | | Vascular Association | | |
|---|---|---|---|---|---|---|---|---|---|---|---|---|---|
| **Coded Subject** | **Group** | BA17 | BA18 | BA19 | BA17 | BA18 | BA19 | BA17 | BA18 | BA19 | BA17 | BA18 | BA19 |
| 1 | Control | 0 | 0 | 0 | 0 | 0 | 0 | 0 | 0 | 0 | 0 | 0 | 0 |
| 2 | Control | 0 | 0 | 0 | 0 | 0 | 0 | 0 | 0 | 0 | 0 | 0 | 0 |
| 3 | Control | 0 | 0 | 0 | 0 | 0 | 0 | 0 | 0 | 0 | 0 | 0 | 0 |
| 4 | Control | 0 | 0 | 0 | 0 | 0 | 0 | 0 | 0 | 0 | 0 | 0 | 0 |
| 5 | Control | 0 | 0 | 0 | 0 | 0 | 0 | 0 | 0 | 0 | 0 | 0 | 0 |
| 6 | Control | 1 | 1 | 3 | 1 | 1 | 4 | 1 | 1 | 2 | 9 | 0 | 27 |
| 7 | Control | 0 | 0 | 0 | 0 | 0 | 0 | 0 | 0 | 0 | 0 | 0 | 0 |
| 8 | CTE Stage 3 | 0 | 0 | 0 | 0 | 0 | 0 | 0 | 0 | 0 | 0 | 0 | 0 |
| 9 | CTE Stage 3 | 0 | 2 | 3 | 0 | 4 | 4 | 0 | 1 | 1 | 0 | 9 | 29 |
| 10 | CTE Stage 3 | 0 | 0 | 1 | 0 | 0 | 1 | 0 | 0 | 1 | 0 | 0 | 6 |
| 11 | CTE Stage 3 | 0 | 0 | 1 | 0 | 0 | 4 | 0 | 0 | 1 | 0 | 0 | 26 |
| 12 | CTE Stage 4 | 2 | 2 | 1 | 4 | 4 | 4 | 1 | 2 | 2 | 19 | 11 | 13 |
| 13 | CTE Stage 4 | 0 | 1 | 1 | 0 | 4 | 4 | 0 | 1 | 2 | 0 | 0 | 27 |
| 14 | CTE Stage 4 | 1 | 1 | 1 | 2 | 4 | 4 | 1 | 2 | 2 | 17 | 17 | 18 |
| 15 | CTE Stage 4 | 0 | 0 | 0 | 0 | 0 | 4 | 0 | 0 | 2 | 0 | 0 | 0 |

**Table 4.6.** Heat map of phosphorylated tau pathology within gyral crowns across brain regions

| | | Plaques | | | NFTs | | | Threads | | | Vascular Association | | |
|---|---|---|---|---|---|---|---|---|---|---|---|---|---|
| **Coded Subject** | **Group** | BA17 | BA18 | BA19 | BA17 | BA18 | BA19 | BA17 | BA18 | BA19 | BA17 | BA18 | BA19 |
| 1 | Control | 0 | 0 | 0 | 0 | 0 | 0 | 0 | 0 | 0 | 0 | 0 | 0 |
| 2 | Control | 0 | 0 | 0 | 0 | 0 | 0 | 0 | 0 | 0 | 0 | 0 | 0 |
| 3 | Control | 0 | 0 | 0 | 0 | 0 | 0 | 0 | 0 | 0 | 0 | 0 | 0 |
| 4 | Control | 0 | 0 | 0 | 0 | 0 | 0 | 0 | 0 | 0 | 0 | 0 | 0 |
| 5 | Control | 0 | 0 | 0 | 0 | 0 | 0 | 0 | 0 | 0 | 0 | 0 | 0 |
| 6 | Control | 3 | 1 | 1 | 1 | 2 | 1 | 1 | 1 | 1 | 8 | 18 | 0 |
| 7 | Control | 0 | 0 | 0 | 0 | 0 | 0 | 0 | 0 | 0 | 0 | 0 | 0 |
| 8 | CTE Stage 3 | 0 | 0 | 0 | 0 | 0 | 0 | 0 | 0 | 0 | 0 | 0 | 0 |
| 9 | CTE Stage 3 | 0 | 2 | 1 | 0 | 4 | 1 | 0 | 1 | 1 | 0 | 14 | 2 |
| 10 | CTE Stage 3 | 0 | 0 | 1 | 0 | 0 | 1 | 0 | 0 | 1 | 0 | 0 | 0 |
| 11 | CTE Stage 3 | 0 | 0 | 1 | 0 | 0 | 0 | 0 | 0 | 0 | 0 | 0 | 3 |
| 12 | CTE Stage 4 | 1 | 3 | 1 | 2 | 4 | 3 | 1 | 2 | 3 | 14 | 26 | 33 |
| 13 | CTE Stage 4 | 0 | 1 | 1 | 0 | 4 | 1 | 0 | 1 | 1 | 0 | 23 | 13 |
| 14 | CTE Stage 4 | 1 | 1 | 1 | 1 | 4 | 2 | 1 | 2 | 2 | 15 | 28 | 18 |
| 15 | CTE Stage 4 | 0 | 0 | 0 | 0 | 0 | 2 | 0 | 0 | 2 | 0 | 0 | 42 |

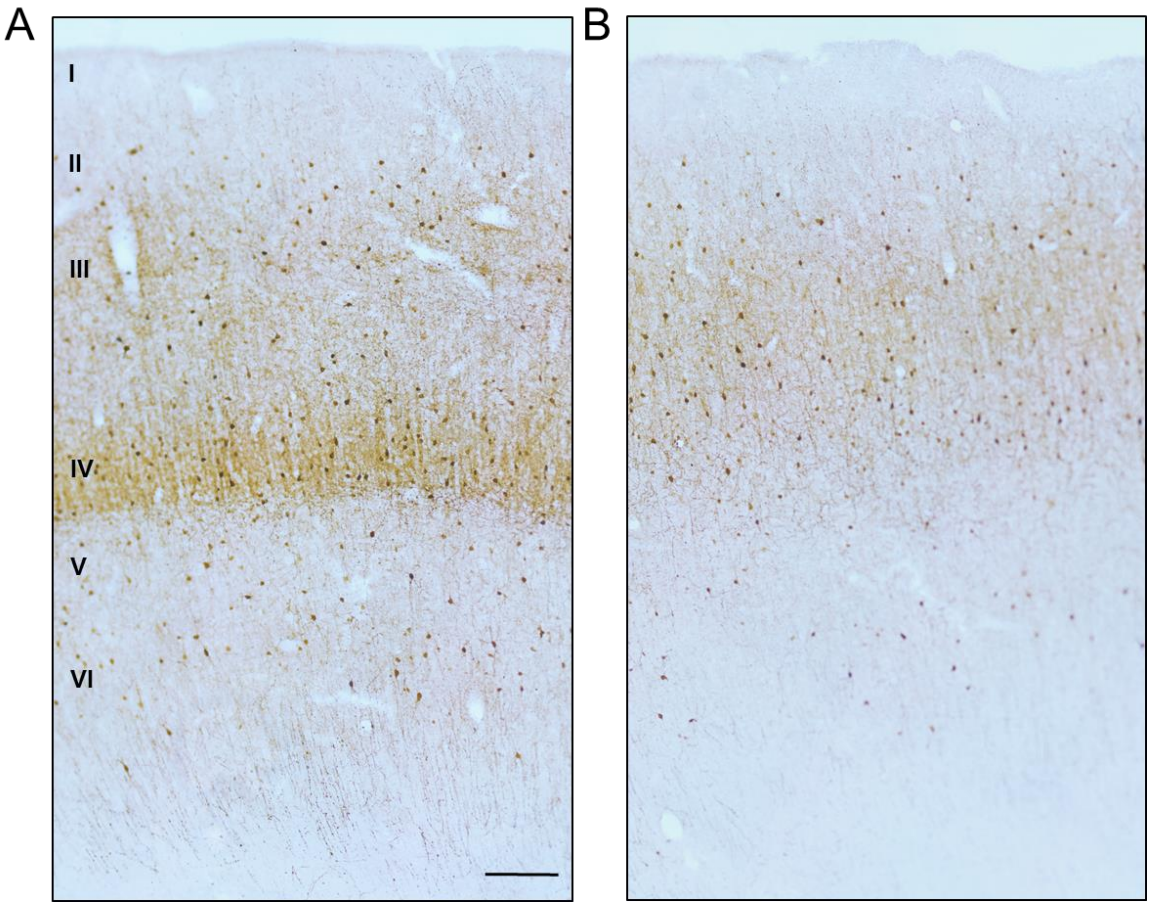


**Figure 4.9.** Low magnification of parvalbumin in primary visual cortex (**A**) and extrastriate cortex (**B**). Roman numerals in (A) denote cortical layers. Scale bar = 100µm.

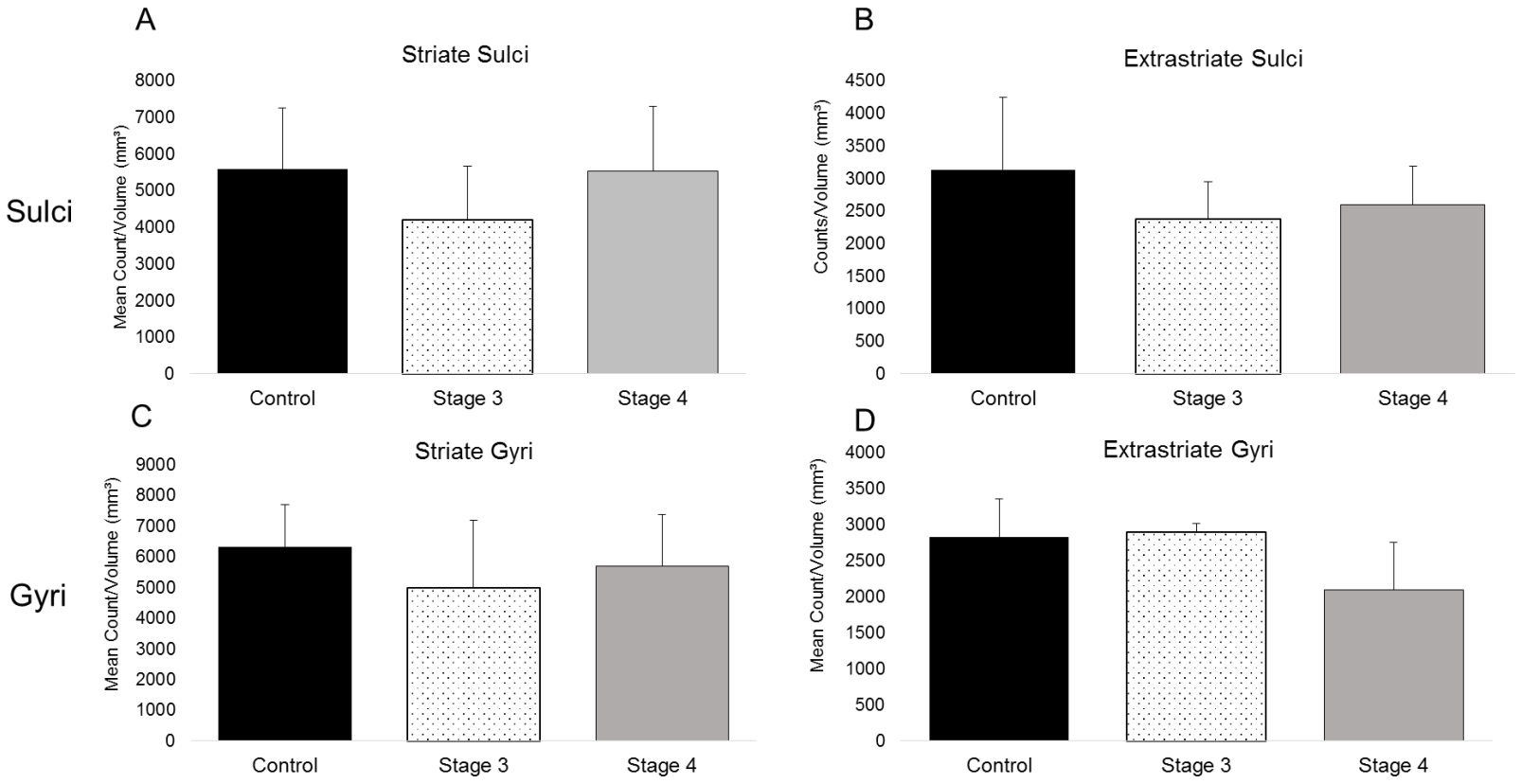


**Figure 4.10.** There was no change in the average number of parvalbumin positive cells within the sulci and gyri in the primary visual cortex (striate) (**A** and **C**) or visual association cortex (extrastriate) (**B** and **D**). Error bars represent SD (control = 7, stage 3 = 4, stage 4 = 4).

## DISCUSSION

No change in the overall number of cells immunoreactive for parvalbumin was apparent in the sulci or gyri in BA 17 and BA 19. However, semi-quantitative analyses revealed a progressive increase in tau pathology in BA 18 and BA 19, despite sparing of primary visual cortex, BA 17. Although a similar progressive trend was apparent, the extent of tau pathology, particularly NFTs and tau positive processes, was greatest in the sulci. As expected, the general increase in tau pathology correlated with advancing CTE stage.

### Tau pathology in the visual cortex of neurodegenerative diseases

The results of this study are similar to previous studies reporting that the visual cortex is largely spared tau pathology in CTE (McKee et al., 2013) and AD (McKee et al., 2006). It has been speculated that the medial location of the primary visual cortex is likely to underlie sparing, particularly in CTE.

Visual cortices are not among the common brain regions examined in the postmortem diagnosis of CTE. It is believed that the presence of pathological lesions in the visual cortex occurs during the last stages of the disease or early on in the most severe forms (McKee et al., 2006; McKee et al., 2013). Although tau pathology is often largely absent in the primary visual cortex, visual association areas are vulnerable (Pikkarainen et al., 2009). Work by Braak reported a striking increase in NFTs when transitioning from striate to parastriate cortex (BA 17 to BA

18) and from parastriate to peristriate cortex (BA 18 to BA 19) (Braak et al., 1989). Similarly, in this study, progressing from the primary visual cortex to visual association areas, there was an increase in the extent of the tau pathology present. Although the small sample size precludes the power needed to robustly analyze the correlation of pathology across brain regions, there is sufficient preliminary evidence to support a more detailed examination with a larger sample size.

The primary visual cortex is a well-characterized brain region that is most easily identified by the myelinated band of axons in layer 4 (stria of Gennari). It represents a pivotal point in the visual pathway, where information received from the lateral geniculate nucleus is organized and distributed to higher order visual association regions (Nolte and Sundsten, 2002). Less is known regarding visual processing in association cortices. However, the higher metabolic demands, and differences in proximity to vascular supplies are speculated to render this region susceptible to pathology in disease states (McKee et al., 2006). Based on the perivascular presence of pathological tau it is possible that some of the visual impairments reported in CTE could result from the pathology in the visual association cortex. However, additional work is needed to document the status of cells and the presence of tau co-localization in these visual association regions.

**Parvalbumin in neurodegeneration and TBI**

The vulnerability of parvalbumin cells in neurodegeneration is still somewhat inconsistent. Several neurodegenerative studies have reported no change in the overall number of parvalbumin cells in diseases such as AD (Hof et al., 1991; Iwamoto and Emson, 1991; Ferrer et al., 1993; Leuba et al., 1998), frontotemporal dementia, and Pick's disease (Arai et al., 1991). However, other studies have found subtle changes in parvalbumin cells. For example, one study found a small percentage (4%) of parvalbumin cells that co-localized with tau compared to 20–31% of pyramidal cells (Iwamoto and Emson, 1991). There are several explanations that could account for the stability of parvalbumin positive interneurons. However, the simplest explanation may relate to their size. Parvalbumin positive neurons are approximately 10 µm in diameter (Blumcke et al., 1990) which is noticeably smaller than the larger projection neurons that are likely to be more vulnerable to the DAI occurring from repetitive trauma. Analysis of the pyramidal cells containing NFTs suggests that smaller cells are less likely to accumulate tau. There have also been reports of significant losses of parvalbumin positive cells (Arai et al., 1987; Satoh et al., 1991). Although some studies reported no overall changes in parvalbumin cells, there can be subtle losses in specific cortical layers despite no change in total cell number (Leuba et al., 1998). In addition, dystrophic and degeneration of processes have been reported (Ferrer et al., 1993).

Despite the stability of parvalbumin cells in the visual cortices in this study, the evaluation of parvalbumin in brain regions highly vulnerable to damage in CTE would be of interest as calcium ions affect the production and release of neurotransmitters, axonal transport and neuronal excitability (Arai et al., 1991). Calcium-binding proteins such as parvalbumin have been shown to play an integral role buffering and redistributing intracellular calcium (Arai et al., 1991). Although dysregulation of calcium in TBI and neurodegenerative disorders such as AD has been widely published (Bezprozvanny and Mattson, 2008; Wojda et al., 2008), no CTE study to date has examined potential changes in the immunoreactivity of parvalbumin, or any other calcium-binding protein.

The present lack of detectable changes in the number of parvalbumin neurons indicates that any effect of CTE on GABAergic neurons is not universal. It is unknown whether cells containing parvalbumin are uniquely spared. One possibility is parvalbumin's unique role as a powerful calcium-binding protein (Marambaud et al., 2009). Perhaps over time increases in the amount of intracellular calcium ions, either due to transient perforations in cells or disrupted intracellular stores from the mild and repetitive brain injuries could be resolved by the buffering and binding of calcium-binding proteins within the cell. Thus, at the onset of CTE symptoms cell types that do not possess the capacity to mitigate the cascades that result from mechanisms associated with ion toxicity could be vulnerable in the disease state.

A more detailed examination of potential cell-specific vulnerability perhaps in other sub-classes of GABAergic neurons across all four clinical stages of CTE within different brain regions will be useful in future studies. It is becoming increasingly evident that GABAergic neurotransmission is affected in neurodegeneration (Abbas et al., 2016; Palop and Mucke, 2016). Alterations in GABAergic networks may either play a primary role or may result from aberrations in excitatory signaling (Li et al., 2016). Although the results of this study revealed no change in the number of parvalbumin immunoreactive cells in the primary visual cortex and visual association cortex, it will be essential for future studies to examine whether there are alterations in GABAergic receptors in the sulci and gyri of primary and associative visual cortices that are affected in CTE. In addition to histopathological evaluations, assessing the functional status of interneurons, despite their apparent resistance, will also be of value especially in the development of therapeutic targets to mitigate the onset and progression of CTE and related tauopathies.

# CHAPTER 5

# DISCUSSION

## Summary

Most of the animal models to date used to study TBI employ invasive methods that result in moderate and severe damage. However, mild TBI accounts for the majority of all injuries and has been associated with CTE. Few studies have probed the region-specific status of specific cell populations following mild blast exposures in animal models and none have examined vulnerability of specific interneuronal populations in CTE. Therefore, the results of this work offer valuable insight regarding region-specific vulnerability to mild blast and advanced CTE.

## Technical considerations in animal models of blast

The extent of injury due to blast exposure has been associated with the magnitude and duration of pressure experienced (Svetlov et al., 2009; Kuehn et al., 2011; Rosenfeld et al., 2013; Mishra et al., 2016). However, as stated in the introduction (Chapter 1), there can be different outcomes due to differences in model construction (Koliatsos et al., 2011; Hines-Beard et al., 2012; Heldt et al., 2014), the presence of anesthetics (Kawaguchi et al., 2005; Statler et al., 2006; Rowe et

al., 2013), the animals used (Xiong et al., 2013), the orientation to blasts (DeMar et al., 2016; Guley et al., 2016), and the time points examined following insults.

To overcome the glaring anatomical differences and relate the injuries experienced by rodents with humans scaling laws have been developed (O'Connor et al., 2011; Jean et al., 2014; Wang et al., 2014). However, there remains considerable variability among studies and although head acceleration does appear to affect injury outcome some question the complications it may exert (Gullotti et al., 2014). To carefully account for the contributions of head accelerations high-speed cameras capturing movement of the animal during primary blast exposure, and kinematic calculations are necessary. Despite careful attention to such details without implanted tissue sensors, the full extent of head mobility is not always possible. Thus, although blast models offer considerable clinical relevance to injuries sustained in special risk groups, there are inherent limitations that may not be possible to fully resolve in animal models of blast.

*Direct cranial blast model technical considerations*

The rodent model of direct cranial blast used in this work was adapted from a previous blast protocol using anesthetized rats (Kuehn et al., 2011). The average maximum blast pressure recorded in this study was 1,034 kPa, which differed greatly from the 515 kPa reported by Kuehn and colleagues. Calibration of the COBIA used a sensor with a 100 kHz maximum sampling frequency. To get a

sense of how the blast wave would have been altered over a larger area, analogous to the dorsal surface of the animal two filters, 2kHz and 12kHz, were used. Both filters were based on methodologies used in two previously published blast studies. The 12 kHz filter was used to more directly compare to the pressure reported by Kuehn and associates in their COBIA validated in rats (Kuehn et al., 2011). The pressures filtered at 12 kHz resulted in a notably lower mean pressure of 322 kPa, which was more comparable to the 515 kPa reported by Kuehn et al. Use of the 2kHz filter resulted in an average pressure of 178 kPa which was similar to the 77kPa reported by Goldstein et al. (2012) following a 2-kHz low pass filter in a shock tube model of mild blast injury in mice. Aside from the difference in blast source (modified nail gun versus shock tube) and animals used (rats versus mice), the presence of head movement is a key difference. In the direct cranial blast model anesthetized rats were immobilized under the COBIA whereas animals in the study conducted by Goldstein et al., were not. In spite of these differences based on the similarities among the magnitude of blast pressures when various frequency filters were applied, and the subtle structural changes observed in blast exposed mice compare to sham, the blast pressures used in this work were considered to recapitulate mild blast(s).

As additional studies focused on blast injury emerges the motivation, to ensure the appropriate application and interpretation of results remain (Panzer et al., 2012; Panzer et al., 2014). A key question that has been posed is whether unrealistic blasts that cause considerable damage in animal models are relevant

to humans (Panzer et al., 2014). Figure 5.1 provides a visual comparison of how the blast pressures used in this study may compare with those previously reported. Based on the peak pressure and scaled duration, the blasts used in this study are within the range of realistic blast exposure. The fact that the blasts in this study are at the low end of the range of realistic blasts further supports the fact that despite a large incident pressure the results obtained simulate responses to mild blasts. It is important to note, however, that all of the studies displayed in Figure 5.1 (modified from work by Panzer et al. in 2014) used a shock tube. In addition, of interest is the fact that several of the reported studies highlighted (Saljo et al., 2010; Cernak et al., 2011; Goldstein et al., 2012; Vandevord et al., 2012) were cited as outside the range of realistic blast exposure.

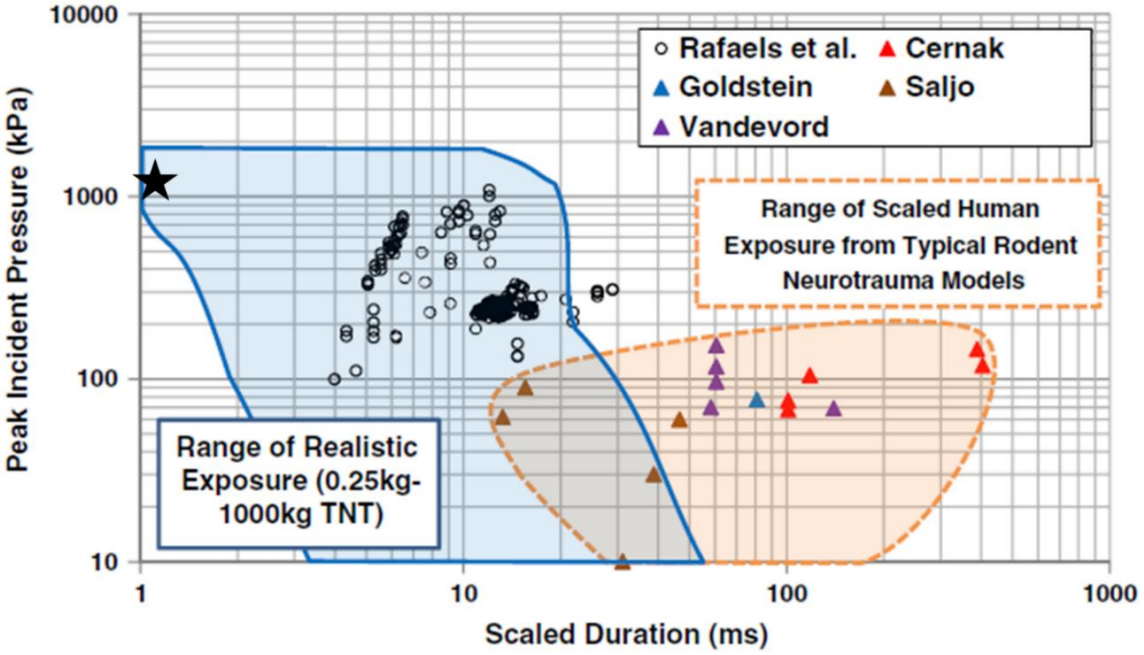


**Figure 5.1.** Comparisons of peak incident pressure versus scaled durations for multiple animal models of TBI due to blast from studies employing shock tubes. The shaded blue region (left) depicts the range of realistic blast exposures while the area enclosed by the dashed orange line (right) depicts published studies whose scaled human exposures are outside of the estimated range of realistic blasts. The black star represents the exposure believed to be represented in the present work despite differences in apparatus used (COBIA used in this study versus shock tube). Image modified from Panzer et al., 2014.

*Blast Intervals in a repetitive injury paradigm*

An important component of this work was the incorporation of multiple blasts. Within the last decade, it has become increasingly evident that incorporating exposure to multiple blasts can offer better insight into TBI pathology as injuries to soldiers and civilians are often due to repetitive insults (Wang et al., 2011). The increased vulnerability following multiple insults is believed to result from a combination of reduced injury thresholds and increased severity of injury due to incomplete cellular recovery between insults (Wang et al., 2011; Gao et al., 2017).

Although repetitive injury paradigms have considerable clinical relevance, there is significant variability among the insult intervals (Wang et al., 2011; Bolton and Saatman, 2014; Lynch et al., 2016; Ferguson et al., 2017). One study evaluated damages sustained from repeated injuries that occurred minutes apart (Wang et al., 2011) while others report injury intervals ranging from 24 to 48 hours (Bolton and Saatman, 2014; Lynch et al., 2016). The choice to utilize a 24 hour latency between blasts was based on a previously published CCI model in mice (Bolton and Saatman, 2014). Behavioral assessments (righting reflexes) and histopathology results comparing a single mild insult to multiple impacts (n=5) with 24 and 48 hour intervals revealed increased gliosis and neurodegeneration when injuries occurred 24 hours apart (Bolton and Saatman, 2014). However, the results of this study did not reveal evidence of a dose response in the neuronal and glial populations examined. One explanation is that the optimal interval to study the effect of repetitive insults could depend on the mode of injury. Most of the published

reports of repeated trauma are based on cortical impact models (Wang et al., 2011; Bolton and Saatman, 2014; Ferguson et al., 2017). Although the reproducibility of impact models is an advantage, they can be invasive and often involve use of anesthetics. In addition, the mechanism of focal trauma versus diffuse axonal injury due to shearing and stretching of neurons during blast compared to impact may effect on injury progression. Therefore, the results of this study provide useful and novel insight into the effect of mild blasts directed onto the dorsal surface of the cranium in unanesthetized wild-type mice.

Although the immunocytochemical evaluation regarding how and where cells seem to be affected following mild blast injury left many questions, the novelty of this blast model adapted for use in mice and the results of this study do provide a good starting point for future studies.

**Considerations for future studies**

*Aim 1: Immunocytochemical evaluation of neuronal and glial responses in the mouse hippocampus following single and repeated blast exposures.* (Chapter 2)

The subtle anatomical alterations reported in this study reveal a unique region specific response in the hippocampus. Glial alterations were observed following acute recovery to both a single and repeated blasts. However, it is possible that the full extent of the pathologies produced by the short duration of blast may have

resolved between the 24 hour intervals or within the recovery windows examined.

It would be of great interest for future studies to identify whether hypertrophic microglia are restricted to the outer molecular layer at more acute time points (minutes to hours) or whether hypertrophic cells are initially widespread within the hippocampus and become limited to the outer molecular layer of the dentate gyrus. There was no positive immunostaining with known pathological glial mediators. Additional efforts to identify the nature of the glial hypertrophy (neuroprotective versus neurotoxic) are warranted.

Although the glial results of this aim provided the greatest evidence of a cellular response, collaborative work using *in vivo* calcium imaging within $CA_1$ showed a decrease in intracellular calcium (data not shown). This decrease was evident in individual cells as well as an overall reduction in spike activity (data not shown). The occurrence of such pronounced yet subtle changes could provide a basis for more detailed work regarding the specific cell populations affected. It would also be valuable to incorporate molecular techniques to provide insight regarding potential changes in gene expression following acute and chronic exposures following mild blast.

*Aim 2: Immunocytochemical examination of glial morphologies following exposure to mild repetitive blasts in the brain and retina.* (Chapter 3)

Most of the blast-related studies reporting retinal pathology have used models of direct ocular injury (blasts directed onto the eye), rather than the cranium (Choi et al., 2014; Bricker-Anthony et al., 2016; DeMar et al., 2016). The absence of hypertrophic glia in this study suggest that either the blast pressures, recovery time points, and/or animal orientation with respect to blast, were insufficient to result in glial activation within major visual structures. Although this study did not specifically evaluate the status of neurons within the retina, collaborative work evaluating the functional integrity of the retina using electroretinograms detected only slight decreases in scotopic responses (contrast sensitivity), one month following exposure to a single blast (data not included). In addition, there were slight decreases in the density of retinal ganglion cells one month following a single blast (data not included). However, even with increased sample sizes, the level of variability between blast and sham groups did not result in statistically significant changes.

Although the mouse retina projects to approximately 46 different brain regions (Morin and Studholme, 2014) only 3 regions (DLG, SC, and visual cortex) were examined in this study. Similar to the retina, no structural changes in glia were observed in the central visual brain regions examined. However, it would be

worthwhile to evaluate potential changes in the functionality of the retina and central visual regions at more acute time points.

It is parsimonious to assume the blasts were insufficient to cause damage or that cellular recovery had occurred by the time points examined. However, the lack of change in both the numbers and appearances of the neurons containing the calcium-binding proteins calretinin and parvalbumin could partially result from a cell-specific resistance to mild blasts. Evaluation of receptors or synaptic proteins may detect subtle neurochemical and anatomical changes following mild blasts. In addition, simple behavioral tests to assess subtle physiological impairments, such as the righting reflex used to assess basic sensory and motor functionality, would be beneficial to correlate with the immunocytochemical results.

*Aim 3: Immunocytochemical evaluation of tau pathology and parvalbumin within visual cortices in advanced chronic traumatic encephalopathy.* (Chapter 4)

The only CTE study to date that evaluated tau pathology within a central visual pathway was work by Armstrong and colleagues (Armstrong et al., 2017). Their results indicated that the tau pathology preferentially affected the intermediate and lower regions of the superior colliculus suggesting motor abnormalities rather than sensory deficits. However, visual impairments are reported in approximately 60% (McKee, 2016) of CTE sufferers and there are no studies that have evaluated the

visual cortex beyond the primary visual cortex. It is likely that the absence of tau pathology in the primary visual cortex, except in the most severe cases (McKee et al., 2013) has motivated efforts to focus on more vulnerable brain regions. However, the presence of tau pathology in visual association areas in this study provides an impetus to explore, in greater detail with a larger sample size, how the central visual pathways may be affected during the course of the disease.

Previous work presented at the Association for Research in Vision and Ophthalmology indicated preliminary evidence of tau aggregates in the retinas of patients diagnosed with CTE (McKee, 2015). It was speculated that the tau present in the retina may be an early diagnostic feature of CTE. Although CTE is distinct from other neurodegenerative disorders, the similarities it shares with AD could help direct future studies. For example, retinal pathology has been reported in AD. Interestingly, the retinal pathology present in AD cases has been reported to precede brain pathology, particularly in the early stages (Kirbas et al., 2013). Therefore it is possible that the retina could serve as a useful proxy in CTE, especially due to the delayed onset of symptoms (Mez et al., 2015). Future studies to systematically examine the progression of tau pathology in the retina and central visual pathways across all four clinical stages of CTE will undoubtedly be of value.

The cross-sectional nature of early CTE studies represented a limitation in the field. However, the correlation of radioactive deposits from functional brain imaging studies (which often lack the resolution with histopathology) has enabled considerable progress in the field to date. Use of positron emission tomography

(PET) imaging has shown promise in detecting brain aggregates whose spatial pattern is analogous to the histological patterns of hyperphosphorylated tau observed postmortem (Barrio et al., 2015). In addition, there have been reports detailing a genetic component because not all individuals with histories of repetitive head trauma will develop CTE (Mez et al., 2013).

The number of parvalbumin cells in this study did not differ between control subjects and those with advanced CTE, in either the primary visual cortex or visual association areas. It is possible that parvalbumin cells are spared from tau pathology. Although large projection neurons have a higher likelihood of tau accumulation, a more comprehensive characterization of the potential vulnerability of different laminar regions and potential changes in other interneuronal populations is warranted. For example, although the primary visual cortex is largely spared from CTE pathology, it would be worthwhile to explore in detail whether cells forming the stria of Gennari, which receives and integrates thalamic input is affected. Furthermore, as discussed in Chapter 4, evaluation of cellular markers to detect subtle changes such as surface receptors and synapses in cells that appear spared would be advantageous.

## BIBLIOGRAPHY

Abbas G, Mahmood W, Kabir N. 2016. Recent progress on the role of GABAergic neurotransmission in the pathogenesis of Alzheimer's disease. Reviews in the Neurosciences 27(4):449–455.

Abdul-Muneer PM, Schuetz H, Wang F, Skotak M, Jones J, Gorantla S, Zimmerman MC, Chandra N, Haorah J. 2013. Induction of oxidative and nitrosative damage leads to cerebrovascular inflammation in an animal model of mild traumatic brain injury induced by primary blast. Free Radical Biology & Medicine 60:282–291.

Adrian H, Marten K, Salla N, Lasse V. 2016. Biomarkers of Traumatic Brain Injury: Temporal Changes in Body Fluids. eNeuro 3(6).

Aertker BM, Bedi S, Cox CS, Jr. 2016. Strategies for CNS repair following TBI. Experimental Neurology 275 Pt 3:411–426.

Almeida-Suhett CP, Prager EM, Pidoplichko V, Figueiredo TH, Marini AM, Li Z, Eiden LE, Braga MF. 2015. GABAergic interneuronal loss and reduced inhibitory synaptic transmission in the hippocampal CA1 region after mild traumatic brain injury. Experimental Neurology 273:11–23.

Alvarez TL, Kim EH, Vicci VR, Dhar SK, Biswal BB, Barrett AM. 2012. Concurrent vision dysfunctions in convergence insufficiency with traumatic brain injury. Optometry and Vision Science 89(12):1740–1751.

Amunts K, Malikovic A, Mohlberg H, Schormann T, Zilles K. 2000. Brodmann's areas 17 and 18 brought into stereotaxic space-where and how variable? Neuroimage 11(1):66–84.

Amunts K, Zilles K. 2015. Architectonic Mapping of the Human Brain beyond Brodmann. Neuron 88(6):1086–1107.

Andersen P. 2007. The hippocampus book. Oxford ; New York: Oxford University Press.

Anderson MA, Ao Y, Sofroniew MV. 2014. Heterogeneity of reactive astrocytes. Neuroscience Letters 565:23–29.

Andriessen TM, Jacobs B, Vos PE. 2010. Clinical characteristics and pathophysiological mechanisms of focal and diffuse traumatic brain injury. Journal of Cellular and Molecular Medicine 14(10):2381–2392.

Arai H, Emson PC, Mountjoy CQ, Carassco LH, Heizmann CW. 1987. Loss of parvalbumin-immunoreactive neurones from cortex in Alzheimer-type dementia. Brain Research 418(1):164–169.

Arai H, Noguchi I, Makino Y, Kosaka K, Heizmann CW, Iizuka R. 1991. Parvalbumin-immunoreactive neurons in the cortex in Pick's disease. Journal of Neurology 238(4):200–202.

Armstrong RA, McKee AC, Cairns NJ. 2017. Pathology of the Superior Colliculus in Chronic Traumatic Encephalopathy. Optometry and Vision Science 94(1):33–42.

Atkins CM. 2011. Decoding hippocampal signaling deficits after traumatic brain injury. Translational Stroke Research 2(4):546–555.

Avila J, Lucas JJ, Perez M, Hernandez F. 2004. Role of tau protein in both physiological and pathological conditions. Physiological Reviews 84(2):361–384.

Azarmina M. 2013. Full-Field versus Multifocal Electroretinography. Journal of Ophthalmic & Vision Research 8(3):191–192.

Ballatore C, Lee VM, Trojanowski JQ. 2007. Tau-mediated neurodegeneration in Alzheimer's disease and related disorders. Nature Reviews. Neuroscience 8(9):663–672.

Barrio JR, Small GW, Wong KP, Huang SC, Liu J, Merrill DA, Giza CC, Fitzsimmons RP, Omalu B, Bailes J, Kepe V. 2015. In vivo characterization of chronic traumatic encephalopathy using [F-18]FDDNP PET brain imaging. Proceedings of the National Academy of Sciences of the United States of America 112(16):E2039–2047.

Baskaya MK, Rao AM, Dogan A, Donaldson D, Dempsey RJ. 1997. The biphasic opening of the blood-brain barrier in the cortex and hippocampus after traumatic brain injury in rats. Neuroscience Letters 226(1):33–36.

Beamer M, Tummala SR, Gullotti D, Kopil K, Gorka S, Ted A, Bass CR, Morrison B, 3rd, Cohen AS, Meaney DF. 2016. Primary blast injury causes cognitive impairments and hippocampal circuit alterations. Experimental Neurology 283(Pt A):16–28.

Bezprozvanny I, Mattson MP. 2008. Neuronal calcium mishandling and the pathogenesis of Alzheimer's disease. Trends in Neurosciences 31(9):454–463.

Bhattacharjee Y. 2008. Neuroscience. Shell shock revisited: solving the puzzle of blast trauma. Science 319(5862):406–408.

Blumcke I, Hof PR, Morrison JH, Celio MR. 1990. Distribution of parvalbumin immunoreactivity in the visual cortex of Old World monkeys and humans. Journal of Comparative Neurology 301(3):417–432.

Bolton AN, Saatman KE. 2014. Regional neurodegeneration and gliosis are amplified by mild traumatic brain injury repeated at 24-hour intervals. Journal of Neuropathology and Experimental Neurology 73(10):933–947.

Braak H, Braak E, Kalus P. 1989. Alzheimer's disease: areal and laminar pathology in the occipital isocortex. Acta Neuropathologica 77(5):494–506.

Bricker-Anthony C, Hines-Beard J, Rex TS. 2014. Molecular changes and vision loss in a mouse model of closed-globe blast trauma. Investigative Ophthalmology & Visual Science 55(8):4853–4862.

Bricker-Anthony C, Hines-Beard J, Rex TS. 2016. Eye-Directed Overpressure Airwave-Induced Trauma Causes Lasting Damage to the Anterior and Posterior Globe: A Model for Testing Cell-Based Therapies. Journal of Ocular Pharmacology and Therapeutics 32(5):286–295.

Bricker-Anthony C, Rex TS. 2015. Neurodegeneration and Vision Loss after Mild Blunt Trauma in the C57Bl/6 and DBA/2J Mouse. PLoS One 10(7):e0131921.

Browne KD, Chen XH, Meaney DF, Smith DH. 2011. Mild traumatic brain injury and diffuse axonal injury in swine. Journal of Neurotrauma 28(9):1747–1755.

Bulson R, Jun W, Hayes J. 2012. Visual symptomatology and referral patterns for Operation Iraqi Freedom and Operation Enduring Freedom veterans with traumatic brain injury. Journal of Rehabilitation Research and Development 49(7):1075–1082.

Buritica E, Villamil L, Guzman F, Escobar MI, Garcia-Cairasco N, Pimienta HJ. 2009. Changes in calcium-binding protein expression in human cortical contusion tissue. Journal of Neurotrauma 26(12):2145–2155.

Byun H, Kwon S, Ahn HJ, Liu H, Forrest D, Demb JB, Kim IJ. 2016. Molecular features distinguish ten neuronal types in the mouse superficial superior colliculus. Journal of Comparative Neurology 524(11):2300–2321.

Caliskan G, Muller I, Semtner M, Winkelmann A, Raza AS, Hollnagel JO, Rosler A, Heinemann U, Stork O, Meier JC. 2016. Identification of Parvalbumin Interneurons as Cellular Substrate of Fear Memory Persistence. Cerebral Cortex 26(5):2325–2340.

Cantu D, Walker K, Andresen L, Taylor-Weiner A, Hampton D, Tesco G, Dulla CG. 2015. Traumatic Brain Injury Increases Cortical Glutamate Network Activity by Compromising GABAergic Control. Cerebral Cortex 25(8): 2306–2320.

Capo-Aponte JE, Urosevich TG, Temme LA, Tarbett AK, Sanghera NK. 2012. Visual dysfunctions and symptoms during the subacute stage of blast-induced mild traumatic brain injury. Military Medicine 177(7):804–813.

Cederberg D, Siesjo P. 2010. What has inflammation to do with traumatic brain injury? Child's Nervous System 26(2):221–226.

Cernak I. 2005. Animal models of head trauma. NeuroRx 2(3):410–422.

Cernak I, Merkle AC, Koliatsos VE, Bilik JM, Luong QT, Mahota TM, Xu L, Slack N, Windle D, Ahmed FA. 2011. The pathobiology of blast injuries and blast-induced neurotrauma as identified using a new experimental model of injury in mice. Neurobiology of Disease 41(2):538–551.

Cernak I, Noble-Haeusslein LJ. 2010. Traumatic brain injury: an overview of pathobiology with emphasis on military populations. Journal of Cerebral Blood Flow and Metabolism 30(2):255–266.

Chalioulias K, Sim KT, Scott R. 2007. Retinal sequelae of primary ocular blast injuries. Journal of the Royal Army Medical Corps 153(2):124–125.

Chamberland S, Topolnik L. 2012. Inhibitory control of hippocampal inhibitory neurons. Frontiers in Neuroscience 6:165.

Chen Y, Swanson RA. 2003. Astrocytes and brain injury. Journal of Cerebral Blood Flow and Metabolism 23(2):137–149.

Cheng H, Nair G, Walker TA, Kim MK, Pardue MT, Thule PM, Olson DE, Duong TQ. 2006. Structural and functional MRI reveals multiple retinal layers. Proceedings of the National Academy of Sciences of the United States of America 103(46):17525–17530.

Cherry JD, Tripodis Y, Alvarez VE, Huber B, Kiernan PT, Daneshvar DH, Mez J, Montenigro PH, Solomon TM, Alosco ML, Stern RA, McKee AC, Stein TD. 2016. Microglial neuroinflammation contributes to tau accumulation in

chronic traumatic encephalopathy. Acta Neuropathologica Communications 4(1):112.

Choi JH, Greene WA, Johnson AJ, Chavko M, Cleland JM, McCarron RM, Wang HC. 2014. Pathophysiology of blast-induced ocular trauma in rats after repeated exposure to low-level blast overpressure. Clinical & Experimental Ophthalmology 43(3):239–246.

Claybon A, Bishop AJ. 2011. Dissection of a mouse eye for a whole mount of the retinal pigment epithelium. Journal of Visualized Experiments: JoVE (48).

Cockerham GC, Goodrich GL, Weichel ED, Orcutt JC, Rizzo JF, Bower KS, Schuchard RA. 2009. Eye and visual function in traumatic brain injury. Journal of Rehabilitation Research and Development 46(6):811–818.

Cockerham GC, Lemke S, Glynn-Milley C, Zumhagen L, Cockerham KP. 2013. Visual performance and the ocular surface in traumatic brain injury. The Ocular Surface 11(1):25–34.

Costanzo M, Zurzolo C. 2013. The cell biology of prion-like spread of protein aggregates: mechanisms and implication in neurodegeneration. Biochemical Journal 452(1):1–17.

Courtney A, Courtney M. 2015. The Complexity of Biomechanics Causing Primary Blast-Induced Traumatic Brain Injury: A Review of Potential Mechanisms. Frontiers in Neurology 6:221.

Dalby NO, Rondouin G, Lerner-Natoli M. 1995. Increase in GAP-43 and GFAP immunoreactivity in the rat hippocampus subsequent to perforant path kindling. Journal of Neuroscience Research 41(5):613–619.

de Lanerolle NC, Bandak F, Kang D, Li AY, Du F, Swauger P, Parks S, Ling G, Kim JH. 2011. Characteristics of an explosive blast-induced brain injury in an experimental model. Journal of Neuropathology and Experimental Neurology 70(11):1046–1057.

DeKosky ST, Blennow K, Ikonomovic MD, Gandy S. 2013. Acute and chronic traumatic encephalopathies: pathogenesis and biomarkers. Nature Reviews.Neurol 9(4):192–200.

DeMar J, Sharrow K, Hill M, Berman J, Oliver T, Long J. 2016. Effects of Primary Blast Overpressure on Retina and Optic Tract in Rats. Frontiers in Neurology 7:59.

Dutca LM, Stasheff SF, Hedberg-Buenz A, Rudd DS, Batra N, Blodi FR, Yorek MS, Yin T, Shankar M, Herlein JA, Naidoo J, Morlock L, Williams N, Kardon RH, Anderson MG, Pieper AA, Harper MM. 2014. Early detection of subclinical visual damage after blast-mediated TBI enables prevention of chronic visual deficit by treatment with P7C3-S243. Investigative Ophthalmology & Visual Science 55(12):8330–8341.

Elder GA, Cristian A. 2009. Blast-related mild traumatic brain injury: mechanisms of injury and impact on clinical care. Mount Sinai Journal of Medicine 76(2):111–118.

Elder GA, Stone JR, Ahlers ST. 2014. Effects of low-level blast exposure on the nervous system: is there really a controversy? Frontiers in Neurology 5:269.

Faden AI, Loane DJ. 2015. Chronic neurodegeneration after traumatic brain injury: Alzheimer disease, chronic traumatic encephalopathy, or persistent neuroinflammation? Neurotherapeutics 12(1):143–150.

Fanselow MS, Dong HW. 2010. Are the dorsal and ventral hippocampus functionally distinct structures? Neuron 65(1):7–19.

Farkas O, Povlishock JT. 2007. Cellular and subcellular change evoked by diffuse traumatic brain injury: a complex web of change extending far beyond focal damage. Progress in Brain Research 161:43–59.

Ferguson S, Mouzon B, Paris D, Aponte D, Abdullah L, Stewart W, Mullan M, Crawford F. 2017. Acute or Delayed Treatment with Anatabine Improves Spatial Memory and Reduces Pathological Sequelae at Late Time-Points after Repetitive Mild Traumatic Brain Injury. Journal of Neurotrauma 34(8):1676–1691.

Ferrer I, Zujar MJ, Rivera R, Soria M, Vidal A, Casas R. 1993. Parvalbumin-immunoreactive dystrophic neurites and aberrant sprouts in the cerebral cortex of patients with Alzheimer's disease. Neuroscience Letters 158(2):163–166.

Finnie JW, Blumbergs PC. 2002. Traumatic brain injury. Veterinary Pathology 39(6):679–689.

Forman MS, Lal D, Zhang B, Dabir DV, Swanson E, Lee VM, Trojanowski JQ. 2005. Transgenic mouse model of tau pathology in astrocytes leading to nervous system degeneration. Journal of Neuroscience 25(14):3539–3550.

Forster E, Zhao S, Frotscher M. 2006. Laminating the hippocampus. Nature Reviews. Neuroscience 7(4):259–267.

Franklin KBJ, Paxinos G. 2008. The Mouse Brain in Stereotaxic Coordinates, Compact, 3rd Edition: Elsevier.

Freire MA, Faber J, Lemos NA, Santos JR, Cavalcanti PF, Lima RH, Morya E. 2015. Distribution and Morphology of Calcium-Binding Proteins Immunoreactive Neurons following Chronic Tungsten Multielectrode Implants. PLoS One 10(6):e0130354.

Freund TF, Buzsaki G. 1996. Interneurons of the hippocampus. Hippocampus 6(4):347–470.

Frost B, Jacks RL, Diamond MI. 2009. Propagation of tau misfolding from the outside to the inside of a cell. Journal of Biological Chemistry 284(19): 12845–12852.

Gao H, Han Z, Bai R, Huang S, Ge X, Chen F, Lei P. 2017. The accumulation of brain injury leads to severe neuropathological and neurobehavioral changes after repetitive mild traumatic brain injury. Brain Research 1657:1–8.

Gavett BE, Stern RA, McKee AC. 2011. Chronic traumatic encephalopathy: a potential late effect of sport-related concussive and subconcussive head trauma. Clinics in Sports Medicine 30(1):179–188, xi.

Geddes DM, LaPlaca MC, Cargill RS, 2nd. 2003. Susceptibility of hippocampal neurons to mechanically induced injury. Experimental Neurology 184(1):420–427.

Gendron TF, Petrucelli L. 2009. The role of tau in neurodegeneration. Molecular Neurodegeneration 4:13.

Ghose D, Maier A, Nidiffer A, Wallace MT. 2014. Multisensory response modulation in the superficial layers of the superior colliculus. Journal of Neuroscience 34(12):4332–4344.

Giannaris EL, Rosene DL. 2012. A stereological study of the numbers of neurons and glia in the primary visual cortex across the lifespan of male and female rhesus monkeys. Journal of Comparative Neurology 520(15):3492–3508.

Giza CC, Hovda DA. 2014. The New Neurometabolic Cascade of Concussion. Neurosurgery 75(suppl_4):S24–S33.

Goldstein LE, Fisher AM, Tagge CA, Zhang XL, Velisek L, Sullivan JA, Upreti C, Kracht JM, Ericsson M, Wojnarowicz MW, Goletiani CJ, Maglakelidze GM, Casey N, Moncaster JA, Minaeva O, Moir RD, Nowinski CJ, Stern RA, Cantu RC, Geiling J, Blusztajn JK, Wolozin BL, Ikezu T, Stein TD, Budson AE, Kowall NW, Chargin D, Sharon A, Saman S, Hall GF, Moss WC, Cleveland RO, Tanzi RE, Stanton PK, McKee AC. 2012. Chronic traumatic encephalopathy in blast-exposed military veterans and a blast neurotrauma mouse model. Science Translational Medicine 4(134): 134ra160.

Goodrich GL, Kirby J, Cockerham G, Ingalla SP, Lew HL. 2007. Visual function in patients of a polytrauma rehabilitation center: A descriptive study. Journal of Rehabilitation Research and Development 44(7):929–936.

Goodrich JA, Kim JH, Situ R, Taylor W, Westmoreland T, Du F, Parks S, Ling G, Hwang JY, Rapuano A, Bandak FA, de Lanerolle NC. 2016. Neuronal and glial changes in the brain resulting from explosive blast in an experimental model. Acta Neuropathologica Communications 4(1):124.

Gouras P. 1970. Electroretinography: Some basic principles. Investigative Ophthalmology 9(8):557–569.

Guley NH, Rogers JT, Del Mar NA, Deng Y, Islam RM, D'Surney L, Ferrell J, Deng B, Hines-Beard J, Bu W, Ren H, Elberger AJ, Marchetta JG, Rex TS, Honig MG, Reiner A. 2016. A Novel Closed-Head Model of Mild Traumatic Brain Injury Using Focal Primary Overpressure Blast to the Cranium in Mice. Journal of Neurotrauma 33(4):403–422.

Gullotti DM, Beamer M, Panzer MB, Chen YC, Patel TP, Yu A, Jaumard N, Winkelstein B, Bass CR, Morrison B, Meaney DF. 2014. Significant head accelerations can influence immediate neurological impairments in a murine model of blast-induced traumatic brain injury. Journal of Biomechanical Engineering 136(9):091004.

Gulyas AI, Hajos N, Freund TF. 1996. Interneurons containing calretinin are specialized to control other interneurons in the rat hippocampus. Journal of Neuroscience 16(10):3397–3411.

Gundersen HJ, Jensen EB, Kieu K, Nielsen J. 1999. The efficiency of systematic sampling in stereology--reconsidered. Journal of Microscopy 193(Pt 3):199–211.

Guo JL, Lee VM. 2014. Cell-to-cell transmission of pathogenic proteins in neurodegenerative diseases. Nature Medicine 20(2):130–138.

Hanger DP, Lau DH, Phillips EC, Bondulich MK, Guo T, Woodward BW, Pooler AM, Noble W. 2014. Intracellular and extracellular roles for tau in neurodegenerative disease. Journal of Alzheimers Disease 40 Suppl 1: S37–45.

Hanrahan F, Campbell M. 2016. Neuroinflammation. In: Laskowitz D, Grant G, eds. Translational Research in Traumatic Brain Injury. Frontiers in Neuroscience. Boca Raton (FL).

Harada H, Kelly PJ, Cole DJ, Drummond JC, Patel PM. 1999. Isoflurane reduces N-methyl-D-aspartate toxicity in vivo in the rat cerebral cortex. Anesthesia and Analgesia 89(6):1442–1447.

Hatashita S, Hoff JT. 1990. Brain edema and cerebrovascular permeability during cerebral ischemia in rats. Stroke 21(4):582–588.

Heldt SA, Elberger AJ, Deng Y, Guley NH, Del Mar N, Rogers J, Choi GW, Ferrell J, Rex TS, Honig MG, Reiner A. 2014. A novel closed-head model of mild traumatic brain injury caused by primary overpressure blast to the cranium produces sustained emotional deficits in mice. Frontiers in Neurology 5:2.

Hertle D, Beynon C, Zweckberger K, Vienenkotter B, Jung CS, Kiening K, Unterberg A, Sakowitz OW. 2012. Influence of isoflurane on neuronal death and outcome in a rat model of traumatic brain injury. Acta Neurochirurgica Supplementum 114:383–386.

Hicks RR, Fertig SJ, Desrocher RE, Koroshetz WJ, Pancrazio JJ. 2010. Neurological effects of blast injury. Journalf of Trauma 68(5):1257–1263.

Hines-Beard J, Marchetta J, Gordon S, Chaum E, Geisert EE, Rex TS. 2012. A mouse model of ocular blast injury that induces closed globe anterior and posterior pole damage. Experimental Eye Research 99:63–70.

Hof PR, Cox K, Young WG, Celio MR, Rogers J, Morrison JH. 1991. Parvalbumin-immunoreactive neurons in the neocortex are resistant to degeneration in Alzheimer's disease. Journal of Neuropathology and Experimental Neurology 50(4):451–462.

Hoon M, Okawa H, Della Santina L, Wong RO. 2014. Functional architecture of the retina: development and disease. Progress in Retinal and Eye Research 42:44–84.

Horstmann L, Kuehn S, Pedreiturria X, Haak K, Pfarrer C, Dick HB, Kleiter I, Joachim SC. 2016. Microglia response in retina and optic nerve in chronic

experimental autoimmune encephalomyelitis. Journal of Neuroimmunology 298:32–41.

Huber BR, Meabon JS, Martin TJ, Mourad PD, Bennett R, Kraemer BC, Cernak I, Petrie EC, Emery MJ, Swenson ER, Mayer C, Mehic E, Peskind ER, Cook DG. 2013. Blast exposure causes early and persistent aberrant phospho- and cleaved-tau expression in a murine model of mild blast-induced traumatic brain injury. Journal of Alzheimers Disease 37(2):309–323.

Huberman AD, Niell CM. 2011. What can mice tell us about how vision works? Trends in Neurosciences 34(9):464–473.

Huusko N, Romer C, Ndode-Ekane XE, Lukasiuk K, Pitkanen A. 2015. Loss of hippocampal interneurons and epileptogenesis: a comparison of two animal models of acquired epilepsy. Brain Structure & Function 220(1): 153–191.

Iqbal K, Alonso Adel C, Chen S, Chohan MO, El-Akkad E, Gong CX, Khatoon S, Li B, Liu F, Rahman A, Tanimukai H, Grundke-Iqbal I. 2005. Tau pathology in Alzheimer disease and other tauopathies. Biochimica et Biophysica Acta 1739(2–3):198–210.

Ivanova E, Toychiev AH, Yee CW, Sagdullaev BT. 2013. Optimized protocol for retinal wholemount preparation for imaging and immunohistochemistry. Journal of Visualized Experiments: JoVE (82):e51018.

Iwamoto N, Emson PC. 1991. Demonstration of neurofibrillary tangles in parvalbumin-immunoreactive interneurones in the cerebral cortex of Alzheimer-type dementia brain. Neuroscience Letters 128(1):81–84.

Iwata A, Chen XH, McIntosh TK, Browne KD, Smith DH. 2002. Long-term accumulation of amyloid-beta in axons following brain trauma without persistent upregulation of amyloid precursor protein genes. Journal of Neuropathology and Experimental Neurology 61(12):1056–1068.

Jean A, Nyein MK, Zheng JQ, Moore DF, Joannopoulos JD, Radovitzky R. 2014. An animal-to-human scaling law for blast-induced traumatic brain injury risk assessment. Proceedings of the National Academy of Sciences of the United States of America 111(43):15310–15315.

Jinno S, Fleischer F, Eckel S, Schmidt V, Kosaka T. 2007. Spatial arrangement of microglia in the mouse hippocampus: a stereological study in comparison with astrocytes. Glia 55(13):1334–1347.

Jinno S, Kosaka T. 2002. Patterns of expression of calcium binding proteins and neuronal nitric oxide synthase in different populations of hippocampal GABAergic neurons in mice. Journal of Comparative Neurology 449(1):1–25.

Johansen FF, Tonder N, Zimmer J, Baimbridge KG, Diemer NH. 1990. Short-term changes of parvalbumin and calbindin immunoreactivity in the rat hippocampus following cerebral ischemia. Neuroscience Letters 120(2): 171–174.

Johnson GV, Stoothoff WH. 2004. Tau phosphorylation in neuronal cell function and dysfunction. Journal of Cell Science 117(Pt 24):5721–5729.

Johnson VE, Stewart W, Smith DH. 2010. Traumatic brain injury and amyloid-beta pathology: a link to Alzheimer's disease? Nature Reviews. Neuroscience 11(5):361–370.

Jones K, Choi JH, Sponsel WE, Gray W, Groth SL, Glickman RD, Lund BJ, Reilly MA. 2016. Low-Level Primary Blast Causes Acute Ocular Trauma in Rabbits. Journal of Neurotrauma 33(13):1194–1201.

Jones S, Yakel JL. 1999. Inhibitory interneurons in hippocampus. Cell Biochemistry and Biophysics 31(2):207–218.

Kanaan NM, Cox K, Alvarez VE, Stein TD, Poncil S, McKee AC. 2016. Characterization of Early Pathological Tau Conformations and Phosphorylation in Chronic Traumatic Encephalopathy. Journal of Neuropathology and Experimental Neurology 75(1):19–34.

Kandel ER. 2013. Principles of neural science. New York: McGraw-Hill Medical. l, 1709 p. p.

Kang K, Song MR. 2010. Diverse FGF receptor signaling controls astrocyte specification and proliferation. Biochemical and Biophysical Research Communications 395(3):324–329.

Kapoor N, Ciuffreda KJ. 2002. Vision Disturbances Following Traumatic Brain Injury. Current Treatment Options in Neurology 4(4):271–280.

Karlstetter M, Scholz R, Rutar M, Wong WT, Provis JM, Langmann T. 2015. Retinal microglia: just bystander or target for therapy? Progress in Retinal and Eye Research 45:30–57.

Karperien A, Ahammer H, Jelinek HF. 2013. Quantitating the subtleties of microglial morphology with fractal analysis. Frontiers in Cellular Neuroscience 7:3.

Karve IP, Taylor JM, Crack PJ. 2016. The contribution of astrocytes and microglia to traumatic brain injury. British Journal of Pharmacology 173(4): 692–702.

Kawaguchi M, Furuya H, Patel PM. 2005. Neuroprotective effects of anesthetic agents. Journal of Anesthesia 19(2):150–156.

Kimbro JR, Kelly PJ, Drummond JC, Cole DJ, Patel PM. 2000. Isoflurane and pentobarbital reduce AMPA toxicity in vivo in the rat cerebral cortex. Anesthesiology 92(3):806–812.

Kirbas S, Turkyilmaz K, Anlar O, Tufekci A, Durmus M. 2013. Retinal nerve fiber layer thickness in patients with Alzheimer disease. Journal of Neuroophthalmology 33(1):58–61.

Klausberger T, Somogyi P. 2008. Neuronal diversity and temporal dynamics: the unity of hippocampal circuit operations. Science 321(5885):53–57.

Kochanek PM, Jackson TC, Ferguson NM, Carlson SW, Simon DW, Brockman EC, Ji J, Bayir H, Poloyac SM, Wagner AK, Kline AE, Empey PE, Clark RS, Jackson EK, Dixon CE. 2015. Emerging therapies in traumatic brain injury. Seminars in Neurology 35(1):83–100.

Kolappan M, Henderson AP, Jenkins TM, Wheeler-Kingshott CA, Plant GT, Thompson AJ, Miller DH. 2009. Assessing structure and function of the afferent visual pathway in multiple sclerosis and associated optic neuritis. Journal of Neurology 256(3):305–319.

Koliatsos VE, Cernak I, Xu L, Song Y, Savonenko A, Crain BJ, Eberhart CG, Frangakis CE, Melnikova T, Kim H, Lee D. 2011. A mouse model of blast injury to brain: initial pathological, neuropathological, and behavioral characterization. Journal of Neuropathology and Experimental Neurology 70(5):399–416.

Kovacs SK, Leonessa F, Ling GS. 2014. Blast TBI Models, Neuropathology, and Implications for Seizure Risk. Frontiers in Neurology 5:47.

Kuehn R, Simard PF, Driscoll I, Keledjian K, Ivanova S, Tosun C, Williams A, Bochicchio G, Gerzanich V, Simard JM. 2011. Rodent model of direct cranial blast injury. Journal of Neurotrauma 28(10):2155–2169.

Langer TP, Lund RD. 1974. The upper layers of the superior colliculus of the rat: a Golgi study. Journal of Comparative Neurology 158(4):418–435.

Lawson LJ, Perry VH, Dri P, Gordon S. 1990. Heterogeneity in the distribution and morphology of microglia in the normal adult mouse brain. Neuroscience 39(1):151–170.

Leist M, Datunashvilli M, Kanyshkova T, Zobeiri M, Aissaoui A, Cerina M, Romanelli MN, Pape HC, Budde T. 2016. Two types of interneurons in the mouse lateral geniculate nucleus are characterized by different h-current density. Scientific Reports 6:24904.

Lemke S, Cockerham GC, Glynn-Milley C, Cockerham KP. 2013. Visual quality of life in veterans with blast-induced traumatic brain injury. JAMA Ophthalmology 131(12):1602–1609.

Leo P, McCrea M. 2016. Epidemiology. In: Laskowitz D, Grant G, eds. Translational Research in Traumatic Brain Injury. Frontiers in Neuroscience. Boca Raton (FL).

Leuba G, Kraftsik R, Saini K. 1998. Quantitative distribution of parvalbumin, calretinin, and calbindin D-28k immunoreactive neurons in the visual cortex of normal and Alzheimer cases. Experimental Neurology 152(2): 278–291.

Li Y, Sun H, Chen Z, Xu H, Bu G, Zheng H. 2016. Implications of GABAergic Neurotransmission in Alzheimer's Disease. Frontiers in Aging Neuroscience 8:31.

Liu L, Drouet V, Wu JW, Witter MP, Small SA, Clelland C, Duff K. 2012. Trans-synaptic spread of tau pathology in vivo. PLoS One 7(2):e31302.

London A, Benhar I, Schwartz M. 2013. The retina as a window to the brain-from eye research to CNS disorders. Nature Reviews. Neurology 9(1):44–53.

Lund-Andersen H. 1979. Transport of glucose from blood to brain. Physiological Reviews 59(2):305–352.

Lynch CE, Crynen G, Ferguson S, Mouzon B, Paris D, Ojo J, Leary P, Crawford F, Bachmeier C. 2016. Chronic cerebrovascular abnormalities in a mouse model of repetitive mild traumatic brain injury. Brain Injury 30(12):1414–1427.

Maccaferri G. 2011. Modulation of hippocampal stratum lacunosum-moleculare microcircuits. Journal of Physiology 589(Pt 8):1885–1891.

Maguire G, Simko H, Weinreb RN, Ayoub G. 1998. Transport-mediated release of endogenous glutamate in the vertebrate retina. Pflügers Archiv: European Journal of Physiology 436(3):481–484.

Majdan M, Steyerberg EW, Nieboer D, Mauritz W, Rusnak M, Lingsma HF. 2015. Glasgow coma scale motor score and pupillary reaction to predict six-month mortality in patients with traumatic brain injury: comparison of field and admission assessment. Journal of Neurotrauma 32(2):101–108.

Majid A, He YY, Gidday JM, Kaplan SS, Gonzales ER, Park TS, Fenstermacher JD, Wei L, Choi DW, Hsu CY. 2000. Differences in vulnerability to permanent focal cerebral ischemia among 3 common mouse strains. Stroke 31(11):2707–2714.

Marambaud P, Dreses-Werringloer U, Vingtdeux V. 2009. Calcium signaling in neurodegeneration. Molecular Neurodegeneration 4:20.

May PJ. 2006. The mammalian superior colliculus: laminar structure and connections. Progress in Brain Research 151:321–378.

McAllister TW. 2011. Neurobiological consequences of traumatic brain injury. Dialogues in Clinical Neuroscience 13(3):287–300.

McKee AC. Vision and Traumatic Brain Injury in Veterans and Athletes. Retinal pathology in Chronic Traumatic Encephalopathy; 2015 May 2; Colorado Convention Center Denver, Colorado. ARVO.

McKee AC. Vision and Traumatic Brain Injury: The Outlook for Therapeutics. Traumatic brain injury and visual function; 2016 April 30; Washington State Convention Center, Seattle. ARVO.

McKee AC, Au R, Cabral HJ, Kowall NW, Seshadri S, Kubilus CA, Drake J, Wolf PA. 2006. Visual association pathology in preclinical Alzheimer disease. Journal of Neuropathology and Experimental Neurology 65(6):621–630.

McKee AC, Cairns NJ, Dickson DW, Folkerth RD, Keene CD, Litvan I, Perl DP, Stein TD, Vonsattel JP, Stewart W, Tripodis Y, Crary JF, Bieniek KF, Dams-O'Connor K, Alvarez VE, Gordon WA, group TC. 2016. The first NINDS/NIBIB consensus meeting to define neuropathological criteria for the diagnosis of chronic traumatic encephalopathy. Acta Neuropathologica 131(1):75–86.

McKee AC, Robinson ME. 2014. Military-related traumatic brain injury and neurodegeneration. Alzheimer's & Dementia 10(3 Suppl):S242–253.

McKee AC, Stern RA, Nowinski CJ, Stein TD, Alvarez VE, Daneshvar DH, Lee HS, Wojtowicz SM, Hall G, Baugh CM, Riley DO, Kubilus CA, Cormier KA, Jacobs MA, Martin BR, Abraham CR, Ikezu T, Reichard RR, Wolozin BL, Budson AE, Goldstein LE, Kowall NW, Cantu RC. 2013. The spectrum of disease in chronic traumatic encephalopathy. Brain 136(Pt 1):43–64.

Menon DK. 2009. Unique challenges in clinical trials in traumatic brain injury. Critical Care Medicine 37(1 Suppl):S129–135.

Mez J, Solomon TM, Daneshvar DH, Murphy L, Kiernan PT, Montenigro PH, Kriegel J, Abdolmohammadi B, Fry B, Babcock KJ, Adams JW, Bourlas AP, Papadopoulos Z, McHale L, Ardaugh BM, Martin BR, Dixon D, Nowinski CJ, Chaisson C, Alvarez VE, Tripodis Y, Stein TD, Goldstein LE, Katz DI, Kowall NW, Cantu RC, Stern RA, McKee AC. 2015. Assessing clinicopathological correlation in chronic traumatic encephalopathy: rationale and methods for the UNITE study. Alzheimer's Research & Therapy 7(1):62.

Mez J, Stern RA, McKee AC. 2013. Chronic traumatic encephalopathy: where are we and where are we going? Current Neurology and Neuroscience Reports 13(12):407.

Mishra V, Skotak M, Schuetz H, Heller A, Haorah J, Chandra N. 2016. Primary blast causes mild, moderate, severe and lethal TBI with increasing blast overpressures: Experimental rat injury model. Scientific Reports 6:26992.

Mohan K, Kecova H, Hernandez-Merino E, Kardon RH, Harper MM. 2013. Retinal ganglion cell damage in an experimental rodent model of blast-mediated traumatic brain injury. Investigative Ophthalmology & Visual Science 54(5):3440–3450.

Morin LP, Studholme KM. 2014. Retinofugal projections in the mouse. Journal of Comparative Neurology 522(16):3733–3753.

Morrison JH, Hof PR. 2002. Selective vulnerability of corticocortical and hippocampal circuits in aging and Alzheimer's disease. Progress in Brain Research 136:467–486.

Moser E, Moser MB, Andersen P. 1993. Spatial learning impairment parallels the magnitude of dorsal hippocampal lesions, but is hardly present following ventral lesions. Journal of Neuroscience 13(9):3916–3925.

Muzaffar R, Shousha MA, Sarajlic L, Osman MM. 2013. Ophthalmologic abnormalities on FDG-PET/CT: a pictorial essay. Cancer Imaging 13:100–112.

Nakagawa A, Ohtani K, Goda K, Kudo D, Arafune T, Washio T, Tominaga T. 2016. Mechanism of Traumatic Brain Injury at Distant Locations After Exposure to Blast Waves: Preliminary Results from Animal and Phantom Experiments. Acta Neurochirurgica Supplementum 122:3–7.

Nolte J, Sundsten JW. 2002. The human brain : an introduction to its functional anatomy. St. Louis, Mo.: Mosby.

O'Brien RJ, Wong PC. 2011. Amyloid precursor protein processing and Alzheimer's disease. Annual Review of Neuroscience 34:185–204.

O'Connor WT, Smyth A, Gilchrist MD. 2011. Animal models of traumatic brain injury: a critical evaluation. Pharmacology & Therapeutics 30(2):106–113.

Obermeier B, Daneman R, Ransohoff RM. 2013. Development, maintenance and disruption of the blood-brain barrier. Nature Medicine 19(12):1584–1596.

Ogundele OM, Omoaghe AO, Ajonijebu DC, Ojo AA, Fabiyi TD, Olajide OJ, Falode DT, Adeniyi PA. 2014. Glia activation and its role in oxidative stress. Metabolic Brain Disease 29(2):483–493.

Palop JJ, Mucke L. 2016. Network abnormalities and interneuron dysfunction in Alzheimer disease. Nature Reviews. Neuroscience 17(12):777–792.

Panzer MB, Bass CR, Rafaels KA, Shridharani J, Capehart BP. 2012. Primary blast survival and injury risk assessment for repeated blast exposures. Journal of Trauma and Acute Care Surgery 72(2):454–466.

Panzer MB, Wood GW, Bass CR. 2014. Scaling in neurotrauma: how do we apply animal experiments to people? Experimental Neurology 261:120–126.

Pardridge WM. 1983. Brain metabolism: a perspective from the blood-brain barrier. Physiologcial Reviews 63(4):1481–1535.

Pascual O, Ben Achour S, Rostaing P, Triller A, Bessis A. 2012. Microglia activation triggers astrocyte-mediated modulation of excitatory neurotransmission. Proceedings of the National Academy of Sciences of the United States of America 109(4):E197–205.

Patt S, Brodhun M. 1999. Neuropathological sequelae of traumatic injury in the brain. An overview. Experiemntal and Toxicologic Pathology 51(2):119–123.

Petras JM, Bauman RA, Elsayed NM. 1997. Visual system degeneration induced by blast overpressure. Toxicology 121(1):41–49.

Pikkarainen M, Kauppinen T, Alafuzoff I. 2009. Hyperphosphorylated tau in the occipital cortex in aged nondemented subjects. Journal of Neuropathology and Experimental Neurology 68(6):653–660.

Porciatti V. 2007. The mouse pattern electroretinogram. Documenta Ophthalmologica. Advances in Ophthalmology 115(3):145–153.

Raghupathi R. 2004. Cell death mechanisms following traumatic brain injury. Brain Pathology 14(2):215–222.

Ramirez AI, Salazar JJ, de Hoz R, Rojas B, Gallego BI, Salinas-Navarro M, Alarcon-Martinez L, Ortin-Martinez A, Aviles-Trigueros M, Vidal-Sanz M, Trivino A, Ramirez JM. 2010. Quantification of the effect of different levels of IOP in the astroglia of the rat retina ipsilateral and contralateral to experimental glaucoma. Investigative Ophthalmology & Visual Science 51(11):5690–5696.

Reid WM, Rolfe A, Register D, Levasseur JE, Churn SB, Sun D. 2010. Strain-related differences after experimental traumatic brain injury in rats. Journal of Neurotrauma 27(7):1243–1253.

Risling M, Plantman S, Angeria M, Rostami E, Bellander BM, Kirkegaard M, Arborelius U, Davidsson J. 2011. Mechanisms of blast induced brain injuries, experimental studies in rats. NeuroImage 54 Suppl 1:S89–97.

Risold PY, Swanson LW. 1996. Structural evidence for functional domains in the rat hippocampus. Science 272(5267):1484–1486.

Rosene DL, Roy NJ, Davis BJ. 1986. A cryoprotection method that facilitates cutting frozen sections of whole monkey brains for histological and histochemical processing without freezing artifact. Journal of Histochemistry and Cytochemistry 34(10):1301–1315.

Rosenfeld JV, McFarlane AC, Bragge P, Armonda RA, Grimes JB, Ling GS. 2013. Blast-related traumatic brain injury. The Lancet. Neurology 12(9): 882–893.

Rowe RK, Harrison JL, Thomas TC, Pauly JR, Adelson PD, Lifshitz J. 2013. Using anesthetics and analgesics in experimental traumatic brain injury. Lab Animal 42(8):286–291.

Royo NC, Conte V, Saatman KE, Shimizu S, Belfield CM, Soltesz KM, Davis JE, Fujimoto ST, McIntosh TK. 2006. Hippocampal vulnerability following traumatic brain injury: a potential role for neurotrophin-4/5 in pyramidal cell neuroprotection. European Journal of Neuroscience 23(5):1089–1102.

Ruff RM, Iverson GL, Barth JT, Bush SS, Broshek DK, Policy NAN, Planning C. 2009. Recommendations for diagnosing a mild traumatic brain injury: a National Academy of Neuropsychology education paper. Archives of Clinical Neuropsychology 24(1):3–10.

Sajja VS, Ereifej ES, VandeVord PJ. 2014. Hippocampal vulnerability and subacute response following varied blast magnitudes. Neuroscience Letters 570:33–37.

Saljo A, Bolouri H, Mayorga M, Svensson B, Hamberger A. 2010. Low-level blast raises intracranial pressure and impairs cognitive function in rats: prophylaxis with processed cereal feed. Journal of Neurotrauma 27(2): 383–389.

Sanders DW, Kaufman SK, DeVos SL, Sharma AM, Mirbaha H, Li A, Barker SJ, Foley AC, Thorpe JR, Serpell LC, Miller TM, Grinberg LT, Seeley WW, Diamond MI. 2014. Distinct tau prion strains propagate in cells and mice and define different tauopathies. Neuron 82(6):1271–1288.

Satoh J, Tabira T, Sano M, Nakayama H, Tateishi J. 1991. Parvalbumin-immunoreactive neurons in the human central nervous system are decreased in Alzheimer's disease. Acta Neuropathologica 81(4):388–395.

Savchenko VL, McKanna JA, Nikonenko IR, Skibo GG. 2000. Microglia and astrocytes in the adult rat brain: comparative immunocytochemical analysis demonstrates the efficacy of lipocortin 1 immunoreactivity. Neuroscience 96(1):195–203.

Schauwecker PE, Steward O. 1997. Genetic determinants of susceptibility to excitotoxic cell death: implications for gene targeting approaches. Proceedings of the National Academy of Sciences of the United States of America 94(8):4103–4108.

Schenk D, Barbour R, Dunn W, Gordon G, Grajeda H, Guido T, Hu K, Huang J, Johnson-Wood K, Khan K, Kholodenko D, Lee M, Liao Z, Lieberburg I, Motter R, Mutter L, Soriano F, Shopp G, Vasquez N, Vandevert C, Walker S, Wogulis M, Yednock T, Games D, Seubert P. 1999. Immunization with amyloid-beta attenuates Alzheimer-disease-like pathology in the PDAPP mouse. Nature 400(6740):173–177.

Schuman JS. 2008. Spectral domain optical coherence tomography for glaucoma (an AOS thesis). Transactions of the American Ophthalmological Society 106:426–458.

Schwartz M, Butovsky O, Bruck W, Hanisch UK. 2006. Microglial phenotype: is the commitment reversible? Trends in Neurosciences 29(2):68–74.

Seoane A, Espejo M, Pallas M, Rodriguez-Farre E, Ambrosio S, Llorens J. 1999. Degeneration and gliosis in rat retina and central nervous system following 3,3'-iminodipropionitrile exposure. Brain Research 833(2):258–271.

Shelah M, Weinberger D, Ofri R. 2007. Acute blindness in a dog caused by an explosive blast. Veterinary Ophthalmology 10(3):196–198.

Sherwood D, Sponsel WE, Lund BJ, Gray W, Watson R, Groth SL, Thoe K, Glickman RD, Reilly MA. 2014. Anatomical manifestations of primary blast ocular trauma observed in a postmortem porcine model. Investigative Ophthalmology & Visual Science 55(2):1124–1132.

Shimada M, Akagi N, Goto H, Watanabe H, Nakanishi M, Hirose Y, Watanabe M. 1992. Microvessel and astroglial cell densities in the mouse hippocampus. Journal of Anatomy 180 ( Pt 1):89–95.

Simard JM, Pampori A, Keledjian K, Tosun C, Schwartzbauer G, Ivanova S, Gerzanich V. 2014. Exposure of the thorax to a sublethal blast wave causes a hydrodynamic pulse that leads to perivenular inflammation in the brain. Journal of Neurotrauma 31(14):1292–1304.

Smith DH, Okiyama K, Gennarelli TA, McIntosh TK. 1993. Magnesium and ketamine attenuate cognitive dysfunction following experimental brain injury. Neuroscience Letters 157(2):211–214.

Sofroniew MV, Vinters HV. 2010. Astrocytes: biology and pathology. Acta Neuropathologica 119(1):7–35.

Sokol S. 1976. Visually evoked potentials: theory, techniques and clinical applications. Survey of Ophthalmology 21(1):18–44.

Somogyi P, Klausberger T. 2005. Defined types of cortical interneurone structure space and spike timing in the hippocampus. Journal of Physiology 562(Pt 1):9–26.

Spaide RF, Koizumi H, Pozzoni MC. 2008. Enhanced depth imaging spectral-domain optical coherence tomography. American Journal of Ophthalmology 146(4):496–500.

Sparks DL, Hartwich-Young R. 1989. The deep layers of the superior colliculus. Reviews of Oculomotor Research 3:213–255.

Statler KD, Alexander H, Vagni V, Dixon CE, Clark RS, Jenkins L, Kochanek PM. 2006. Comparison of seven anesthetic agents on outcome after experimental traumatic brain injury in adult, male rats. Journal of Neurotrauma 23(1):97–108.

Stelmack JA, Frith T, Van Koevering D, Rinne S, Stelmack TR. 2009. Visual function in patients followed at a Veterans Affairs polytrauma network site: an electronic medical record review. Optometry 80(8):419–424.

Steward O, Schauwecker PE, Guth L, Zhang Z, Fujiki M, Inman D, Wrathall J, Kempermann G, Gage FH, Saatman KE, Raghupathi R, McIntosh T. 1999. Genetic approaches to neurotrauma research: opportunities and potential pitfalls of murine models. Experimental Neurology 157(1):19–42.

Steward O, Torre ER, Tomasulo R, Lothman E. 1991. Neuronal activity up-regulates astroglial gene expression. Proceedings of the National Academy of Sciences of the United States of America 88(15):6819–6823.

Strange BA, Witter MP, Lein ES, Moser EI. 2014. Functional organization of the hippocampal longitudinal axis. Nature Reviews. Neuroscience 15(10): 655–669.

Suh M, Basu S, Kolster R, Sarkar R, McCandliss B, Ghajar J, Cognitive, Neurobiological Research C. 2006. Increased oculomotor deficits during target blanking as an indicator of mild traumatic brain injury. Neuroscience Letters 410(3):203–207.

Svetlov SI, Larner SF, Kirk DR, Atkinson J, Hayes RL, Wang KK. 2009. Biomarkers of blast-induced neurotrauma: profiling molecular and cellular mechanisms of blast brain injury. Journal of Neurotrauma 26(6):913–921.

Svetlov SI, Prima V, Kirk DR, Gutierrez H, Curley KC, Hayes RL, Wang KK. 2010. Morphologic and biochemical characterization of brain injury in a model of controlled blast overpressure exposure. Journal of Trauma 69(4): 795–804.

Tang Y, Le W. 2016. Differential Roles of M1 and M2 Microglia in Neurodegenerative Diseases. Molecular Neurobiology 53(2):1181–1194.

Thored P, Heldmann U, Gomes-Leal W, Gisler R, Darsalia V, Taneera J, Nygren JM, Jacobsen SE, Ekdahl CT, Kokaia Z, Lindvall O. 2009. Long-term accumulation of microglia with proneurogenic phenotype concomitant with persistent neurogenesis in adult subventricular zone after stroke. Glia 57(8):835–849.

Tong F. 2003. Primary visual cortex and visual awareness. Nature Reviews. Neuroscience 4(3):219–229.

Toth K, Eross L, Vajda J, Halasz P, Freund TF, Magloczky Z. 2010. Loss and reorganization of calretinin-containing interneurons in the epileptic human hippocampus. Brain 133(9):2763–2777.

Toth K, Magloczky Z. 2014. The vulnerability of calretinin-containing hippocampal interneurons to temporal lobe epilepsy. Frontiers in Neuroanatomy 8:100.

Townsend KA, Wollstein G, Schuman JS. 2008. Clinical application of MRI in ophthalmology. NMR in Biomedicine 21(9):997–1002.

Tual-Chalot S, Allinson KR, Fruttiger M, Arthur HM. 2013. Whole mount immunofluorescent staining of the neonatal mouse retina to investigate angiogenesis in vivo. Journal of Visualized Experiments: JoVE (77): e50546.

Vandevord PJ, Bolander R, Sajja VS, Hay K, Bir CA. 2012. Mild neurotrauma indicates a range-specific pressure response to low level shock wave exposure. Annals of Biomedical Engineering 40(1):227–236.

Vecino E, Rodriguez FD, Ruzafa N, Pereiro X, Sharma SC. 2016. Glia-neuron interactions in the mammalian retina. Progress in Retinal and Eye Research 51:1–40.

Walsh DV, Capo-Aponte JE, Jorgensen-Wagers K, Temme LA, Goodrich G, Sosa J, Riggs DW. 2015. Visual field dysfunctions in warfighters during different stages following blast and nonblast mTBI. Military Medicine 180(2):178–185.

Wang HC, Choi JH, Greene WA, Plamper ML, Cortez HE, Chavko M, Li Y, Dalle Lucca JJ, Johnson AJ. 2014. Pathophysiology of blast-induced ocular trauma with apoptosis in the retina and optic nerve. Military Medicine 179(8 Suppl):34–40.

Wang J, Fox MA, Povlishock JT. 2013. Diffuse traumatic axonal injury in the optic nerve does not elicit retinal ganglion cell loss. Journal of Neuropathology and Experimental Neurology 72(8):768–781.

Wang Y, Mandelkow E. 2016. Tau in physiology and pathology. Nature Reviews. Neuroscience 17(1):5–21.

Wang Y, Wei Y, Oguntayo S, Wilkins W, Arun P, Valiyaveettil M, Song J, Long JB, Nambiar MP. 2011. Tightly coupled repetitive blast-induced traumatic brain injury: development and characterization in mice. Journal of Neurotrauma 28(10):2171–2183.

Weber JT. 2012. Altered calcium signaling following traumatic brain injury. Frontiers in Pharmacology 3:60.

Werner C, Engelhard K. 2007. Pathophysiology of traumatic brain injury. British Journal of Anaesthesia 99(1):4–9.

Williams PA, Howell GR, Barbay JM, Braine CE, Sousa GL, John SW, Morgan JE. 2013. Retinal ganglion cell dendritic atrophy in DBA/2J glaucoma. PLoS One 8(8):e72282.

Woerman AL, Aoyagi A, Patel S, Kazmi SA, Lobach I, Grinberg LT, McKee AC, Seeley WW, Olson SH, Prusiner SB. 2016. Tau prions from Alzheimer's disease and chronic traumatic encephalopathy patients propagate in cultured cells. Proceedings of the National Academy of Sciences of the United States of America 113(50):E8187–E8196.

Wojda U, Salinska E, Kuznicki J. 2008. Calcium ions in neuronal degeneration. IUBMB Life 60(9):575–590.

Wolfe MS. 2012. The role of tau in neurodegenerative diseases and its potential as a therapeutic target. Scientifica (Cairo) 2012:796024.

Xiong Y, Mahmood A, Chopp M. 2013. Animal models of traumatic brain injury. Nature Reviews. Neuroscience 14(2):128–142.

Xiong Y, Zhang Y, Mahmood A, Chopp M. 2015. Investigational agents for treatment of traumatic brain injury. Expert Opinion on Investigational Drugs 24:743–760.

Xu X, Roby KD, Callaway EM. 2010. Immunochemical characterization of inhibitory mouse cortical neurons: three chemically distinct classes of inhibitory cells. Journal of Comparative Neurology 518(3):389–404.

Xu X, Warrington AE, Bieber AJ, Rodriguez M. 2011. Enhancing CNS repair in neurological disease: challenges arising from neurodegeneration and rewiring of the network. CNS Drugs 25(7):555–573.

Yadav NK, Ciuffreda KJ. 2013. Optimization of the pattern visual evoked potential (VEP) in the visually-normal and mild traumatic brain injury (mTBI) populations. Brain Injury 27(13–14):1631–1642.

Yi J, Padalino DJ, Chin LS, Montenegro P, Cantu RC. 2013. Chronic traumatic encephalopathy. Current Sports Medicine Reports 12(1):28–32.

Zamanian JL, Xu L, Foo LC, Nouri N, Zhou L, Giffard RG, Barres BA. 2012. Genomic analysis of reactive astrogliosis. Journal of Neuroscience 32(18):6391–6410.

Zeisel A, Munoz-Manchado AB, Codeluppi S, Lonnerberg P, La Manno G, Jureus A, Marques S, Munguba H, He L, Betsholtz C, Rolny C, Castelo-Branco G, Hjerling-Leffler J, Linnarsson S. 2015. Brain structure. Cell types in the mouse cortex and hippocampus revealed by single-cell RNA-seq. Science 347(6226):1138–1142.

Zetterberg H, Smith DH, Blennow K. 2013. Biomarkers of mild traumatic brain injury in cerebrospinal fluid and blood. Nature Reviews. Neurology 9(4): 201–210.

Zhang J, Puvenna V, Janigro D. 2016. Biomarkers of Traumatic Brain Injury and Their Relationship to Pathology. In: Laskowitz D, Grant G, eds. Translational Research in Traumatic Brain Injury. Frontiers in Neuroscience. Boca Raton (FL).

Zhao X, Ahram A, Berman RF, Muizelaar JP, Lyeth BG. 2003. Early loss of astrocytes after experimental traumatic brain injury. Glia 44(2):140–152.

Zhivotovsky B, Orrenius S. 2011. Calcium and cell death mechanisms: a perspective from the cell death community. Cell Calcium 50(3):211–221.

Zou YY, Kan EM, Lu J, Ng KC, Tan MH, Yao L, Ling EA. 2013. Primary blast injury-induced lesions in the retina of adult rats. Journal of Neuroinflammation 10:79.

# Vita